92PC92104-TPR-14

DOE/PC/92104--T14

ADVANCED THERMALLY STABLE JET FUELS

Technical Progress Report
October 1995 - December 1995

H.H. Schobert, S. Eser, C. Song, P.G. Hatcher, A. Boehman, M.M. Coleman

Contributions from:

J. Atria, T. Edwards, J. Yu. P. Sanghani. J. Li, M. Sobkowiak, S. Martin, and W.-C. Lai

April 1996

Prepared for U.S. Department of Energy
under
Contract No. DE-FG22-92PC92104

OBJECTIVES

The Penn State program in advanced thermally stable jet fuels has five components: 1) development of mechanisms of degradation and solids formation; 2) quantitative measurement of growth of sub-micrometer and micrometer sized particles suspended in fuels during thermal stressing; 3) characterization of carbonaceous deposits by various instrumental and microscopic methods; 4) elucidation of the role of additives in retarding the formation of carbonaceous solids; and 5) assessment of the potential of producing high yields of cycloalkanes and hydroaromatics by direct liquefaction of coal.

SUMMARY

Norpar-13, a mixture of *n*-alkanes, was found to be a useful model for observing the effects of high-temperature stressing of jet fuels. Norpar was stable in the oxidative regime and increased the amount of pyrolytic deposition detected. The increased pyrolytic deposits made observing the mitigating effects of additives easier than in an authentic jet fuel. Tetrahydroquinoline (THQ), benzyl alcohol, and tetralin all increased the thermal stability of Norpar-13 in a flow reactor. THQ was the most effective, consistent with batch reactor results, although an oxidative deposit formed with THQ addition.

Norpar-13 was also studied under supercritical conditions, both at 425°C in a glass tube reactor and at 450°C in the conventional microautoclave (tubing bomb) batch reactors.

Homogeneous processes occurring in the bulk fuel (in this case, jet fuels blended with tetradecane) form reactive species, but nucleation of coke particles does not occur at 723K under supercritical conditions. Cycloalkanes, xylene, toluene, and benzene are stable and do not contribute to the formation of solid deposits. Indan and C_1 and C_2 indans are very stable. Radicals formed from tetradecane and other alkanes can abstract hydrogen from these stable compounds to form reactive radicals. Deposit formation in jet fuel / tetradecane mixtures is proportional to the initial concentration of tetradecane, but the direct correlation between deposit mass and tetradecane conversion is poor. Using an appropriate functional form that incorporates the induction period for deposition may lead to an improved correlation. With an appropriate description of the induction process and further statistical analysis, it should be possible to develop a rate equation for deposit formation in terms of the concentration of reactive compounds in the mixture.

Further flow reactor experiments have been conducted with Norpar-13 to study metal surface effects on deposit formation. Large amounts of carbon deposit are formed at

500 psig, 550°C for 5 hours. Filamentous and platelet carbon form under these conditions, neither of which is normally expected to form under these flow reactor conditions. There is a narrow temperature window for the formation of large amounts of filamentous carbon and thick carbon platelets, since no collectable carbon deposits were formed at 525° or 575°.

Norpar-13 created a large amount of catalytic filament deposits in stainless steel flow reactor tubes. A fused silica coating (Silicosteel) created a barrier from the stainless steel surface, eliminating filament formation and greatly reducing the amount of pyrolytic deposits formed.

Work has begun on a screening test to evaluate deposit formation with various additives in the 200–300°C temperature range. Initial tests used dodecane and Jet A-1 treated with THQ and benzyl alcohol at 250°C. Based on preliminary results, plans are being developed to perform systematic experiments at 250°C and 200 psi air as a function of time.

Scouting studies on seeking a non-radical hydrogen transfer mechanism to coal at low-temperature conditions continued. Such a reaction pathway offers the potential of a substantial reduction in cost of any coal-derived components that might be the basis of, or additives to, jet fuels.

Platinum- and palladium-loaded mordenites proved to be very effective catalysts for conformational isomerization of *cis*-decalin to *trans*-decalin at 473 K under hydrogen. The selectivity to *trans*-decalin is nearly 100%, with a *trans*-/*cis*- ratio of nearly 13.

Task 1. Investigation of the Quantitative Degradation Chemistry of Jet Fuels

1. High Temperature Cracking and Deposition Behavior of an n-Alkane Mixture (Contributed by Joseph Atria and Tim Edwards)

Introduction

Advanced jet engine designs and the need for jet fuel in aircraft to handle increasing heat loads have generated much interest in investigating the thermal stability of jet fuels at temperatures greater than 450°C. The deposits that form from jet fuel at elevated temperatures can inhibit and degrade the performance of fuel lines, heat exchangers, nozzles and other aircraft systems. Two types of carbon deposits can form. Oxidative deposits form by autoxidation reactions at temperatures from 120°C to 200°C. Pyrolytic deposits begin to form from the gas phase when the fuel begins to crack at temperatures above 450°C. The thermal cracking of jet fuel proceeds via a free radical mechanism which can lead to the formation of deposits.

A cost-effective model compound mixture was needed to study the chemical breakup of jet fuel at high temperatures, along with providing the ability to observe the effects of thermal stabilizers on the fuel products. The many complex species found in jet fuel can often mask these effects. An *n*-alkane mixture, consisting of mainly dodecane, tridecane and tetradecane, called Norpar-13 (from Exxon Corporation) was used in these experiments. Norpar-13 was both cost effective and allowed for comparison to past batch reactor work done with these alkanes (1-3).

Several compounds have been shown to help increase the thermal stability of jet fuel in batch reactor tests at temperatures greater than 400°C (3-6). The stabilizers used in this study were tetrahydroquinoline (THQ), benzyl alcohol (BzOH), and tetrahydronapthalene (tetralin). These stabilizers donate hydrogen to react with the fuel radicals that form during thermal stressing. This hydrogen transfer will help suppress the thermal decomposition of the fuel and inhibit the pyrolytic carbon deposition. The use of these compounds at lower temperatures was also of interest to observe their effects on oxidative deposition. In addition, the effects of a dispersant additive, Betz SPEC-AID 8Q405, used to eliminate thermal oxidative deposition were examined in the Norpar under pyrolytic deposition conditions. The goal of the current work was to observe both the cracking behavior of Norpar-13 and observe mitigation effects of the thermal stabilizers on the carbon deposition in a flow reactor environment.

Experimental

The flow reactor apparatus consisted mainly of a fuel tank and a single tube running through a Lindbergh laboratory furnace with a 91.5 cm actively heated zone. A schematic of the flow reactor is shown in Figure 1. The temperature profile of the fuel through the heated flow-tube section, as calculated by a NIST Supertrapp program (7), is also plotted in Figure 1. The fuel was pumped through the system with a SSI high pressure liquid chromatography pump, and the system pressure was regulated by a back pressure valve. Liquid and gas products were sampled through a three-way valve downstream of the back pressure valve. Tube wall temperatures were determined by type K thermocouples spot welded to the outside of the tube, and a thermocouple was inserted at the end tube section to determine the final fuel temperature. The fuel in the tank could be sparged with either air or nitrogen (70 ppm O_2 (w/w) in air saturated fuel (0.0018 molar)), and the system was sparged with nitrogen prior to each test. Further information of the experimental set up has been reported by Edwards (8).

The tube section used in each test was 122 cm long, 6.4 mm OD, 4.7 mm ID, stainless steel 304. The tube was rinsed prior to testing with acetone to remove any hydrocarbon residue. The Norpar also passed through a 0.45 μm filter before reaching the test section to remove any particulates. The flow rate was 12 mL/min with a system pressure through the tube of 5 MPa. These conditions create linear flow through the tube with the Norpar reaching supercritical conditions at the end of the 122 cm tube. Each test was run for 5 hours at a final fuel temperature of 550°C which corresponded to a maximum wall temperature (Tw) from 600°C to 620°C. The thermal stabilizers benzyl alcohol and tetralin were acquired from Aldrich at 99+% purity. The tetrahydroquinoline was acquired from TCI America at 95+% purity. The Betz dispersant is a proprietary additive. The thermal stabilizers were added to the Norpar at 2.0 wt%, and the Betz dispersant at 125 mg/L in the fuel tank without further purification. Norpar-13 is made up of 0.2 wt% undecane, 14.4% dodecane, 52.9% tridecane, 32.0% tetradecane, and 0.5% pentadecane.

After each test, the stainless steel tube was cut into 5 cm sections, washed with hexane, vacuum dried at 120°C for 2 hours, and analyzed by carbon burnoff (Leco surface carbon analyzer) to measure the carbon deposition. At the three-way valve both liquid and gas products were sampled and analyzed off-line. The gas formation (cracking) of the Norpar-13 was calculated as the volume percent of the liquid that was cracked into gases (C_1–C_6) and was determined by measuring the fuel flow before and after heating. The liquid products were analyzed by gas chromatography/mass spectrometry (GC/MS) on a Hewlett Packard 5890 series GC/MS with a HP Ultra 1 Crosslinked Methyl Silicone Gum column. Gas samples were analyzed using a gas chromatograph with a flame ionization detector (GC FID) on a Hewlett

Packard 5890 series GC and a J & W Scientific GS-Q column. Oxidative studies were conducted in a quartz crystal microbalance system (9). The tests were conducted with 60 mL of Jet A fuel with 500 ppm of the thermal stabilizers stressed in a 100 mL Parr bomb reactor. The fuel was stressed for 15 hours at 140°C. The quartz crystal was resonated at 5 MHz within the fuel. At constant temperature, deposit formation on the crystal will cause a change in frequency which can be used to measure the amount of carbon deposited over time (9).

Results and Discussion

Norpar-13 was observed to crack into a series of smaller alkanes and alkenes a shown in the sample chromatogram, Figure 2. Larger amounts of unsaturates to saturates were formed in the smaller chains (C_6–C_{11}). Under nitrogen saturation conditions, larger alkenes along with methylcyclohexanes were formed. These results are similar to results of the pyrolysis of large *n*-alkanes shown by Hazlett (10).

The distribution of compounds, in volume percent, found in the gaseous products of Norpar stressed under both nitrogen- and air-saturation conditions are plotted in Figure 3. A total of 12 volume percent of the Norpar cracked to gas. The three largest components found in the gas were ethane, propylene, and propane. The largest species under air-saturation conditions was ethane, while under nitrogen-saturation conditions propylene became the largest volume fraction. The ratio of saturates, alkanes, (including methane) to unsaturates, alkenes, in the gas products were also calculated. Air-saturated conditions had products with a saturates to unsaturates ratio of 1.35, and under nitrogen-saturation conditions the amount of unsaturates increased, lowering the ratio to 1.11. The increased amount of unsaturates under nitrogen conditions may be an indication that a larger amount of catalytic decomposition was occurring. Increased pyrolytic deposition was observed in the nitrogen-saturation test. Large amounts of unsaturated gasses have been observed to show increased deposition in the case of ethylene steam cracking (11).

The deposition profiles of tests run with Norpar-13 under both air- and nitrogen-saturation conditions are plotted along with the results from a test using a Jet A 3084 fuel in Figure 4. The wall temperatures along the tube for each test are also given in Figure 4. Under nitrogen conditions the Norpar will show twice the amount, 14,000 µg, of pyrolytic deposits (maximum deposit found in a 5 cm section) than under air-saturation conditions. Pyrolytic deposits are also found earlier in the tube section at lower wall and fuel temperatures under nitrogen conditions. Norpar-13 does remain stable at the oxidative regime. This oxidative deposit regime can be observed along the tube from the 25–45 cm where the fuel temperature reaches temperatures above 150°C. The Jet A 3084 fuel shows an oxidative deposit peak in this regime and deposits an equal amount in the pyrolytic regime. Jet A fuel deposits much less than

Norpar-13 under pyrolytic conditions with a deposit peak of only 1000 µg. Jet A fuel contains many species which are more thermally stable than long-chain alkanes at temperatures greater than 400°C and contains other species such as hydrogen donors to further help increase the stability over that of Norpar-13.

Thermal Stabilizers . The effects of the high temperature thermal stabilizers, tetralin, THQ, and BzOH, on the deposition profile of Norpar-13 under air-saturation conditions are shown in Figure 5. All three stabilizers were found to reduce the pyrolytic deposits in the tube. Tetralin showed the least effect on deposition and THQ reduced the pyrolytic peak the most, to below 800 µg. The THQ added to the Norpar also created a significant oxidative deposit peak of over 1000 µg. The GC/MS analysis of liquid products from tests with thermal stabilizers added showed increased stability of the C_{12}–C_{15} from cracking to smaller-chain alkenes and alkanes. Also, higher numbered alkenes and methylcyclohexanes were not formed. The gas products showed a small reduction in unsaturated compounds, propylene and ethylene.

Batch reactor work with THQ added to dodecane has shown similar increased stability results (4,5). The transferable hydrogen still has enough time to stabilize thermal radical formation in Norpar in the short residence time of the flow reactor environment. Residence times are on the order of minutes to hours in the batch reactor tests while the flow reactor conditions used in these tests resulted in residence times under a minute. Greater than 90 wt% of the THQ in the Norpar remained after stressing. Nitrogen-saturated Norpar behaved very differently with the thermal stabilizers in the flow reactor tests. Both THQ and tetralin showed no increased stabilization of the Norpar while BzOH continued to lower the amount of deposits. The GC/MS analysis continued to show increased stabilization effects on the long-chain alkanes.

The dispersant 8Q405, when added to Jet A 3084 fuel at 125 mg/L, eliminated the oxidative deposition as expected but doubled the pyrolytic deposition. QCM results were used to measure the effects of the high-temperature stabilizers at lower temperatures where autoxidation occurs. Both tetralin and benzyl alcohol were found to significantly reduce the amount of mass accumulated on the quartz crystal. Benzyl alcohol also increased the rate of oxygen consumption of the fuel. Tetrahydroquinoline increased the amount of deposit accumulated on the quartz crystal. This increased deposition in THQ corresponds with the result observed in the flow reactor tests. A flow reactor test was run with both THQ and 8Q405 added to Norpar-13, but significant oxidative and pyrolytic deposits were still detected.

Summary

Norpar-13 was found to be a useful model solvent in observing the effects of high temperature stressing of jet fuels. Norpar was both stable in the oxidative regime and increased

the amount of pyrolytic deposition detected. The increased pyrolytic deposits made observing the mitigation effects of the additives easier than in a jet fuel. The effects of stabilizers on the liquid products could be determined and results could be related to prior work done with single model compounds such as dodecane and tetradecane.

Tetrahydroquinoline, benzyl alcohol, and tetralin all increased the thermal stability of Norpar-13 under flow reactor conditions. THQ was observed to increase the pyrolytic stability the most, as was seen in batch reactor tests. However, an adverse oxidative deposit formed from the addition of THQ. Nitrogen-saturating the Norpar-13 will cause increase deposits and eliminate the benefits from THQ and tetralin. Species formed by air in the Norpar, oxygen functionalities formed by the addition of BzOH and components within jet fuel may all contribute to increasing the pyrolytic stability.

References

1) Song, C., Lai, W., Schobert, H. H., I & EC Research, 33, 534 (1994).
2) Song, C., Lai, W., Schobert, H. H., I & EC Research, 33, 548 (1994).
3) Selvaraj, L., Sobkowiak, M., Song, C., Stallman, J. B., and Coleman, M. M., Energy & Fuels, 8, 839 (1994).
4) Yoon, E., Selvaraj, L., Song, C., Stallman, J. B., and Coleman, M. M., Energy & Fuels, Submitted.
5) Yoon, E., Selvaraj, L., Eser, S., and Coleman, M. M., Energy & Fuels, Submitted.
6) Song, C., Eser, S., Schobert, H.H., and Hatcher, P. G., Energy & Fuels, 7, 234 (1993).
7) Ely, J. F., and Huber, M. L., NIST Standard Reference Database 4-NIST Thermophysical Properties of Hydrocarbon Mixtures, February 1990.
8) Edwards, T., PREPRINTS, Div. of Petrol. Chem., ACS, 39(1), 92 (1984).
9) Zabarnick, S., and Grinstead R. R., I & EC Research , 33, 2771 (1994).
10) Hazlett, R. N., Frontiers of Free Radical Chemistry, W. A. Pryor, Editor, Academic Press, New York, 1980, pp. 195-223.
11) Brown, D. E., Clark, J. T. K., Foster, A. I., McCarroll, J. J., and Sims, M.L., Coke Formation on Metal Surfaces, L. F. Albright and R. T. Baker, Editors, American Chemical Society, Washington, Symposium Series 202, 1989, pp. 23-44.

2. Thermal Decomposition of Norpar-13 under Supercritical Conditions (Contributed by Jian Yu and Semih Eser)

Introduction

We have previously reported the results from the thermal decomposition of pure normal alkanes, namely *n*-C_{10}, *n*-C_{12}, and *n*-C_{14}, under supercritical conditions [1,2]. It was found that the thermal decomposition of *n*-alkanes can be represented well by the first-order kinetics. Pressure has significant effects on the first-order rate constant and product distribution in the near-critical region. The major products are a series of *n*-alkanes and 1-alkenes. The relative yields of *n*-alkanes and 1-alkenes depend on the reaction conditions. The observed product distributions and changes in product composition with reaction conditions were explained by a modified free-radical mechanism.

In this work, the thermal decomposition of a mixture of *n*-alkanes, Norpar-13, was studied under supercritical conditions. The thermal stressing experiments were carried out at 425 °C in the glass tube reactor and at 450 °C in the tubing bomb reactor.

Results and Discussion

Norpar-13 is composed of *n*-C_{11} (0.43 wt%), *n*-C_{12} (12.59%), *n*-C_{13} (50.80%), *n*-C_{14} (35.71%), *n*-C_{15} (0.41%), and small amount of impurities. In the following discussion, the overall conversion of Norpar-13 was calculated using eq 1

$$x = (y_{12}^{\circ} \times x_{12} + y_{13}^{\circ} \times x_{13} + y_{14}^{\circ} \times x_{13}) / (y_{12}^{\circ} + y_{13}^{\circ} + y_{14}^{\circ}) \qquad (1)$$

where y_{12}°, y_{13}°, and y_{14}° are molar fractions of *n*-C_{12}, *n*-C_{13}, and *n*-C_{14} in Norpar-13 and x_{12}, x_{13} and x_{14} are apparent individual conversions for *n*-C_{12}, *n*-C_{13}, and *n*-C_{14}, respectively.

Figure 6 shows the changes in conversions of individual compounds with loading ratio from the thermal decomposition of Norpar-13 at 425 °C for 15 min. Also included is the change in overall conversion with loading ratio. As loading ratio increases, the conversion of *n*-C_{12} decreases while the conversion of *n*-C_{14} first increases and then decreases. The conversion of *n*-C_{13} remains almost unchanged before 0.25 loading ratio and then decreases with loading ratio. The compound with longer chain has higher conversion in the mixture. It seems that individual compounds interact with each other in the mixture thermal reaction. While the conversions for the thermal decomposition of *n*-C_{12} in Norpar-13 are similar to those for the decomposition of pure *n*-C_{12}, the conversions of *n*-C_{14} are decreased from about 10–12%, depending on loading ratio, in the thermal decomposition of pure compound at 425 °C for 15 min to 6–7% in the thermal reaction of Norpar-13 at similar conditions, indicating significant

inhibition of the heavier alkane by the lighter alkane. Figures 6 and 7 show the changes in conversions of *n*-C_{12} and *n*-C_{14} with reaction time from the thermal decomposition of the pure compound and Norpar-13. Also included are the results from the thermal reactions of a petroleum-derived jet fuel, JP-8P. It can be seen that the conversions for the thermal decomposition of *n*-C_{14} in Norpar-13 are lower than those obtained for the decomposition of pure *n*-C_{14}. The real conversions for the decomposition of *n*-C_{12} in Norpar-13 should be higher than those shown in Figure 6 because some portions of remainder *n*-C_{12} after reaction result from decomposition of *n*-C_{13} and *n*-C_{14}. Since the initial amount of *n*-C_{12} in Norpar-13 is only about 13% while the total amount of *n*-C_{13} and *n*-C_{14} are above 86%, the amount of *n*-C_{12} from the decomposition of *n*-C_{13} and *n*-C_{14} may be significant. In other words, the real conversions for the decomposition of *n*-C_{12} in Norpar-13 could be larger than those obtained for the decomposition of pure *n*-C_{12}.

From Figures 7 and 8 one can also see that the conversions for the thermal decomposition of *n*-C_{12} and *n*-C_{14} in JP-8P are much lower than those obtained for the decomposition of pure compounds. This is because JP-8P contains significant amounts of cycloalkanes and aromatics which inhibit the decomposition of *n*-alkanes.

Figures 9 and 10 show the changes in molar yields of C_6-C_{10} *n*-alkanes and 1-alkenes with reaction time from the thermal decomposition of Norpar-13 at 425 °C for two different loading ratios. The product yields are expressed as the number of moles based on 100 moles of the feed converted. It can be seen that the product yield decreases as chain length increases. While the yields of *n*-alkanes slightly increase, those of 1-alkenes decrease with increased reaction time. The reaction with the higher loading ratio gives higher *n*-alkane yields and lower 1-alkene yields than that with the lower loading ratio, indicating the increased rates of hydrogen abstraction and radical addition reactions with increased loading ratio.

Figures 11 and 12 show the changes in product yields with reaction time from the thermal decomposition of Norpar-13 at 450 °C in the tubing bomb reactor for two different loading ratios. The molar yields of both C_7-C_{10} *n*-alkanes and 1-alkenes decrease with increased reaction time, indicating significant secondary reactions at higher temperature and longer reaction time. Among the gaseous products, the yields of hydrogen, methane, ethane, and propane increase while the yields of ethylene and propylene decrease as reaction time increases. The yields of benzene, toluene, *m*-xylene and *o*-xylene (BTX) steadily increase with increased reaction time. The comparison of the product distributions from two different loading ratios reveals that the higher loading ratio gives higher yields of *n*-alkanes, lower yields of 1-alkene, BTX and gases. This is because the bimolecular reactions, such as hydrogen abstraction and radical addition, are favored over radical decomposition reactions at high loading ratio (high pressure). The increased hydrogen abstraction rate will increase the formation of *n*-alkanes and

the increased radical addition rate will suppress the production of 1-alkenes. Also, the depressed radical decomposition rate would result in lower gaseous yields at higher loading ratio. Since the monoaromatics, such as BTX, are produced from the reactions of 1-alkenes, their yields would be lower at higher loading ratio because of lower 1-alkene yields. Because the monoaromatics will undergo further reactions to form polyaromatics, which are the precursors for the deposit formation, one will expect that the deposit formed at higher loading ratio would be lower than that formed at lower loading ratio. This is the case. For example, the amounts of the deposits from the thermal decomposition of Norpar-13 at 450 ℃ for 5 h are 2.4%, 2.0% and 1.4% of the feeds for the three different loading ratios, 0.14, 0.25, and 0.36 respectively.

References

1. Schobert, H. H.; Eser, S.; Song, C.; Hatcher, P. G.; Boehman, A.; Coleman, M. M. *Advanced Thermally Stable Jet Fuels.* Technical Progress Report (January 1995 - March 1995), June 1995, The Pennsylvania State University.

2. Schobert, H. H.; Eser, S.; Boehman, A.; Song, C.; Hatcher, P. G.; Coleman, M. M. *Advanced Thermally Stable Jet Fuels.* Technical Progress Report (April 1995 - June 1995), August 1995, The Pennsylvania State University.

Task 2 Investigation of Incipient Deposition

Deposit Growth During Heating of Coal-Derived Aviation Gas Turbine Fuels (Contributed by Prashant C. Sanghani and Andre L. Boehman)

Abstract

The kinetics of coke formation from coal-derived jet fuel were studied using statistical methods. The degree of correlation between deposit (coke) growth and species concentration has been examined. Formation of deposits from the mixtures of jet fuel and tetradecane was proportional to the initial concentration of tetradecane present in the fuel. Decomposition of tetradecane was found to be first order with correlation coefficient of 0.98. Other normal alkanes species, such as dodecane, tridecane, and pentadecane, which are present in very small amount also contribute significantly to deposit growth. Cycloalkanes, alkylated C_1, C_2, C_3 benzenes, and alkylated naphathalenes present in coal derived jet fuel were very stable compared to tetradecane. The statistical approach helps in identifying or arranging species in terms of their contribution to deposit formation. Grouping species on the basis of their correlation with deposit formation clarifies the required structure for a general kinetic model of the jet fuel degradation process.

Introduction

Currently jet fuel is used as the primary coolant to cool aircraft components during flight. In high-speed aircraft, cooling requirements have increased significantly and the fuel provides the only practical means of cooling. In future aircraft the fuel may reach temperatures as high as 700°C for a fraction of a second before its combustion [1]. A portion of the fuel also experiences a moderate heat flux for a long residence time [2]. Under such conditions, the fuel forms carbonaceous coke deposits which foul heat exchangers and reduce the flow through fuel injection nozzles. Coke particles also form in the bulk and can be carried to the turbine combustor creating performance problems. Because of the increasing thermal management needs in aircraft, there is an increasing need for development of a fundamental model for the prediction of the extent of coke formation in fuel lines.

Coke formation occurs by secondary reactions. In the case of coal-derived jet fuel there are 150 identifiable compounds. To simulate pyrolytic reactions and predict coke formation in terms of elementary reaction steps of individual compounds would require consideration of hundreds of reaction steps. The complexity of the network of reactions precludes a mechanistic modeling study on fuel pyrolysis and it will not be possible to develop rate equations in terms of elementary steps. Although some efforts have been made to model deposition in the autoxidation regime [3,8] the high-temperature pyrolytic domain of fuel decomposition has not

been considered. This paper describes a study of the deposition process for a coal-derived jet fuel, using statistical methods and quantitative chemical analysis to correlate deposition kinetics. Deposit formation correlations can be developed in terms of the concentrations of the reactive species. The base fuel in these experiments is JP-8C, to which a small amount of tetradecane was added as a reactive species. Experiments were conducted at 450 °C (723 K) for period of 2 to 12 hours. Pressures reached values in excess of 1400 psi after two hours and the reaction occurs in the supercritical phase.

Experimental

This study used a coal-derived jet fuel mixture consisting of 1.5g of tetradecane in 6.68g of neat JP-8C fuel. The mixture was then pyrolyzed at 450°C for a period of 2 to 12 hours in a tubing bomb reactor. Before reaction, the reactor was pressurized to 6.9 MPa with ultra high purity nitrogen and then purged to atmospheric pressure 7 times. This method of pressurizing and purging practically removed all oxygen from the reactor. The tubing bombs were then pressurized to 0.69 MPa with N_2 before pyrolysis. After the desired reaction time, the reactors were quenched in water at room temperature. The reactors were opened and products were collected separately and analyzed. In another set of experiments, tetradecane was mixed with JP-8C in different proportions starting from 0% to 100% tetradecane. These mixtures were also pyrolyzed under similar conditions for 6 hours.

About 3% *n*-decylcyclohexane was added to the pyrolyzed products as an internal standard for quantification. Compounds in the liquid products were identified by capillary gas chromatography-mass spectrometry (GC-MS). The column used for GC separation was a 30 m x 0.25 mm-i.d. fused silica capillary column (J&W DB-17). Mass spectrometric identification was confirmed by injecting sixty different compounds and comparing their spectra and retention time with the unknown compounds of liquid products of the pyrolyzed fuel. Compounds such as substituted decalins, tetralins, indans and cycloalkanes for which standards are not available were identified using knowledge of their fragmentation pattern. Quantification of liquid products was accomplished by using a Perkin Elmer 8500 capillary GC equipped with an FID and a DB-17 column. Those compounds which coelute in the GC were quantified using single ion monitoring in the mass spectrometer. Gaseous products were analyzed by a Perkin Elmer Auto System gas chromatograph equipped with FID and TCD detectors. The TCD column was used to separate ethane from ethylene. The FID used a Chemipack C18 column (6 ft x 1/8'' i.d.). The TCD used a 60/80 Carboxen 1000 column (15 ft x 1/8" i.d.).

The growth of coke in the bulk fuel was measured by first mixing the stressed fuel with 8 parts toluene and allowing it to stand in the dark for 10–12 hours at room temperature. This mixture was then filtered through 0.1 μ filter paper. The filter paper was then dried in vacuum

for a few hours. The amount of toluene insoluble (T.I.) deposit that remained on the filter was determined by weighing the filter after drying. Toluene was removed from the filtrate by a rotary evaporator. The filtrate was then mixed with 100 parts *n*-pentane and was allowed to stand in the dark for 10 hours. This solution of pentane and filtrate was then filtered through 0.1μ filter paper. The mass of pentane insoluble that remained on the filter paper was reported as toluene soluble and pentane insolubles (T.S.-P.I).

Results and Discussion

Deposits can form by surface reactions on the reactor walls as well as by homogeneous reactions occurring in the bulk [3]. Deposits formed on the reactor walls were found to be insoluble in solvents like toluene and THF. No toluene-insolubles were found in the stressed fuel. However, small but measurable amounts of pentane insoluble and toluene soluble compounds were found in the stressed liquid product. Figure 13 shows the amount of deposits formed on the wall (which is toluene insoluble, i.e. T.I.) and the amounts of toluene soluble-pentane insoluble (T.S-P.I.) formed in the bulk. It can be seen that solid growth occurs directly on the wall rather than through a homogeneous nucleation such as occurs during soot formation. Thus, as soon as the reactive species form they go to the wall and react with deposit mass present there. This does not mean than deposit formation is a heterogeneous process. Stainless steel surfaces (SS 316) remain inert during pyrolysis [4]. However, when Ni and Cu are present, these surfaces do catalyze deposit formation [5]. Instead, the initial layer of deposit on the wall acts as a sink for reactive species.

The next step in the experimental procedure was to identify the reactive species or the compounds which can furnish such reactive species during pyrolysis. Coal-derived fuel contains at least 150 identifiable compounds and we might suspect that each of these can contribute more or less to deposit formation. To resolve which species are involved one can rely upon a number of model compound studies that have elucidated the degree to which many of these compounds contribute to deposit formation [6]. During these model compound studies, tetradecane, dodecane, and *n*-butylbenzene were found to produce the maximum amount of solids during pyrolysis at 450°C for 4 hours. Neat coal-derived jet fuel was found to produce deposits only after 8 hours of stressing. Because tetradecane was found to produce more solids we concluded that tetradecane will act as a reactive species during coke formation in a complex mixture such as jet fuel. Results of deposit formation for a particular, initial concentration of tetradecane added to the neat jet fuel are shown in Figure 14. Deposit mass has been expressed as the mass fraction of solid produced. The correlation coefficient between the amount of deposit produced and initial weight percent tetradecane present in the mixture was found to be 0.987. Thus, deposit formation is directly proportional to the concentration of tetradecane

present in the fuel. Mixtures of 18% tetradecane in neat JP-8C were pyrolyzed at 450°C for different time periods. The natural logarithm of concentration of the tetradecane remaining in the mixture at a specific time is plotted in Figure 15. The correlation coefficient for tetradecane decomposition versus time was found to be 0.98 and therefore, tetradecane decomposition is first-order under these conditions. First-order decomposition of tetradecane has been reported by other workers as well [7].

The highly correlated relationship between initial tetradecane concentration and deposition of solids motivates an examination of other compounds in the fuel and stressed fuel products from a statistical viewpoint. The concentration of compounds such as hexane, heptane, octane, nonane, decane, undecane, dodecane, tridecane, cyclohexane, methyl- cyclohexane, ethylcyclohexane, propylcyclohexane, benzene, toluene, xylenes, ethylbenzene, ethylmethylcyclohexanes, dimethylcyclohexanes, tetralin, decalin, C_1-tetralin, C_2-tetralin, C_1-decalins, C_2-decalins, naphathalene, C_1-naphathalenes, C_2-naphathalenes, measured at various time intervals is shown in Figures 16-21. What follows is a determination of the role these compounds play in the stressed fuel during pyrolysis, based on observations of the time history of their concentration. We are looking for the degree to which concentration correlates with deposit mass over time.

The concentration of toluene, xylenes, ethyl benzene, naphathalenes and substituted naphathalenes increased with reaction time. These compounds therefore are primary products of the fuel decomposition reactions. Because their concentration increases with time these compounds are very stable and do not contribute to deposit formation. In the figure xylenes and ethylbenzene are lumped together as one compound because of difficulty in quantifying separately since they have very similar mass spectra.

The concentration of methylcyclopentane steadily increases with time. It has been shown previously [7] that methylcyclopentane forms from cyclization reactions of radicals formed from tetradecane, tridecane and dodecane. Since this compound shows a continuous increase, we conclude that it does not contribute to solid formation either. Cyclohexane concentration remains constant for 6 hours and then decreases slightly. Since a rich radical pool exists because of the decomposition of tetradecane and other long-chain alkanes, these radicals can abstract hydrogen from cyclohexane. These reactions should proceed very slowly because of instability associated with formation of the cyclohexyl radical. Since cyclohexane concentration remains constant for considerable time, it will not form any reactive species that lead to coke formation. The concentration of compounds such as ethylcyclohexane, propyl- cyclohexane, methylethylcyclohexanes decreases slowly but steadily with time. These compounds will form substituted aromatics such as xylenes, ethylbenzenes, and dimethylethyl- benzenes by dehydrogenation, which is possible under supercritical conditions. Correlation among

ethylcyclohexane, propylcyclohexane, methylethylcyclohexanes, xylenes, ethyl- benzenes, and dimethylethylbenzenes needs to be established. Since the concentration of compounds such as ethylcyclohexane, propylcyclohexane, methylethylcyclohexanes decreases slowly and they will preferentially undergo dehydrogenation, they will not contribute to solid formation. Methylcyclohexane concentration remained constant for 9 hours and then it decreased slightly, showing that it does not contribute to solid formation either.

The concentration of tetralin, decalin, C_1-decalins, C_2-decalins, C_1-tetralins, and C_2-tetralins, decreases steadily with time. It has already been shown by Song et al. that compounds such as tetralin and decalin function as hydrogen donors and that they inhibit deposit formation [9]. These two compounds are converted to naphathalene, which is thermally stable. Substituted tetralins and decalins will be converted to substituted naphathalenes and are therefore less likely to form reactive species. The concentration of indan, C_1-indans, C_2-indans decreases slightly. These compounds might be converted to naphathalene and C_1-naphathalenes, which should preclude them from forming deposits.

The concentration of dodecane, tridecane, and tetradecane has been plotted in Figure 18. Their concentration decreases continuously with time. We already have shown that the amount of solid formation is directly proportional to the initial concentration of tetradecane in JP-8C. It will also be proportional to dodecane and tridecane concentration. However, an attempt to model deposit growth based solely on tetradecane concentration failed to reproduce an observed induction period shown in Figure 21. During the induction period, tetradecane decomposes prior to significant deposit formation. Deposit selectivity calculated as the mass of coke produced divided by initial mass of tetradecane present, is plotted against the conversion of tetradecane in Figure 23. From this curve it is evident that a measurable amount (> 4 mg) of deposit appears only after 63% conversion of tetradecane. This means that either the reactive species formed from tetradecane will form more reactive radicals or the generation of radicals from tetradecane is a very slow process.

The concentration of normal hexane, heptane, octane, nonane, decane, and undecane increases from 0 to 4 hours and then it starts to decrease. In the individual model compound studies, the coking tendency was found to decrease with a decrease in carbon number. Therefore hexane, heptane and octane might not contribute to solid formation. Only nonane, decane, and undecane will contribute to solid formation among the normal alkanes from hexane to undecane.

Conclusion

Deposit formation occurs by the addition of reactive species to the initial deposit layer formed on the reactor wall. Homogeneous processes occurring in the bulk form reactive species

but nucleation of coke particles does not occur at 723K under supercritical conditions. Compounds such as cycloalkanes, xylenes, toluene, benzene, are stable compounds and do not contribute to the formation of solid deposits. Compounds such as indan and C_1- and C_2-indans are very stable and do not trigger formation of radicals that can add to the already growing layer of deposits. However, radicals formed from tetradecane and other comparable alkanes can abstract hydrogen from these stable compounds, thereby forming reactive radicals. Yet, it may not be possible for radicals generated from indans and cycloalkanes to add to deposits on the reactor wall due to steric factors or some other reason not known at present.

From these quantitative analyses of jet fuel pyrolysis, it is possible to develop a statistical correlation between conversion of alkanes to cycloalkanes and solid deposits. During this conversion process compounds such as dodecane and tetradecane form reactive radicals whose nature needs to be determined. Though deposit formation is proportional to the initial concentration of tetradecane, the direct correlation between deposit mass and tetradecane conversion is very poor. However, using an appropriate functional form that incorporates the induction period for deposition may lead to an improved correlation between these observations. With an appropriate description of the induction process and further statistical analysis, it should be possible to develop a rate expression for deposit formation in terms of the concentration of reactive compounds such as tetradecane, dodecane, tridecane, undecane, butyl benzenes and substituted higher benzenes.

References

1. Edwards, T., U.S. Air Force Wright Laboratory, WPAFB, Personal communication, October 1995.
2. Roquemore, W. M., Pearce, J.A., Harrison III, W.E., Krazinski, J.L., Vanka, S.P., *Prepr.- Am. Chem. Soc., Div. Pet. Chem.* 1989, 34 (4), 841-849.
3. Krazinski, J. L., Vanka, S. P., December 1989, Final Report WRDC-TR-89-2139.
4. Eser, S., Pennsylvania State University, Fuel Science Program, Personal Communication 1995.
5. Li, J., Eser, S., in Extended Abstracts. 21st Biennial Conference on Carbon, p.527 American Carbon Society (1993.)
6. Eser, S., Song, C., Schobert, H. H., Hatcher P. G., Technical Progress Report WL-TR-90-2117.
7. Song, C., Lai, W., Schobert, H. H., I & EC Research 1994, 33, 534-547.
8. Zabarnick, S. Ind. Eng. Chem. Res. 1993, 32, 1012-1017.
9. Song, C., Lai, W., Schobert, H. H., I & EC Research 1994, 33, 548-557.

Task 3. Characterization of Solid Gums, Sediments, and Carbonaceous Deposits.

1. Surface Effects on Deposit Formation in a Flow Reactor System (Contributed by Jun Li and Semih Eser)

Introduction

We have reported some results regarding metal surface effects on deposit formation from thermal stressing of jet fuel (JP-8P) in our flow reactor [1]. More experiments have been conducted in the flow reactor using Norpar 13 (a mixture of C_{12} - C_{15} *n*-alkanes) to study the metal surface effects on deposit formation. The combination of an on-line GC capillary column with a FID and a packed column with a TCD enables a complete account of the reaction products distribution. The liquid products collected from the gas/liquid separator of the reactor system were analyzed with a UV-VIS spectrophotometer. Deposits collected from the reactor (walls) and foils were analyzed by polarized-light microscopy (PLM), SEM, and TEM.

Experimental

The flow reactor used in this study has been described in a previous report [1]. Reactant used in the experiments was Norpar 13, a mixture of C_{11}-C_{15} *n*-alkanes (0.32%wt *n*-C_{11}, 11.3%wt *n*-C_{12}, 49.51%wt *n*-C_{13}, 38.47%wt *n*-C_{14}, and 0.39%wt *n*-C_{15}). Liquid reactants were pumped into the reactor system at a flow rate of 2 mL/min. UHP N_2 was also fed to the reactor with Norpar 13 during the reaction (N_2 was used before the reaction to purge and stabilize the reactor system). The effects of temperature, pressure, and the metal surface on the pyrolysis of Norpar 13 and on deposit formation were studied. Parameters studied included temperatures from 500 to 600 °C, pressures from 0 to 1000 psig., and with/without the insertion of nickel coupons. Space time was approximately 25 seconds when studying the effects of temperature, and 5–50 seconds when studying the effects of pressure. The reaction products were analyzed by the on-line GCs. Liquid products collected from the gas/liquid separator were diluted with hexane and analyzed by an AVIV Spectrophotometer (Model 118 OS UV-VIS). Deposits collected from the reactor walls as well as on the foils were analyzed by an ISI ABT SX-40A scanning electron microscope (SEM), a JEOL JSM6300F Field Emission SEM, and a transmission electron microscope (TEM). The optical texture of the deposits was examined in a Nikon Microphot FXA-II polarized-light microscope. The coupons were embedded in a Spurr (Polysciences, PA) low-viscosity epoxy.

Results and Discussion

Response Factors The response factors for different compounds eluting from a capillary column with FID depend on the column used and the operation conditions. Using a standard mixture containing C_6–C_{16} normal alkanes, the response factor for each of alkane was determined. It is noted that the differences between the response factors for different alkanes cannot be ignored under the typical GC conditions used (GC temperature program, carrier gas pressure, FID cell temperature, Air/H_2 ratio). In addition, it is noted that due to the vaporization of the light alkanes (C_6 and C_7), the response factors for hexane and heptane can be determined more accurately by extrapolation than those obtained by direct measurement. Therefore, the response factors for pentane, hexane, and heptane were calculated from the extrapolated data. The response factors for 1-alkenes are assumed to be the same as those of *n*-alkanes with the same carbon number. These response factors are listed in Table 1.

For the packed column with a TCD, it is claimed [2] that the relative response factor (determined using benzene as an internal standard and helium as a carrier) appears to be independent of the experimental parameters. Relative response factors that are used in this analysis are also compiled in Table 1.

Since the reaction products are mostly kept in vapor state during the reaction before sending to the GC columns, TCD and FID are actually analyzing the same compositions of reaction products. The TCD and FID data are correlated using pentene as a reference component and then normalized. It is later confirmed that the errors of the quantitative analyses are within 10 %.

Gas Phase Analysis. Basically four sets of experiments have been conducted: (1) temperature effects (500, 525, 550, 575, 600 °C) without the presence of nickel coupons; (2) pressure effects (0, 250, 500, 750, 1000 psig.) without the presence of nickel coupons; (3) temperature effects (500, 525, 550, 575 °C) with the presence of nickel coupons; and (4) pressure effects (0, 500, 1000 psig.) with the presence of nickel coupons. A typical GC chromatogram (Norpar 13, 550°C, 500 psig., no metal coupons, 25 second space time, 1 hour run) of the reaction products is shown in Figure 23. Figure 24 shows that the packed column with TCD can separate C_1–C_6 *n*-alkanes and 1-alkenes well. Reaction products include C_1–C_{15} *n*-alkanes and C_2–C_{11} 1-alkenes. Very small amounts of heavier components (>C_{15}) can be detected. The amounts of possible aromatic products are also too small to be detected by the on-line GC.

The complete products distribution (ignoring the small amounts of branched alkanes and alkene isomers, total of less than 2 % at the highest level) is shown in Tables 2–5. These products distribution are consistent with those expected from the well-known radical reaction mechanisms and the effects of temperature and pressure. Tables 2 and 4 show that high temperature favors β-scission reactions, leading to higher 1-alkenes and ethylene and lower *n*-

alkane yields. For example, from Table 2, at 600° and 500 psig., the ethylene yield is as high as 3.99 % (wt). The butene yield under the same conditions is 5.29 %, while butane is only 2.99 %. Tables 3 and 5 show that high pressures favor bimolecular hydrogen abstraction reactions and radical addition reactions, leading to a higher *n*-alkane yield and lower 1-alkene yield. For example, from Table 3, the ethylene yield is only 0.74 % (wt) at 550 °C and 1000 psig, while the ethane yield is 2.53 % (wt). A full description of the products distribution and mechanistic implications of the data will be presented later.

Liquid Phase Analysis. The liquid products collected from the gas /liquid separator are analyzed using GC, and GC/MS in order to identify the aromatic products. No aromatic peaks were detected due possibly to the very low concentration of these products. Since UV absorption is very sensitive to the aromatic compounds, a UV spectrophotometer was used to analyze the liquid products. Figures 25 and 26 show the UV absorbance spectra of the liquid products. It can be seen that aromatics are present (note the shoulder peaks at 254 nm and at about 238 nm) in the liquid products. The concentration is in the order of ppm (based on the comparison with a naphthalene standard). With or without the presence of nickel coupons, the concentration of the aromatic compounds appears to increase exponentially with the reaction temperature, but linearly with the reaction pressure. A preliminary HPLC analysis of the liquid products suggests that one-ring aromatics (benzene and alkylbenzenes) are the most abundant aromatic compounds.

Deposit Characterization. Consistently large amounts of carbon deposit (around 900 mg) are formed at 550 °C, under 500 psig for 5 hours. Figures 27 and 28 show the typical morphology of the deposit formed under these conditions. It can be seen that the deposit is predominately in two forms: filamentous carbon and segregated platelets. The mechanism of filamentous carbon formation is well known, but it is surprising that filaments are formed under the experimental conditions used in the flow reactor.

Similarly, the formation of a large amount of platelet carbon is not normally expected under the conditions used in our experiments. These platelets are quite different from those reported in the literature. They are much thicker than those formed on catalytic nickel surfaces [3-6]. It is therefore doubtful that the proposed dissolution-precipitation model [5] or surface diffusion model [6] can be used here to fully explain the platelet formation. TEM micrographs (Figures 29 and 30) show that these platelets are not attached to any metal particles (except in Figure 30a the platelet is entangled with filamentous carbon). The cracks at one side of these platelets look like they were caused by growth cones of pyrolytic carbon. Polarized-light optical microscopy reveals that these platelets are highly anisotropic, the entire block of the platelets is in either yellow or blue color (Figure 31). This indicates that the platelets are highly ordered, maybe in graphitic structure. These highly ordered carbon platelets may also be a form of

pyrolytic carbon. The existence of aromatics in the reaction products show that the formation of carbon by aromatization and polymerization is also a possible route. It is, therefore, plausible to suggest that the formation of these thick platelets takes place through a combination of catalytic initiation and pyrolytic growth processes.

Experiments also show that there is a narrow temperature window for the formation of large amounts of filamentous carbon and especially thick carbon platelets. At 525 °C and 575°C, no collectable amount of carbon deposits are formed in the reactor tube. Morphologies of deposits on nickel coupons are mostly filamentous.

References

1. H. H. Schobert, S. Eser, C. Song, P.G. Hatcher, A.Boehman, and M.M. Coleman, *Advanced Thermally Stable Jet Fuels*, Technical Progress Report, 92PC92104-TPR-10, 36-40, 1995
2. D. M. Rosie and E. F. Barry, *J. Chromatographic Sci.* **11**, 237-250, 1973
3. S. D. Robertson, *Carbon*, **8**, 365-374, 1970
4. T. Baird, *Fuel*, **63**, 1081-1099, 1984
5. F. J. Derbyshire, A. E. B. Presland, and D. L. Trimm, *Carbon*, **13**, 111-113, 1975
6. A. E. B. Presland and P. L. Walker Jr., *Carbon* ,**7**, 1-8, 1969

2. Nature of High Temperature Deposits from N-Alkanes in Flow Reactor Tubes (Contributed by Joseph V. Atria)

Introduction

Higher temperatures in jet engines are causing increased concerns for system fouling due to carbon deposits in heat exchangers, nozzles, and fuel lines. Current aircraft can heat the fuel to temperatures around 150°C, but future designs may cause the fuel to heat up to temperatures approaching 540°C prior to combustion (1). At 150°C, the carbon deposits which form are due to autoxidative reactions. At 540°C the fuel will begin to thermally break down under pyrolysis and form gas. This will lead to gas-phase or pyrolitic carbon deposits.

An Exxon solvent, Norpar-13, which consists of C_{12}–C_{15} normal alkanes, was used to help model the pyrolitic deposition of jet fuel in a single-tube flow reactor. Norpar-13 forms large amounts of pyrolytic deposits but will remain stable in the autoxidation regime. This stability of Norpar-13 allows it to be a good model mixture to observe the chemistry and deposit formation of jet fuels under pyrolytic conditions. Thermal stability of a fuel, as measured by deposit formation, can be increased different ways. Higher thermally stable components can be engineered into the jet fuel, additives can be added to the fuel to stabilize radicals formed by thermal stressing, or surface effects from the metal walls which can cause catalytic decomposition of the fuel at high temperatures can be mitigated. The goal of this work was to investigate the surface catalytic effects of stainless steel on the deposition behavior and deposit morphology of Norpar-13. The behavior of an inert fused silica coating called Silcosteel, from Restek Corporation, was also investigated. Experimentation with Silcosteel in the oxidative regime on thermally stressed jet fuels has recently been conducted (2). In addition, the morphology of the pyrolytic deposits were compared with oxidative deposits formed from a Jet A fuel.

Experimental

The flow reactor apparatus consisted mainly of a fuel tank and a single tube running through a Lindberg laboratory furnace with a 91.5 cm actively heated zone. The fuel was pumped through the system with a SSI high pressure liquid chromatography pump, and the system pressure was regulated by a back pressure valve. Liquid and gas products were sampled through a three-way valve downstream of the back-pressure valve. Tube wall temperatures were determined by type K thermocouples spot welded to the outside of the tube, and a thermocouple was inserted at the end tube section to measure the final fuel temperature. The fuel in the tank could be sparged with either air or nitrogen (70 ppm O_2 (w/w) in air saturated fuel (0.0018

molar)), and the system was sparged with nitrogen prior to each test. Further information and a schematic of the experimental set up have been reported by Edwards (3).

The stainless steel 304 tubes used in each test were 122 cm long, 6.4 mm OD, 4.7 mm ID and rinsed with acetone to remove any hydrocarbon residue prior to experimentation. The Norpar also passed through a 0.45 μm filter before reaching the test section to remove any particulates. The flow rate was 12 mL/min with a system pressure through the tube of 5 MPa. Each test was run for 5 hours at a final fuel temperature of 550°C which corresponded to a maximum wall temperature from 600°C to 620°C. These conditions create linear flow through the tube with the Norpar-13 reaching supercritical conditions in the pyrolytic regime at temperatures greater than 400°C. The gas formation (cracking) of Norpar-13 was calculated as the volume percent of the liquid that was converted to gas (C_1–C_6) and was determined by measuring the fuel flow before and after reaction through the tube.

The Norpar-13 obtained from Exxon was made up of 0.2 wt% undecane, 14.4% dodecane, 52.9% tridecane, 32.0% tetradecane, and 0.5% pentadecane. The Silcosteel from Restek consisted of a stainless steel 304 tube coated with a uniform fused silica layer. Silcosteel tubes with coating thickness of 450Å and 1000Å, with and without a deactivation layer consisting of phenyl and methyl groups, were used in experiments. Jet A 3084 jet fuel was used in obtaining oxidative deposits.

After each test, the stainless steel tube was cut into 5 cm sections, washed with hexane, vacuumed dried at 120°C for 2 hours, and analyzed by carbon burnoff (Leco surface carbon analyzer) to measure the carbon deposition. Some 5 cm sections were not analyzed by carbon burnoff but further cut by a wafer saw and analyzed in a field emission scanning electron microscope (JEOL JSM6300F) to observe the inner tube surface and carbon deposit morphology. The FESEM uses lower acceleration voltages (20 kV used in this work) as compared to a typical scanning electron microscope, SEM. Due to the low acceleration voltage, samples did not need to be gold coated and remained untouched, so that samples could be further tested in the future by other characterization techniques.

Results and Discussion

The Norpar-13 under nitrogen-saturation conditions was found to crack to 12 volume percent gas as compared to 6 volume percent gas formation for the Jet A 3084. Gas analysis also showed the Norpar-13 product gases to contain higher amounts of unsaturated species such as ethylene and propylene, as compared to Jet A gas products. The larger formation of gas and unsaturated species help explain the larger amount of pyrolitic deposits found in Norpar tests.

The carbon deposition profiles comparing deposits in a stainless steel tube to deposits in Silcosteel tubes are shown in Figure 32. The plot also contains the wall temperatures along the

tubes in each test. Experiments in the stainless steel tubes showed large amounts of pyrolytic deposits to a maximum amount of over 14,000 μg (for a 5 cm tube section). Significant deposits were still observed on the 450Å thick Silcosteel with a deactivation layer. However, the 450Å Silcosteel tube was also able to significantly reduce deposits to a maximum of 5,500 μg as compared to the stainless steel tube. Increasing the thickness of the fused silica layer to 1000Å and eliminating the deactivation layer reduces the deposits detected to below 800 μg.

Morphology of the Deposits. A FESEM micrograph of a typical pyrolytic deposit formed on stainless steel is shown in Figure 33. Large bundles of deposits can be seen rising up from the tube surface. Due to the increased resolution and sharpness of the FESEM over the SEM, these carbon bundles could be further enhanced, Figure 34. The bundles were observed to be made up thousands of long string-like deposits, filaments. The entire stainless steel surface in the pyrolytic regime was found to contain these filaments. The micrograph in Figure 35 further magnifies the structure of the filaments. A metallic particle can be seen at the tip of the filaments. Carbon filaments have been found to form in the steam cracking of ethane (4) and many researchers have begun to investigate the catalytic effects of metal particles in forming carbon filaments (5-7). A metal particle from the stainless tube surface is pitted away from the tube surface and catalyzes tubular carbon growth from the surface of the metal Both iron and nickel have been shown to greatly catalyze filament deposition (6,7). This catalytic deposition can lead to system fouling and weaken the strength of metal surfaces contacted by the fuel. This could be a serious problem for thin-walled heat exchangers.

After observing the catalytic filaments on the stainless steel tube, the benefit of using Silcosteel became apparent in creating an inert barrier between the metal surface and the stressed fuel. A FESEM micrograph of the deposits formed in the 450Å coated Silcosteel tube is presented in Figure 36. The coating seems to have restricted or delayed the formation of the carbon filaments. Filaments are just beginning to develop on the surface of the Silcosteel and no bundling of deposits were found. The 1000Å coated Silcosteel completely eliminated the formation of filaments.

A comparison between the morphology of the pyrolitic deposits from Norpar-13 and Jet A 3084 fuel was also conducted. A FESEM micrograph of the oxidative deposit from the jet fuel as deposited on a stainless steel tube is shown in Figure 37. These deposits had to be examined at a lower acceleration voltage of 5 kV due to charging effects. The charging effects encountered indicate the oxidative deposits have a different structure than the pyrolytic deposits. The oxidative deposits were made up of very small, less than 1 μm, bundles of condensed carbon. The oxidative deposits also seemed to be very amorphous as compared to the pyrolytic filament deposits.

Conclusions

Norpar-13 stressed above 450°C in stainless steel flow reactor tubes was found to create a large amount of catalytic filament deposits. The addition of a sufficiently thick fused silica coating in the Silcosteel reactor tubes created a barrier from the catalytic stainless steel surface, eliminating filament formation and greatly reducing the amount of pyrolytic deposits formed. Oxidative deposits from a Jet A fuel were found to be very different in morphology than the pyrolytic deposits from Norpar-13. The oxidative deposits were made up of submicron carbon bundles which seem to condense together.

Acknowledgments

I would like to acknowledge Dr. T. Edwards at Wright Labs for his assistance and expertise with the flow reactor experiments and the opportunity to work with Mr. W. Cermignani, from Penn State's Ceramic Science program, on the FESEM..

References

1) Edwards, T. and Atria, J. V., PREPRINTS, Div. of Petrol. Chem., ACS, 40(4), 649 (1995).

2) Jones, G. E., Balster, W. J., and Rubey, W. A., PREPRINTS, Div. of Petrol. Chem., ACS, 40(4), 655 (1995).

3) Edwards, T., PREPRINTS, Div. of Petrol. Chem., ACS, 39(1), 92 (1984).

4) Kim, M. S., Rodriguez, N. M., Baker, R. T. K., and Milks, D., PREPRINTS, Div. of Petrol. Chem., ACS, 40(4), 618 (1995).

5) Baker, R. T. K., Yates, D. J. C., and Dumesic, J. A., Coke Formation on Metal Surfaces, L. F. Albright and R. T. Baker, Editors, American Chemical Society, Washington, Symposium Series 202, 1989, pp. 1-22.

6) Park, C., Baker, R. T. K., and Rodriguez, N. M., PREPRINTS, Div. of Petrol. Chem., ACS, 40(4), 646 (1995).

7) Rodriguez, N. M., Kim, M. S., Fortin, F., Mochida, I., and Baker, R. T. K., PREPRINTS, Div. of Petrol. Chem., ACS, 40(4), 625 (1995).

Task 4. Coal-based Fuel Stabilization Studies

Towards the Design of Thermally Stable Jet Fuels at Both Moderate (<250°C) and High (>400°C) Temperatures. (Contributed by Michael M. Coleman, Leena Selvaraj and Maria Sobkowiak)

We have previously demonstrated that if certain hydrogen donors, the most effective being 1,2,3,4-tetrahydroquinoline (THQ), are blended into jet fuels (or similar hydrocarbon mixtures) they enhance thermal stability and retard the formation of carbonaceous solids at temperatures in the range of 400–500°C. The superior performance of THQ in the pyrolysis regime was determined to be predicated on a number of factors. First, THQ and its dominant reaction product, quinoline, are highly stable at 400–450°C and there are no substituents on the aromatic or aliphatic rings which can be cleaved at these temperatures to produce radicals and promote degradation. Secondly, THQ is an efficient radical scavenger at these temperatures. Initial hydrogen atom transfer to an aliphatic hydrocarbon radical is facile and the THQ radical formed after initial hydrogen abstraction is well stabilized by resonance through delocalization into the aromatic ring. Finally, the transfer of three more hydrogens to hydrocarbon radicals is also facile with excellent resonance stabilization at every step towards the formation of quinoline. Details of screening and kinetic studies have been presented in previous reports and are integrated in two recent papers[1,2].

Having successfully discovered compounds that act as thermal stabilizers for hydrocarbon mixtures at temperatures in excess of 400°C, we are now confronted with a number of questions, the answers to which have important ramifications in the design, formulation and development of commercially viable high temperature stable jet fuels. Such fuels must also be stable (both thermally and oxidatively) at storage and moderately elevated temperatures (from ambient to say 300°C) which is in the autoxidative regime. Will the high temperature (> 400°C) thermal stabilizers such as THQ, benzyl alcohol (BzOH) etc. also act as antioxidants at these lower temperatures? Even if THQ and BzOH are inherently poor antioxidants at the lower temperatures, will the relatively high concentration (≈1–10 mol% compared to <500 ppm for a classic antioxidant) of the hydrogen donor offset this drawback? This represents the next real challenge, because classic antioxidants like the sterically hindered phenolics that operate well in the autoxidation regime actually *promote* free radical reactions in the pyrolysis regime. In other words, the additive introduced to prevent degradation of the fuel in storage and at moderately elevated temperatures can adversely affect the efficacy of the additive put in to retard the formation of carbonaceous solids at high temperatures (>400°C).

We may also find solutions to these problems in a related field, that of vulcanization chemistry. In the vulcanization of diene elastomers accelerators (e.g. mercaptobenzothiazole, tetramethylthiuram disulfide, etc.) are used in conjunction with sulphur and other activators to produce the active crosslinking agent. In mixing the ingredients on a two-roll mill, premature vulcanization, or as it commonly called "scorch", is prevented by adding a "retarder" (often a sulphenamide). The retarder acts as a "sacrificial lamb", mopping up any active crosslinking agent until it is all consumed, thus delaying the onset of normal vulcanization. In a similar vein, one can envisage a jet fuel formulation that contains a relatively small amount (<500 ppm) of a classic antioxidant (e.g. a sterically hindered phenolic) and a relatively large amount (≈5%) of a high temperature stabilizer (e.g. THQ). The former should work well in the autoxidative regime, but as the temperature rises and approaches ≈400°C cleavage of the antioxidant side groups will occur and the free radicals formed need to be capped by hydrogen donation from the high temperature stabilizer. In effect, some of the THQ will be sacrificed to mop up the excess radicals formed by the cracking of the antioxidant at the higher temperatures.

Before we can test any of these ideas, we needed to develop a simple screening test, similar to the "tubing bomb" methodology used in our high temperature screening of thermal stabilizers at 400–500°C, that can be performed reproducibly in a reasonable time period at temperatures in the range of 200–300°C. The screening methodology employed at 400–500°C is not applicable at 200–300°C, because of the inordinately long time periods required to produce measurable changes. After several miscues, the following simple procedure was adopted which accelerates the oxidative degradation process. Samples of pure Dod (or Jet A-1 fuel) and mixtures containing 5 vol% of THQ or BzOH based on Dod (or Jet A-1) were prepared. Thermal stressing was performed at 250°C in 25mL type 316 stainless steel microreactors. The microreactor containing the sample was purged five times with UHP-grade N_2 at 1000 psi to minimize the presence of dissolved oxygen and finally pressurized with air at various specific pressures from 100 to 400 psi. The microreactor was then placed in a preheated oil bath at 250°C for 1h, followed by quenching into cold water. The liquid products were examined visually in terms of color and the absence or presence of oils or solids. The results for the Dod and Jet A-1 mixtures are summarized in Tables 6 and 7, respectively.

Let us first consider the preliminary results obtained from neat Dod and the Dod mixtures. As indicated in Table 6, no evidence of carbonaceous solid formation occurs in the samples of neat Dod thermally stressed at 250°C under air pressures up to 200 psi. There is some discoloration of the liquid at 150 and 200 psi, however. At 250 psi air a trace of

carbonaceous solids is observed and the liquid is yellow. At 300 and 400 psi air there are obvious amounts of carbonaceous solids present and the liquids are highly colored. In the Dod mixtures with THQ, there are no large amounts of carbonaceous solids formed up to pressures of 400 psi, but the liquids are colored throughout and there is evidence of a small amount of oily material in the samples subjected to the higher air pressures. At this stage, before further analysis of the products, it is reasonable to presume that THQ is reacting with oxygen and retarding the formation of carbonaceous solids. The Dod/BzOH mixtures were clear and contained no carbonaceous solids at 100 psi air, but at 200 psi and higher both the presence of oil and carbonaceous solids was apparent and the liquid was discolored. This is not an improvement over neat Dod.

The analogous results for the neat Jet A-1 and mixtures with THQ and BzOH are given in Table 7. In the case of the neat Jet A-1 fuel there is no evidence of carbonaceous solid formation occurs in the samples of neat Dod thermally stressed at 250°C under an air pressure of 100 psi, but there is some discoloration of the liquid. Above 100 psi air, however, carbonaceous solids are obvious and the liquids are highly colored. In the Jet A-1 fuel mixtures with both THQ and BzOH, there appears to be a significant improvement. While the liquids are highly colored, carbonaceous solid formation appears to be retarded *vis-à-vis* neat Jet A-1 fuel.

These preliminary results are encouraging and we intend to perform systematic experiments of the type described above at 250°C under an initial air pressure of 200 psi as a function of time. In this manner, we hope to be able to formulate a jet fuel that will have enhanced thermal stability in both the autoxidative and pyrolysis regimes.

References

1. *High Temperature Stabilizers For Jet Fuels And Similar Hydrocarbon Mixtures. 1. Comparative Studies Of Hydrogen Donors.* E. M. Yoon, L. Selvaraj, C. Song, J. B. Stallman and M. M. Coleman, *Energy & Fuels*, submitted.

2. *High Temperature Stabilizers For Jet Fuels And Similar Hydrocarbon Mixtures. 2. Kinetic Studies.* E. M. Yoon, L. Selvaraj, S. Eser and M. M. Coleman, *Energy & Fuels*, submitted.

Task 5. Exploratory Studies on the Direct Conversion of Coal to High-Quality Jet Fuels.

1. Exploratory Studies on the Possibility of Non-Radical Hydrogen Transfer under Low Temperature Liquefaction Conditions. (contributed by Shona Martin)

Introduction

In view of the economic constraints placed on current coal processing, attractive options for the future include reducing production temperature and H_2 consumption. To date, the exact role of much of the mineral matter in coals remains unclear [1-3]. Catalytic activity, mainly attributed to pyrite, is well documented [1,4]. Conversely, removal of naturally occurring anions such as Na^+, Ca^{2+} and K^+ has been shown to enhance liquefaction conversions [5]. In recent tests [6], a higher gas-phase H_2 consumption was observed in comparative non-catalytic runs, with raw and dried low rank coals at 350°C. Preliminary studies were subsequently conducted on a demineralized sample to examine the possibility that the reaction with H_2 may be mineral matter catalyzed, where it was observed that demineralization had no serious detrimental effect on liquefaction under low temperature conditions [7,8]. Indeed, in terms of liquid product distribution, tests conducted in the presence of 1-methylnaphthalene yielded the best results. It may be that elimination of such species allows for better access for gaseous H_2. Nevertheless, this raises questions as to possible hydrogenation mechanisms.

Experimental.

During the last reporting period, a further series of non-catalytic baseline tests were conducted at 300°C, again with Wyodak (DECS-8) coal. Again, experimental procedures were outlined previously [6].

Results and Discussion.

Table and Figures 38 and 39 summarize the product distribution for the tests completed at 300 and 350 °C, 1000 psi H_2, 30 min. In terms of total conversion (dmmf wt%), these complement those reported previously by Saini et al. [9]. However, product distributions, especially in the case where no solvent was present, show variation with previous results. Determination of liquid product distribution shows that the most significant changes occur in the presence of solvent, both H-donor and non-donor. Oil yield increases the most with the H-donor solvent, by *ca* 4 wt%, almost double that observed at 350°C; non-donor solvent affords little change, of the order 1.2 wt%. However, it must be noted that oils yields from both runs, i.e. in the presence of both solvents and under two temperatures, are comparable. Asphaltene

concentration increases by approximately 1.5 % in the presence of both tetralin and 1-methylnaphthalene; the corresponding increases are 5 wt% and 3.2 wt%, respectively, for the runs at 350°C. The yield of pre-asphaltenes (THF-sols) in the presence of both solvent systems decreases approximately 2 wt%. This in contrast to the results given previously, where, at 350°C, presence of 1-methylnaphthalene was shown to exert a favorable influence on conversion to preasphaltene. Therefore, as anticipated, relative to runs at 300°C, 350°C affords higher overall conversions and better liquid product distribution. This trend becomes more apparent when either an H-donor (tetralin) or non-donor (1-mn) solvent are used.

The FTIR spectra of the THF-extracted raw coal and the residues from the runs conducted at 350 °C are shown in Figures 40 to 43, where it was observed that under all conditions, i.e. in both the presence and absence of solvent, no marked changes were evident. The residue from this set of experiments is currently undergoing further analysis by Py-GC-MS, in an attempt to evaluate in more detail the fundamental differences in speciation resulting from non-catalytic treatment under different regimes.

Future Work.

For the next reporting period, the specific objects will be further demineralization of Wyodak (DECS-8) by successive HCl/HF treatments, followed by liquefaction in microautoclaves under low temperature conditions (300°C; 1000 psi H_2; 30 min) to detect changes induced by removal of specific minerals and evaluate the possible catalytic effect of such species. Additional analytical techniques, such as ICP-AAS, XRD, FTIR, NMR and Py-GC-MS, will lead to identification of the species contributing to possible low temperature mechanisms.

References:

1. Maldonado-Hodar, F.J., Rivera-Utrilla, J., Mastral-Lamarca, A.M., Ferro-Garcia, M.A. Fuel **74**(6), 818 (1995) and references therein.
2. Mochida, I., Yufu, A., Sakanishi, K., Korai, Y. Fuel **67**, 114 (1988)
3. Serio, M.A., Solomon, P.R., Kroo, E., Bassilakis, R., Malhotra, R., McMillen, D. Am. Chem. Soc., Div, Fuel Chem., Prep. **35**(1), 61 (1990)
4. Garcia, A.B., Schobert, H.H. Fuel **68**, 1613 (1989) and references therein.
5. Joseph, J.T., Forrai, T.R. Fuel **71**, 75 (1992)
6. S.C. Martin, H.H. Schobert Advanced Thermally Stable Jet Fuels, Technical Progress Report, 92PC92104-TPR-11, p74

7. S.C. Martin, H.H. Schobert Advanced Thermally Stable Jet Fuels, Technical Progress Report, 92PC92104-TPR-12, p35
8. S.C. Martin, H.H. Schobert Advanced Thermally Stable Jet Fuels, Technical Progress Report, 92PC92104-TPR-13, p22
9. Saini, A.J., Song, C., Schobert, H.H. Am. Chem. Soc., Div. Fuel Chem., Prep. **37**(3), 1235 (1992)

2. Conformational Isomerization of cis-Decahydronaphthalene over Zeolite Catalysts.
(Contributed by Wei-Chuan Lai and Chunshan Song)

Introduction

Commercial decalin (decahydronaphthalene, abbreviated as DeHN) solvents from industrial hydrogenation processes consist of almost equimolar mixtures of *cis*- and *trans*-DeHN. Although the physical properties of these two isomers are similar, their chemical reactivities are different. One example is their difference in thermal stability at high temperatures. We have previously shown that as jet fuel components, *trans*-DeHN is superior to *cis*-DeHN because the former is much more stable at high temperatures [1]. The excellent thermal stability at high temperatures is desirable for use as fuel for future high Mach aircraft [2]. It was reported in the literature that decalin may be one of the potential endothermic jet fuels that also serve as the primary heat sink to cool the hot surfaces and system components of aircraft [3-5]. In addition, *trans*-DeHN has the desirable ability of inhibiting the solid deposit formation from jet fuels and their components at high temperatures [6]. Although *cis*-DeHN also has some potential industrial applications, it is desirable to convert *cis*-DeHN to *trans*-DeHN for enhancing fuel stability at high temperatures.

Although there has been much research on cracking, hydrocracking and dehydrogenation of decalin at temperatures generally in excess of 673 K under elevated pressures [7-12]. Little information is available about the conformational isomerization of *cis*-DeHN into *trans*-DeHN at lower temperatures. Our earlier exploratory work [13-15] has shown that some zeolites can promote the isomerization of *cis*-DeHN into *trans*-DeHN, as shown in Scheme 1, at 523 K for 2 h under N_2 environment. This work is a continuation of our exploratory studies on the zeolite-catalyzed conformational isomerization of *cis*-DeHN into *trans*-DeHN. The objectives of this report are to examine the effects of catalyst type, reaction temperature, noble metals and gas atmosphere on the catalytic reaction, and to develop an overall kinetic model for the catalytic reaction and empirical equations to predict the product yields.

Experimental

1. Reactants and catalysts. The chemicals, *cis*-DeHN, *trans*-DeHN, and DeHN (an almost equimolar mixture of *cis*- and *trans*-DeHN) were obtained from Aldrich Chemical Company and were used as received. Their purities (>99%) were analyzed using gas chromatography (GC) and gas chromatography-mass spectrometry (GC-MS). The six catalysts used in the catalytic isomerization reactions include: a hydrogen Y zeolite (HY), a metal ion-exchanged Y zeolite (LaHY), a hydrogen mordenite (HM30A), and three noble metal loaded

mordenites (Pt/HM30A, Pd/HM30A, and Pt/HM20A). The Y zeolites (HY and LaHY) were prepared according to the procedures described elsewhere [16]. The HM30A mordenite was prepared by heat treatment of a commercial ammonium mordenite sample [17] and has a SiO_2 to Al_2O_3 mole ratio of 38. The noble metal loaded mordenites were prepared by dispersing the salt of platinum or palladium into the mordenites by incipient wetness impregnation method. The noble metal loading on the zeolites was kept at 6 wt%. The details of the preparation and properties of the catalysts are described elsewhere [14,18].

2. Reaction procedure and product analysis. Catalytic isomerization reactions were carried out in 28-mL horizontal type stainless steel tubing bomb reactors, which were generally charged with 1 g of *cis*-DeHN, *trans*-DeHN, or DeHN (7.23 mmol) and 0.2 g of catalyst, at 473–573 K for 0.15-8 h under an initial pressure of 0.79 MPa UHP N_2 or H_2. The reactor was agitated vertically at 240 cycles/min. After the reaction, the gas products were collected in a gas bag and were quantitatively analyzed using a Perkin-Elmer Autosystem GC equipped with two detectors, a thermal conductivity detector (TCD) and a flame ionization detector (FID). The liquid products were recovered by washing with acetone and were analyzed on an HP 5890II GC coupled with an HP 5971A Mass Selective Detector (MSD) and quantified by a Perkin-Elmer GC 8500 equipped with an FID. More analytical details may be found elsewhere [19].

Results and discussion

1. Effect of catalyst type and reaction conditions. Table 9 shows the products distribution from catalyzed isomerization of *cis*-DeHN over three catalysts (LaHY, HY, and HM30A) at 473-573 K for 0.5-8 h under an initial pressure of 0.79 MPa UHP N_2 or H_2 using 1-g commercial DeHN as reactant. The purity analysis of the starting material is also presented in Table 9. The as-received reactant contains about 48.3% of *trans*-DeHN, 50.6% of *cis*-DeHN, 0.7% of tetralin, and 0.34% of *n*-decane impurity. Figure 44 presents an expanded retention time window of three GC profiles for the liquid products over LaHY at 473, 523, and 573 K. The window covers DeHN and its major products.

No apparent reaction was observed when the experiment was carried out at 473 K for 2 h without a catalyst or with a LaHY catalyst. However, reactions proceed over LaHY when the temperature was raised to 523 K, as shown in Figure 43. Isomerization is the dominant reaction under the conditions employed. The major products from *cis*-DeHN are *trans*-DeHN (from conformational isomerization), which dominated at 523 K with higher selectivity (defined as the ratio of molar yield of the product to the conversion), and other products from ring-opening or ring-contraction isomerization, which prevailed at 573 K. Cracking products are, in general, of little significance and are not shown in Table 9. Trace amounts of hydrocarbon gases, mainly C_1-C_3 gases, were detected but their total yields were negligible. There was no apparent

dehydrogenation reaction from decalin to tetralin, judging from the gradually decreasing yield of tetralin, which initially existed as an impurity (0.7 wt%). It was experimentally observed in this work that LaHY at 573 K also enhances the isomerization of tetralin to form 1-methylindane, with a selectivity of about 0.3.

Table 9 shows that the hydrogen Y zeolite (HY) performed about as well as the metal ion-exchanged Y zeolite (LaHY), and the catalyst with the lowest acidity (HM30A) is the least effective one, displaying the lowest activity as well as selectivity to *trans*-DeHN, among the three catalysts. Reaction conditions at 548-573 K for 0.5 h seem too severe for the isomerization reaction of *cis*-DeHN to form *trans*-DeHN, judging from the low selectivity towards *trans*-DeHN. Enhanced competitive side reactions or secondary reactions including ring-opening, ring-contraction, and cracking reactions contributed to the low selectivity of *trans*-DeHN at severe conditions. Petrov et al. [20] reported the isomerization of *cis*- and *trans*-DeHN on a nickel catalyst in the temperature range of 393–453 K. They reported that the isomerization took place only in the presence of hydrogen. However, the present results clearly showed that the isomerization of *cis*-DeHN into *trans*-DeHN could occur over HY, LaHY, and HM30A even under N_2. It is also interesting to note that gas environment (N_2 or H_2) has no impact on the performance of LaHY as shown in Table 9.

2. Reaction pathways and kinetic data. We further investigated the performance of LaHY and HY, with an intention to obtain relevant kinetic data. These isomerization reactions were carried out using pure *cis*-DeHN instead of DeHN mixture, and 0.2 g of catalyst, at 508–548 K for 0.15–8 h under an initial pressure of 0.79 MPa UHP N_2. The experimental results are shown in Table 10. Figure 45 presents the *trans*-DeHN selectivity versus *cis*-DeHN conversion plots for LaHY and HY catalysts at four different temperatures.

There are several features that can be seen from examining Table 10 and Figure 45. First, HY performs slightly better than LaHY in terms of activity and selectivity. This observation for runs using pure *cis*-DeHN is slightly different from the trend observed for runs with commercial DeHN mixture, where the two catalysts performed equally well (Table 9). Second, selectivity towards *trans*-DeHN decreases with increasing temperature. This is not unexpected since the isomerization from *cis*-DeHN to *trans*-DeHN is exothermic, 13,212 J/mol (95 J/g or 3.16 kcal/mol) at 523 K (from thermodynamic calculation to be discussed later). Third, the product (*trans*-DeHN) selectivity decreases with increasing conversion level under isothermal condition, and displays a concave downward behavior, which could be empirically fitted by a second-degree polynomial as demonstrated later. The trend of selectivity versus conversion in Figure 45 provided useful information about the reaction pathways. It implied that the reactions proceeded through a parallel-consecutive network [21].

Based on the previous observations, a simple reaction pathway model for the catalytic reaction of *cis*-DeHN to products was proposed. The overall reaction is modeled as the parallel-consecutive kinetic scheme shown in Figure 46. The isomerization between *cis*- and *trans*-DeHN was known to be a reversible process; thus the inter conversion between them was also included in Figure 46. However, our experimental data using both *cis*- and *trans*-DeHN have shown that the forward reaction from *cis*- to *trans*-DeHN is much faster than the backward reaction, i.e., $k_1 >> k_{-1}$. In addition, for the reaction conditions studied, the reactions were taken to be approximately first order. With these assumptions, the rate equations may be written as the following:

$$\frac{dD}{dt} = -(k_1 + k_2) D \tag{1}$$

$$\frac{dB}{dt} = k_1 D - k_3 B \tag{2}$$

$$\frac{dC}{dt} = k_2 D + k_3 B \tag{3}$$

where D and B are *cis*-DeHN and *trans*-DeHN, respectively, and C, denoted as the "others" in Figure 45, represents the grouped products from dehydrogenation, ring-contraction, and cracking reactions. Equations 1-3 can be solved to give

$$D/D_0 = \exp[-(k_1+k_2) t] = \exp[-k t] \tag{4}$$

$$B/D_0 = [k_1/(k_1+k_2-k_3)] [\exp(-k_3 t) - \exp(-k t)] \tag{5}$$

$$C = D_0 - D - B \tag{6}$$

Because we are mainly interested in the yield of *trans*-DeHN and only limited data are available in the current work, we did not intend to find all the kinetic parameters. Instead, we used the experimental data to find the lumped rate constant k (equal to k_1+k_2 in Eq. 4) and then developed empirical equations to predict the product yield of *trans*-DeHN. The procedures are described as follows. First, the rate constant k was determined by using Eq. (4) for all the experiments shown in Table 10. Then, the rate constant (k) was correlated by the Arrhenius law as shown in Eq. (7)

$$k = A\, e^{-E_a / RT} \tag{7}$$

where A (h^{-1}) is the frequency (or preexponential) factor, E_a is the apparent activation energy (kcal/mol), and R is the gas constant (kcal mol^{-1} K^{-1}). The apparent E_a and A values determined from Arrhenius plots (as shown in Figure 47) are as follows:

$$\text{for HY} \quad E_a = 49.9 \pm 2.6 \text{ kcal/mol} \quad \text{and} \quad A = 6.03 \times 10^{20} \text{ h}^{-1} \tag{8}$$

$$\text{for LaHY} \quad E_a = 54.6 \pm 2.6 \text{ kcal/mol} \quad \text{and} \quad A = 3.36 \times 10^{22} \text{ h}^{-1} \tag{9}$$

Third, empirical equations were developed to predict the product yield of *trans*-DeHN. Based on the results in Figure 45, we found that the selectivity of *trans*-DeHN can be presented by a second-degree polynomial as shown in Eq. (10)

$$\text{Selectivity of } \textit{trans}\text{-DeHN} = a_1 + a_2 X + a_3 X^2 + a_4 T + a_5 X T \tag{10}$$

where X is the *cis*-DeHN conversion, T is the temperature in K, and a_i (i=1,...,5) are the empirical parameters to be found. Using the data in Table 10, we have determined the parameters a_i as follows:

$$\text{for HY} \quad \text{Sel.} = 1.938 + 0.779 X - 0.285 X^2 - 0.00228 T - 0.0012 X T \tag{11}$$

$$\text{for LaHY} \quad \text{Sel.} = 1.534 + 2.745 X - 0.082 X^2 - 0.00146 T - 0.0054 X T \tag{12}$$

In order to check the reliability of these equations in predicting the conversion and selectivity, predictions based on equations 4, 8, 9, 11, and 12 are compared with experimental results. Figure 48 compares the experimental selectivity of *trans*-DeHN to the values predicted from the empirical equations for both catalysts. The line corresponding to exact agreement is drawn as a diagonal. It is clear that the predicted values are generally in good agreement with experimental values over a wide range of conversion. Similarly, Figure 49 compares the predicted and measured *trans*-DeHN yield, which is the product of conversion and selectivity. Again, there is good general agreement. These examples demonstrated the reliability and potential usefulness of the aforementioned equations in predicting conversion and product yield.

3. Effect of noble metals. Recall that the experimentally determined activation energies for HY and LaHY, as shown in Eqs. 8 and 9, are unusually high for catalytic reactions. There are two possible explanations for this. First, the first-order reaction was assumed to simplify the calculation of rate constant, but the isomerization of *cis*-DeHN into *trans*-DeHN may not be a real first-order reaction and can involve several reaction steps. Second, these two catalysts are not effective in some of the key reaction steps; thus the apparent activation energy values are higher than expected.

In considering the possible reaction mechanisms, it occurred to us that this isomerization may proceed through a two-step process involving dehydrogenation of *cis*-DeHN to form an olefinic intermediate (possibly $\Delta^{1,9}$-octalin, or $\Delta^{9,10}$-octalin, or both) followed by addition of hydrogen to this olefinic intermediate to give *trans*-DeHN, as illustrated in Scheme 2. It should be noted that *trans*-DeHN can be formed by hydrogen addition to either $\Delta^{1,9}$-octalin, or $\Delta^{9,10}$-octalin [22,23]. If this two-step process is the case, then the high values of apparent activation energy with HY and LaHY catalysts suggest that either the dehydrogenation or the subsequent hydrogenation or both are relatively difficult over HY and LaHY under the conditions used. These considerations prompted us to examine the effect of noble metals, because they are known to be good catalysts for both dehydrogenation and hydrogenation. We then tested Pt- and Pd-loaded mordenites for this reaction.

Table 11 shows the products distribution from catalyzed isomerization of *cis*-DeHN using 0.2-g noble metal loaded catalysts and 1-g commercial DeHN as starting reactant at 473 K under an initial pressure of 0.79 MPa UHP H_2 or N_2. Pt- and Pd-loaded mordenites, i.e., Pt/HM30A, Pt/HM20A, and Pd/HM30A, are very effective catalysts under H_2 atmosphere for the conformational isomerization of *cis*-DeHN to *trans*-DeHN even at low temperature, 473 K. Their selectivity towards *trans*-DeHN reached nearly 100%; in other words, there were almost no side-reactions. Take Pt/HM30A as an example. The experimental product composition of 92.3% *trans*-DeHN and 7.3% *cis*-DeHN at 473 K (as shown in Table 11) is very close to calculated thermodynamic equilibrium composition (95.3% *trans*-DeHN, 4.7% *cis*-DeHN, in Table 13 to be discussed later).

Changing the gas environment from H_2 to N_2 significantly affects the effectiveness of noble metal loaded catalysts and therefore the final product distribution. Although Pt- and Pd-loaded mordenites are effective catalysts under H_2 atmosphere, they are much less effective under N_2 atmosphere (see Table 11). Pt/HM30A is a better catalyst than Pd/HM30A at 473 K under N_2 atmosphere in terms of conversion and *trans*-DeHN selectivity although they are almost equally effective under H_2. It is also interesting to note the yield change of tetralin, which initially existed as an impurity (0.7 wt%), under different gas environment. Table 11 shows that tetralin was completely hydrogenated into decalin under H_2 environment due to the good hydrogenation ability of Pt and Pd. On the other hand, the noble metals under N_2 served to dehydrogenate decalin to tetralin and thus increased the yield of tetralin.

To improve the effectiveness of noble metal loaded mordenites under N_2, we explored the possible effect of catalyst pre-reduction. Table 12 shows the results at 453 and 443 K over Pt/HM30A using *cis*-DeHN as the starting material. Three types of experiments were carried out. The first one was carried out in N_2 using catalyst without pre-reduction; the second was carried out in N_2 using pre-reduced catalyst, and the third was carried out in H_2 with the catalyst

being reduced in situ. The catalyst performs the best in the presence of H_2, and the worst in N_2 atmosphere using catalyst without pre-reduction. The effectiveness of catalyst was apparently improved at 453 K when the catalyst was pre-reduced, judging from the higher *trans*-DeHN yield. Similar improvement was also observed for the reaction at 443 K. It is speculated that the isomerization of *cis*-DeHN to *trans*-DeHN starts with dehydrogenation occurring on the metal surface to form olefinic intermediates, for example, $\Delta^{1,9}$-octalin. The olefinic compounds later are hydrogenated to *trans*-DeHN. Since the dehydrogenation and hydrogenation steps occur on the metal and involve hydrogen, pre-reduction of the catalyst and the presence of H_2 could facilitate the isomerization reaction.

The above results present an interesting case of molecular H_2-promoted conformational isomerization of a bicyclic alkane. Combined analysis of the above results also suggests that the noble metals loaded on mordenites strongly promote the isomerization by catalyzing both the initial dehydrogenation of *cis*-DeHN to form the olefinic intermediates and the subsequent hydrogen addition to the olefinic intermediate to form *trans*-DeHN. This consideration is supported by the following facts: 1) these catalysts became much less effective for isomerization but enhanced dehydrogenation of *cis*-DeHN under N_2; 2) the pre-reduction improved the catalytic activity for isomerization under N_2; and 3) these catalysts can drive the reaction to equilibrium quickly and highly selectively under H_2 atmosphere.

4. Calculated equilibrium composition. The equilibrium compositions of *trans*-DeHN and *cis*-DeHN at several temperatures were calculated to establish the theoretical upper limit of the catalytic conversion. The equilibrium constant (K) is related to the Gibbs energy change (ΔG^0) by Eq. (13)

$$\ln K = \frac{-\Delta G^0}{RT} \tag{13}$$

Thermochemical data such as standard enthalpy of formation, standard Gibbs energy of formation, and isobaric heat capacity, are needed to establish the equilibrium constant as a function of temperature Using the thermochemical data in Reid et al. [24] for *cis*-DeHN and *trans*-DeHN, we have determined the general expression for the equilibrium constant as a function of temperature as shown in Eq. (14)

$$R \ln K = \frac{15370}{T} + 14.83 \ln T - 0.0365\, T + 1.885\times10^{-5}\, T^2 - 4.49\times10^{-9}\, T^3 - 85.2 \tag{14}$$

where R is the gas constant (8.314 J mol^{-1} K^{-1}) and T is the temperature in K. The calculated heat of reaction, equilibrium constant, and composition are shown in Table 13. It should be noticed that because of the exponential nature of Eq. (13), the calculated results are highly dependent on the thermodynamic parameters used. For example, if the Gibbs energy was off by

only 5–10%, the estimation error for the equilibrium constant at 473 K may be as large as 16–35%.

The theoretical calculation results show that the isomerization from *cis*-DeHN to *trans*-DeHN is exothermic (Table 13), and the equilibrium conversion of *cis*-DeHN decreases with increasing temperature. Therefore, a lower reaction temperature is thermodynamically favorable. The yield of *trans*-DeHN could reach over 90% for the temperature range studied (below 573 K). Comparing the calculated mixture compositions with experimental data for the six catalysts studied in this work, we could find that the optimal product yields, i.e., the theoretical equilibrium compositions, could be approached by using very effective catalysts (Pt- and Pd-loaded mordenites) under appropriate conditions (under H_2 atmosphere at 473 K). The data in Table 9 also showed that reactions at 573 K for 0.5 h over LaHY and HY seemed to have approached the equilibrium state for *trans*- and *cis*-isomers because the experimental ratios of *trans*- to *cis*- are very close to the theoretical value (11.4 at 573 K, as shown in Table 13). It is kinetically desirable to run the reaction under the condition that could quickly push the reaction to near equilibrium stage. However, some conditions (at 573 K for 0.5 h over LaHY and HY) may be too severe for the isomerization reaction of *cis*-DeHN to *trans*-DeHN because of the undesirable side reactions. In any case, the theoretically calculated equilibrium compositions (in Table 13) are useful and can be used as guidelines for the evaluation of reaction conditions and the effectiveness of catalysts.

Conclusions

Pt- and Pd-loaded mordenites are very effective catalysts under H_2 for the conformational isomerization of *cis*-DeHN to *trans*-DeHN at 473 K. The selectivity towards *trans*-DeHN with these catalysts is very high (nearly 100%) with a *trans*-DeHN/*cis*-DeHN ratio of near 13. On the other hand, they are less effective under a hydrogen-deficient environment such as under N_2. The isomerization of *cis*-DeHN to *trans*-DeHN is thought to involve dehydrogenation and hydrogenation on the metal surface. The effectiveness of Pt/HM30A in N_2 environment could be improved by pre-reduction in H_2. Pt/HM30A is a better catalyst than Pd/HM30A at 473 K under N_2 atmosphere, in terms of conversion and *trans*-DeHN selectivity, although they are almost equally effective under H_2. HY, LaHY, and HM30A are not as effective as Pt- and Pd-loaded mordenites, and their activities under N_2 and under H_2 are similar to each other. Among these three catalysts, HY performs slightly better than LaHY, and the catalyst with the lowest acidity (HM30A) displayed the lowest activity. The observed activity for *cis*-DeHN conversion is: Pt/HM30A ≈ Pd/HM30A ≈ Pt/HM20A > HY > LaHY > HM30A. Selectivity towards *trans*-DeHN decreases with both increasing temperature and increasing conversion level (under isothermal condition).

A simple reaction pathways model containing parallel-consecutive kinetic schemes was proposed. Empirical equations capable of predicting product yields were developed. The equations 4, 8, 9, 11, and 12 may be used to predict reaction conversion and major products. The theoretical equilibrium compositions of *trans*-DeHN and *cis*-DeHN at several temperatures were calculated and compared with experimental data. The experimental results for very effective catalysts such as Pt- and Pd-loaded mordenites, corroborated well with theoretical calculations. The calculated equilibrium compositions are useful as guidelines for evaluating the effects of catalysts and reaction conditions.

References

1. C. Song, W.-C. Lai and H. H. Schobert, Prepr.-Am. Chem. Soc., Div. Fuel Chem., 37 (1992) 1655.

2. C. Song, S. Eser, H. H. Schobert and P. G. Hatcher, Energy & Fuels, 7 (1993) 234.

3. E. E. Donath and M. Hess, Chemical Engineering Progress, 56 (1960) 68.

4. H. R. Lander and A. C. Nixon, Prepr.-Am. Chem. Soc., Div. Pet. Chem., 32 (1987) 504.

5. P. H. Taylor and W. A. Rubey, Prepr.-Am. Chem. Soc., Div. Pet. Chem., 32 (1987) 521.

6. C. Song, W.-C. Lai and H. H. Schobert, Ind. Eng. Chem. Res., 33 (1994) 548.

7. A. W. Ritchie and A. C. Nixon, Prepr.-Am. Chem. Soc., Div. Pet. Chem., 12 (1967) 117.

8. J. Shabtai, R. Ramakrishnan and A. G. Oblad, in A. G. Obald and H. G. Davis and R. T. Eddinger (Editors), Thermal Hydrocarbon Chemistry, Advances in Chemistry Series 183, American Chemical Society, Washington, D. C., 1979, pp 297-328.

9. W. D. Constant, G. L. Price and E. McLaughlin, Fuel, 65 (1986) 8.

10. H. B. Mostad, T. U. Riis and O. H. Ellestad, Applied Catalysis, 58 (1990) 105; H. B. Mostad, T. U. Riis and O. H. Ellestad, Applied Catalysis, 63 (1990) 345.

11. M. Nimz, Zeolites, 10 (1990) 297.

12. E. F. Sousa-Aguiar, M. Pinhel da Silva, M. L. Murta Valle and D. Forte da Silva, Prepr.-Am. Chem. Soc., Div. Pet. Chem., 39 (1994) 356.

13. C. Song and K. Moffatt, Prepr.-Am. Chem. Soc., Div. Pet. Chem., 38 (1993) 779.

14. C. Song and K. Moffatt, Microporous Materials, 2 (1994) 459.

15. W.-C. Lai and C. Song, in *Advanced Thermally Stable Jet Fuels.* Technical Progress Report (October 1994 - December 1994), H. H. Schobert, S. Eser, C. Song, P. G. Hatcher, A. Boehman, M. M. Coleman, Eds., The Pennsylvania State University, February **1995**, pp19-23.

16. C. Song, H. H. Schobert and H. Matsui, Prepr.-Am. Chem. Soc., Div. Fuel Chem., 36 (1991) 1892.

17. C. Song and S. Kirby, Microporous Materials, 2 (1994) 467.

18. A. D. Schmitz, G. Bowers and C. Song, Prepr.-Am. Chem. Soc., Div. Fuel Chem., 40 (1995) 930.

19. C. Song, W.-C. Lai and H. H. Schobert, Ind. Eng. Chem. Res., 33 (1994) 534.

20. L. Petrov, L. Angelova and D. Shopov, Bokl. Bolg. Akad. Nauk, 30 (1977) 85.

21. G. C. Bond, Heterogeneous Catalysis: Principles and Applications, Second Edition, Oxford University Press, Oxford, 1987, pp 52-53.

22. A. W. Weitkamp, in D. D. Eley, H. Pines and P. B. Weisz (Editors), Advances in Catalysis and Related Subjects, Academic Press, New York, 1968, Volume 18, pp1-110.

23. J.F. Sauvage, R. H. Baker and A. S. Hussey, J. Am. Chem. Soc., 83 (1961) 3874.

24. R. C. Reid, J. M. Prausnitz and B. E. Poling, The Properties of Gases & Liquids, Fourth Edition, McGraw-Hill Book Company, New York, 1987.

APPENDIX I

TABLES

Table 1. The Response Factor of the FID and TCD.

Compound	RRF_9 for FID *	RWR for TCD**
CH4		2.25
C2H4		1.71
C2H6		1.7
[illegible]		
C4H8	1.21	1.44
C4H10	1.21	1.47
[illegible]		
C6H12	1.12	1.39
C6H14	1.12	1.43
[illegible]		
C8H16	1.03	
C8H18	1.03	
[illegible]		
C10H20	0.94	
C10H22	0.94	
[illegible]		
C12H24	0.83	
C12H26	0.83	
[illegible]		
C14H30	0.74	
[illegible]		
* C4-C7 response factors are extrapolated data		
** From Ref. 2 with He as a carrier gas		

Table 2. Temperature Effects on Products Distribution of Norpar 13 Reacted in the Flow Reactor at 500 psig., Space Time 25 Seconds, and 1 Hour Run.

Compound	Wi %	Wi %	Wi %	Wi %	Wi %
	500 °C	525 °C	550 °C	575 °C	600 °C
CH4	0.01	0.10	0.38	0.56	1.58
C2H4	0.08	0.40	1.07	1.63	3.99
C2H6	0.15	0.66	1.63	2.18	5.20
C3H6	0.35	1.17	2.38	[illegible]	[illegible]
C3H8	0.38	1.23	2.14	[illegible]	[illegible]
C4H8	0.36	1.06	1.64	2.86	5.29
C4H10	0.27	0.77	1.12	1.75	2.99
C5H10	0.42	1.56	[illegible]	[illegible]	[illegible]
C5H12	0.28	0.85	[illegible]	[illegible]	[illegible]
C6H12	0.62	1.67	2.84	4.50	5.69
C6H14	0.26	0.54	1.01	1.42	1.77
C7H14	0.58	1.44	2.33	[illegible]	[illegible]
C7H16	0.21	0.57	0.84	[illegible]	[illegible]
C8H16	0.55	1.23	2.66	3.28	3.41
C8H18	0.18	0.41	0.82	0.74	0.81
C9H18	0.45	0.88	2.22	[illegible]	[illegible]
C9H20	0.36	0.81	[illegible]	[illegible]	[illegible]
C10H20	0.45	0.82	1.83	1.84	2.79
C10H22	0.16	0.20	0.51	0.44	0.53
C11H22	0.41	0.54	1.23	[illegible]	[illegible]
C11H24	0.38	0.67	[illegible]	[illegible]	[illegible]
C12H24	0.22	0.38	0.82	0.90	0.88
C12H26	12.86	8.55	8.79	7.50	5.27
C13H26	46.75	47.81	[illegible]	[illegible]	[illegible]
C14H30	33.96	36.12	24.63	20.14	10.75
C15H30	0.00	[illegible]	[illegible]	[illegible]	[illegible]

Table 3. Pressure Effects on Products Distribution of Norpar 13 Reacted in the Flow Reactor at 550 °C, and 1 Hour Run.

Compound	Wi %	Wi %	Wi %	Wi %	Wi %
	0 psig	250 psig.	500 psig.	750 psig.	1000 psig.
CH4	0.03	0.01	0.38	0.48	0.57
C2H4	0.11	0.08	1.07	1.01	0.74
C2H6	0.05	0.15	1.63	2.13	2.53
C4H8	0.14	0.36	1.64	2.39	2.65
C4H10	0.00	0.27	1.12	2.23	3.13
C6H12	0.07	0.62	2.84	2.81	3.64
C6H14	0.03	0.26	1.01	1.45	2.58
C8H16	0.04	0.55	2.66	2.08	2.66
C8H18	0.00	0.18	0.82	1.32	2.06
C10H20	0.00	0.45	1.83	1.77	1.49
C10H22	0.00	0.16	0.51	0.78	1.11
C12H24	0.00	0.22	0.82	0.94	0.78
C12H26	12.52	12.86	8.79	8.20	6.44
C14H30	37.00	33.96	24.63	22.29	18.17

Table 4. Temperature Effects on Products Distribution of Norpar 13 Reacted in the Flow Reactor at 500 psig., Space Time 25 Seconds, and 1 Hour Run with Ni Coupons.

Compound	Wi %	Wi %	Wi %	Wi %
	500 °C	525 °C	550 °C	575 °C
CH4	0.02	0.03	0.12	0.75
C2H4	0.07	0.10	0.44	1.69
C2H6	0.14	0.21	0.77	2.31
[illegible]	0.23	0.33	1.33	3.22
[illegible]	0.26	0.36	1.32	3.01
C4H8	0.21	0.33	1.09	2.25
C4H10	0.18	0.29	0.95	1.74
[illegible]	0.24	0.36	[illegible]	[illegible]
[illegible]	0.18	0.26	[illegible]	[illegible]
C6H12	0.35	0.67	1.75	2.67
C6H14	0.16	0.30	0.59	0.76
[illegible]	0.32	0.85	[illegible]	[illegible]
[illegible]	0.15	0.31	0.65	0.82
C8H16	0.37	0.63	1.62	2.04
C8H18	0.14	0.23	0.53	0.56
[illegible]	0.42	[illegible]	[illegible]	[illegible]
[illegible]	0.18	0.27	[illegible]	[illegible]
C10H20	0.45	0.69	1.41	1.52
C10H22	0.20	0.27	0.45	0.40
[illegible]	0.40	0.35	[illegible]	[illegible]
[illegible]	0.68	0.76	[illegible]	[illegible]
C12H24	0.27	0.39	0.67	0.67
C12H26	12.13	12.22	10.45	7.59
[illegible]	46.22	44.57	[illegible]	[illegible]
C14H30	35.71	33.94	29.66	26.54
[illegible]	0.49	[illegible]	[illegible]	[illegible]

Table 5. Pressure Effects on Products Distribution of Norpar 13 Reacted in the Flow Reactor at 550 °C, and 1 Hour Run with Nickel Coupons.

Compound	Wi %	Wi %	Wi %
	0 psig.	500 psig.	1000 psig.
CH4	0.03	0.12	0.40
C2H4	0.09	0.44	0.47
C2H6	0.07	0.77	1.78
[illegible]	0.09	[illegible]	[illegible]
[illegible]	0.05	[illegible]	[illegible]
C4H8	0.06	1.09	1.89
C4H10	0.01	0.95	2.75
[illegible]	0.05	[illegible]	[illegible]
[illegible]	[illegible]	[illegible]	[illegible]
C6H12	0.07	1.75	2.61
C6H14	0.06	0.59	1.93
[illegible]	0.05	[illegible]	[illegible]
[illegible]	[illegible]	[illegible]	[illegible]
C8H16	0.06	1.62	2.15
C8H18	0.00	0.53	1.68
[illegible]	0.05	[illegible]	[illegible]
[illegible]	[illegible]	[illegible]	[illegible]
C10H20	0.09	1.41	1.35
C10H22	0.00	0.45	1.00
[illegible]	[illegible]	[illegible]	[illegible]
[illegible]	[illegible]	[illegible]	[illegible]
C12H24	0.00	0.67	0.54
C12H26	12.51	10.45	7.28
[illegible]	[illegible]	[illegible]	[illegible]
C14H30	38.40	29.66	24.55
[illegible]	[illegible]	[illegible]	[illegible]

Table 6. Description of the products of thermal stressing for 1h @ 250°C.

Air Pressure (psi)	Dodecane (Dod) Mixtures		
	Neat Dod	+ 5% THQ	+ 5% BzOH
100	Clear liquid No solids	Yellow liquid No solids	Clear liquid No solids
150	Pale yellow liquid No solids		
200	Pale yellow liquid No solids	Yellow/orange liquid No solids	Pale yellow liquid Oily drop + black solids
250	Yellow liquid Trace black solids		
300	Dark yellow liquid Significant black solids	Orange liquid Trace of oil	Pale yellow liquid Oily drop + black solids
400	Yellow/green liquid Obvious black solids	Orange liquid Small oily deposit	

Table 7. Description of the products of thermal stressing for 1h @ 250°C.

Air Pressure (psi)	Jet A-1 Mixtures		
	Neat Jet A-1	Jet A-1 + 5% THQ	Jet A-1 + 5% BzOH
100	Yellow liquid No solids	Yellow/orange liquid No solids	Yellow liquid No solids
200	Dark orange liquid Significant black solids	Orange/brown liquid No solids	Bright yellow liquid No solids
300	Dark orange liquid Significant black solids	Dark brown liquid Trace solids (?)	Bright yellow liquid No solids
400	Dark orange liquid Large deposit on reactor	Red/brown liquid Small amount of solids	Orange liquid Significant black solids

Table 8 . Results of Non-Catalytic Liquefaction of Wyodak Coal at 300 °C and 350 °C for 30 min. Under 6.9 MPa H_2.

Reaction Temperature (°C)	Solvent	Gaseous Distribution			Liquid Distribution			Total Liquids	% Conv.
		CO	CO_2	C_1-C_4	Oil	Asph.	Preasph.		
300	-	0.2	3.2	0.12	0.2	0.3	4.3	4.8	7.6
350	-	0.2	4.5	0.2	2.1	2.6	4.5	9.2	12.5
300	Tetralin	0.4	7.4	0.2	4.3	1.8	2.3	8.4	15.9
350	"	0.2	4.1	0.2	4.1	7.6	10.0	21.7	25.9
300	1-MN	0.2	4.3	0.1	1.4	1.9	2.4	5.7	14.0
350	"	0.2	4.3	0.2	1.1	5.8	7.4	14.3	18.3

Table 9. Catalyzed Isomerization of *cis*-Decalin under an Initial Pressure of 0.79 MPa UHP N_2 or H_2 Using Commercial Decalin as Reactant.

Catalyst	Temp.	Time	Gas	Product (wt % of feed)				*trans/cis*	X[c]	Sel.[d]
type	(K)	(h)		*trans*-DeHN	*cis*-DeHN	Tetralin	Others[b]	ratio	(%)	
		a		48.34	50.62	0.70	0.34			
LaHY	473	2.0	N_2	48.29	50.73	0.68	0.30	0.95	0	-
LaHY	508	8.0	N_2	59.67	32.32	0.62	7.07	1.85	18.3	0.62
LaHY	523	0.5	N_2	57.36	36.25	0.67	5.35	1.58	14.4	0.63
LaHY	523	2.0	N_2	65.15	18.82	0.61	15.42	3.5	31.8	0.53
LaHY	523	2.0	H_2	65.79	16.73	0.59	16.89	3.9	33.9	0.52
LaHY	573	0.5	N_2	47.83	4.48	0.36	46.55	10.68	46.1	-
HY	508	8.0	N_2	64.76	25.26	0.59	9.06	2.56	25.4	0.65
HY	523	0.5	N_2	52.38	44.68	0.64	1.97	1.17	5.9	0.68
HY	523	2.0	N_2	65.92	19.04	0.60	14.44	3.5	31.6	0.56
HY	548	0.5	N_2	62.18	7.36	0.43	29.49	8.45	43.3	0.32
HY	573	0.5	N_2	45.60	3.74	0.33	49.34	12.19	46.9	-
HM30A	523	2.0	N_2	53.02	31.60	0.38	15.00	1.7	19.0	0.25

a) This row presents the purity of as-received commercial decalin including 0.34% *n*-decane.

b) Unreacted *n*-decane plus products of ring-contraction and ring-opening reactions.

c) Conversion of *cis*-decalin (weight % of feed).

d) Selectivity to *trans*-decalin, defined as a fraction of *cis*-decalin conversion.

Table 10. Catalyzed Isomerization of Pure *cis*-Decalin under an Initial Pressure of 0.79 MPa UHP N_2.

	Catalyst: 0.2 g of LaHY													
temperature (K)	508	508	508	508	523	523	523	523	538	538	538	548	548	548
residence time[a] (min)	60	120	240	480	30	60	120	120	9	18	60	9	18	60
reaction time[b] (min)	54	114	234	474	25	55	115	115	4	13	55	5	14	56
product yield[c] (wt %)														
trans-DeHN	7.4	11.5	22.7	43.0	20.4	29.0	47.7	46.3	11.7	32.7	50.4	24.2	37.9	42.5
cis-DeHN	90.5	85.2	70.8	42.8	72.0	60.1	29.4	32.5	83.5	51.4	10.2	61.2	31.2	4.7
trans-/*cis*-DeHN ratio	0.08	0.13	0.32	1.00	0.28	0.48	1.62	1.42	0.14	0.64	4.94	0.40	1.21	9.08
cis-DeHN conversion[c]	9.1	14.4	28.8	56.8	27.6	39.5	70.2	67.1	16.1	48.2	89.4	38.4	68.4	94.9
rate constant, k (h^{-1})	0.11	0.08	0.09	0.11	0.78	0.55	0.63	0.58	2.62	3.02	2.45	5.83	4.92	3.19
trans-DeHN selectivity	0.80	0.79	0.79	0.76	0.73	0.73	0.68	0.69	0.72	0.68	0.56	0.63	0.55	0.45

	Catalyst: 0.2 g of HY												
temperature (K)	508	508	508	523	523	523	538	538	538	538	548	548	548
residence time[a] (min)	120	240	480	30	60	120	9	18	30	60	9	18	30
reaction time[b] (min)	114	234	474	25	55	115	4	13	25	55	5	14	26
product yield[c] (wt %)													
trans-DeHN	21.1	47.6	57.0	23.1	46.1	52.7	20.7	34.6	51.9	54.5	35.8	47.8	50.3
cis-DeHN	73.9	37.8	23.0	69.3	36.8	25.6	71.6	51.1	19.4	7.4	45.9	23.1	10.2
trans-/*cis*-DeHN ratio	0.28	1.26	2.48	0.33	1.25	2.06	0.29	0.68	2.67	7.35	0.78	2.07	4.93
cis-DeHN conversion[c]	25.8	61.8	76.6	30.3	62.9	74.0	28.0	48.5	80.3	92.2	53.7	76.5	89.4
rate constant, k (h^{-1})	0.16	0.25	0.18	0.87	1.08	0.70	4.91	3.06	3.89	2.78	9.16	6.19	5.17
trans-DeHN selectivity	0.81	0.77	0.74	0.76	0.73	0.71	0.73	0.71	0.64	0.59	0.67	0.62	0.56

a) Reactor residence time in sand bath preheated to reaction temperature.

b) Corrected reaction time (reactor residence time minus experimentally measured heat-up time).

c) Based on the initial amount of *cis*-DeHN.

Table 11. Catalyzed Isomerization of *cis*-Decalin under an Initial Pressure of 0.79 MPa UHP H_2 or N_2 Using Commercial Decalin as Reactant.

Catalyst type	Temp. (K)	Time (h)	Gas	Product (wt % of feed)				*trans/cis* ratio	X[c] (%)	Sel.[d]
				trans-DeHN	*cis*-DeHN	Tetralin	Others[b]			
		a		48.34	50.62	0.70	0.34			
Pt/HM30A	473	2.0	N_2	62.40	33.46	2.26	1.88	1.9	17.2	0.82
Pd/HM30A	473	2.0	N_2	54.50	42.43	1.84	1.23	1.3	8.2	0.75
Pt/HM30A	473	2.0	H_2	92.34	7.25	0	0.41	12.7	43.4	1.00
Pd/HM30A	473	2.0	H_2	92.31	7.23	0	0.46	12.8	43.4	1.00
Pt/HM20A	473	8.0	H_2	91.50	7.95	0	0.55	11.5	42.7	1.00

a) This row presents the purity of as-received commercial decalin including 0.34% *n*-decane.

b) Unreacted *n*-decane plus products of ring-contraction and ring-opening reactions.

c) Conversion of *cis*-decalin (weight % of feed).

d) Selectivity to *trans*-decalin, defined as a fraction of *cis*-decalin conversion.

Table 12. Catalyzed Isomerization of Pure *cis*-Decalin over Pt/HM30A.

Temp. (K)	Time (h)	Catalyst H_2 treated?	Gas	Product (wt % of feed)		
				trans-DeHN	*cis*-DeHN	Tetralin
453	0.25	No	N_2	0.6	98.1	1.3
453	0.25	Yes	N_2	23.7	75.1	1.2
453	0.25	No	H_2	52.1	47.9	
443	0.25	No	N_2	0.6	97.9	1.5
443	0.25	Yes	N_2	9.6	88.3	2.1
443	0.25	No	H_2	69.3	30.7	

Table 13. Calculated Heat of Reaction, Equilibrium Constant and Composition for a Binary Mixture System of *cis*-Decalin and *trans*-Decalin.

Temperature	Heat of reaction	Equilibrium	Composition (wt %)	
(K)	ΔH (J/mol)[a]	constant[b]	*cis*-DeHN	*trans*-DeHN
473	-13206	20.5	4.65%	95.35%
508	-13210	16.3	5.79%	94.21%
523	-13212	14.9	6.30%	93.70%
538	-13214	13.7	6.82%	93.18%
548	-13215	12.9	7.17%	92.83%
573	-13216	11.4	8.06%	91.94%
623	-13211	9.1	9.87%	90.13%
673	-13193	7.6	11.69%	88.31%
723	-13160	6.4	13.48%	86.52%

a) The values of standard enthalpy of formation for *cis*- and *trans*-DeHN at 298.2 K are -1.691×10^5 and -1.824×10^5 J/mol. respectively.

b) Equilibrium constant for the reaction: *cis*-DeHN ↔ *trans*-DeHN

$$K = \frac{[trans\text{-DeHN}]}{[cis\text{-DeHN}]}$$

APPENDIX II

FIGURES

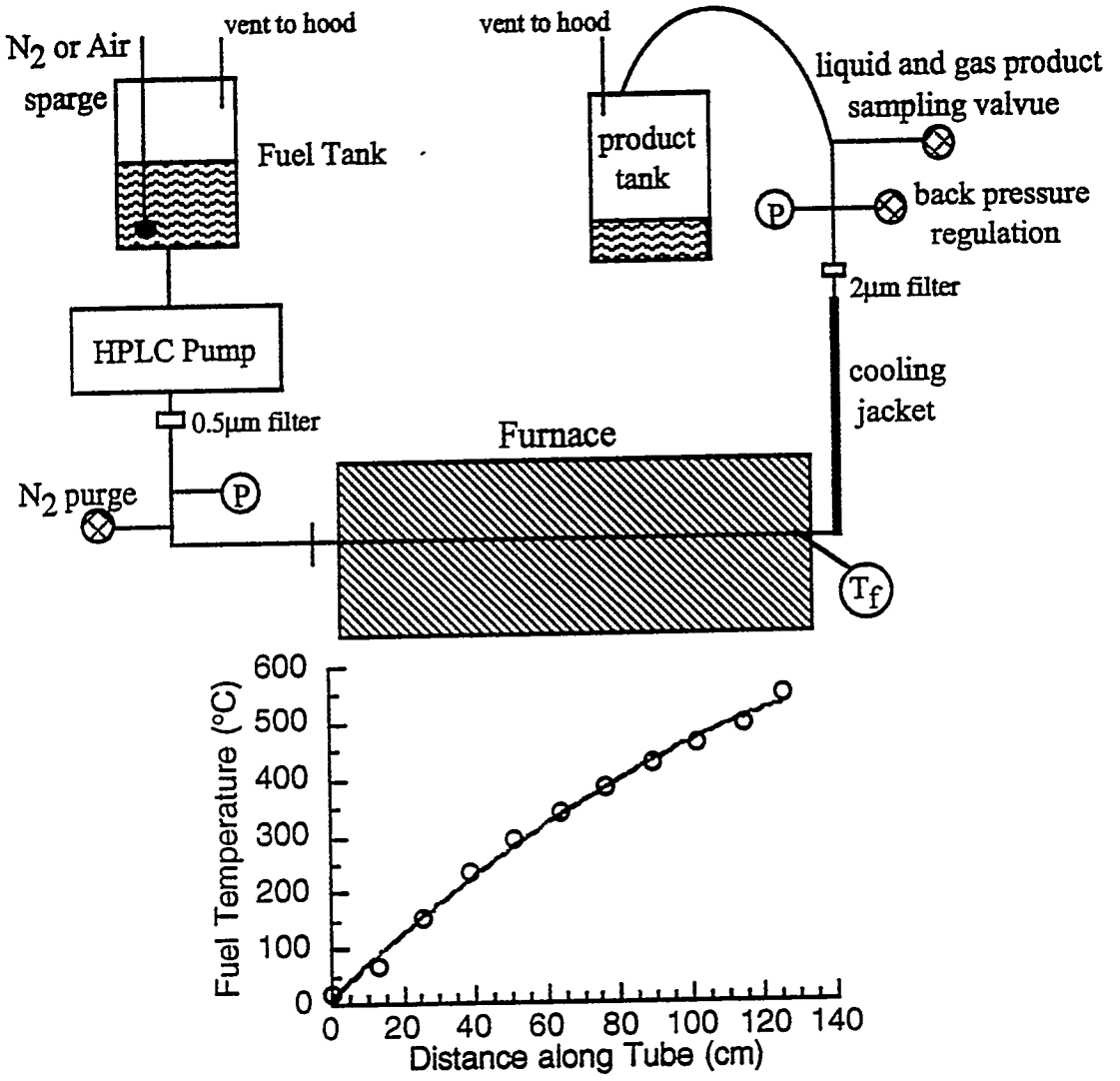

Figure 1. Schematic of test apparatus with calculated fuel temperature along the flow tube.

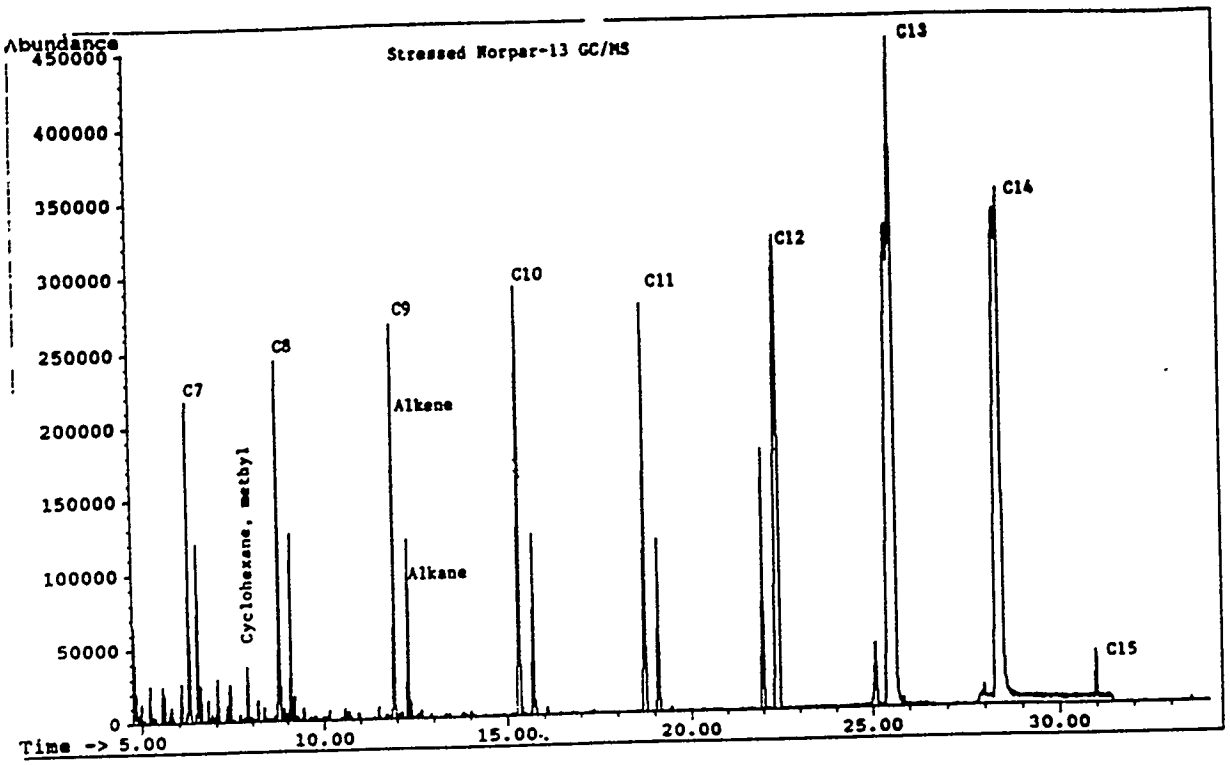

Figure 2. Liquid GC/MS chromatograph of nitrogen-saturated Norpar-13.

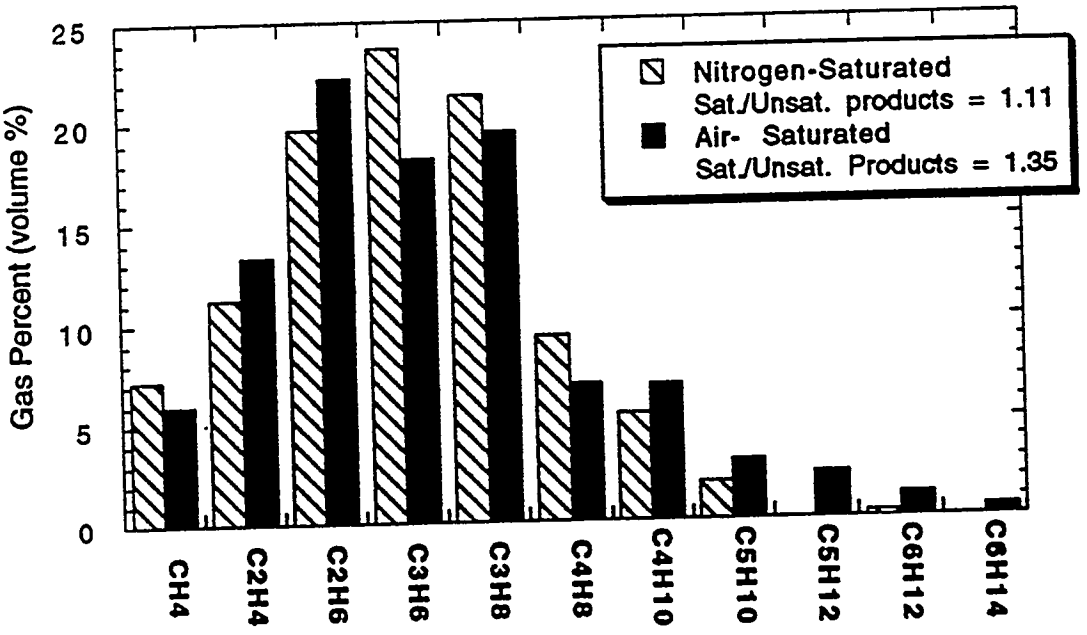

Figure 3. Gas products of Norpar-13 after stressing to a final fuel temperature of 550C.

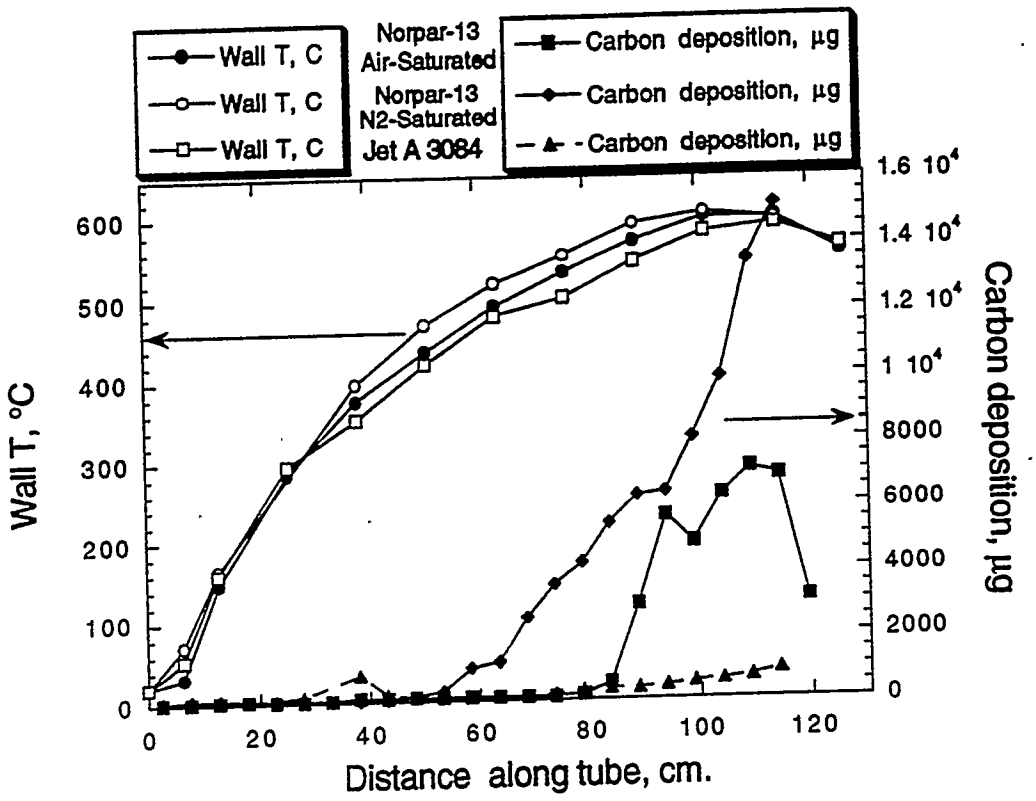

Figure 4. Deposition profile of Norpar-13 compared to a jet A fuel.

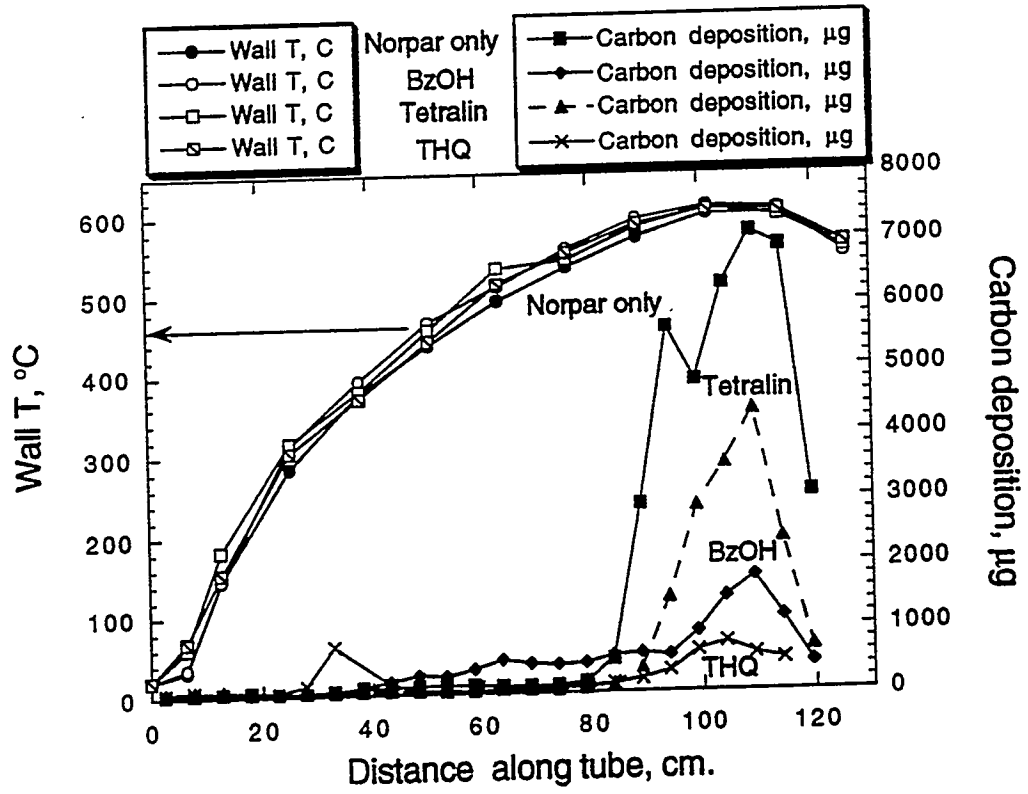

Figure 5. Deposition profile of Norpar-13 with 2.0 wt% thermal stabilizers added.

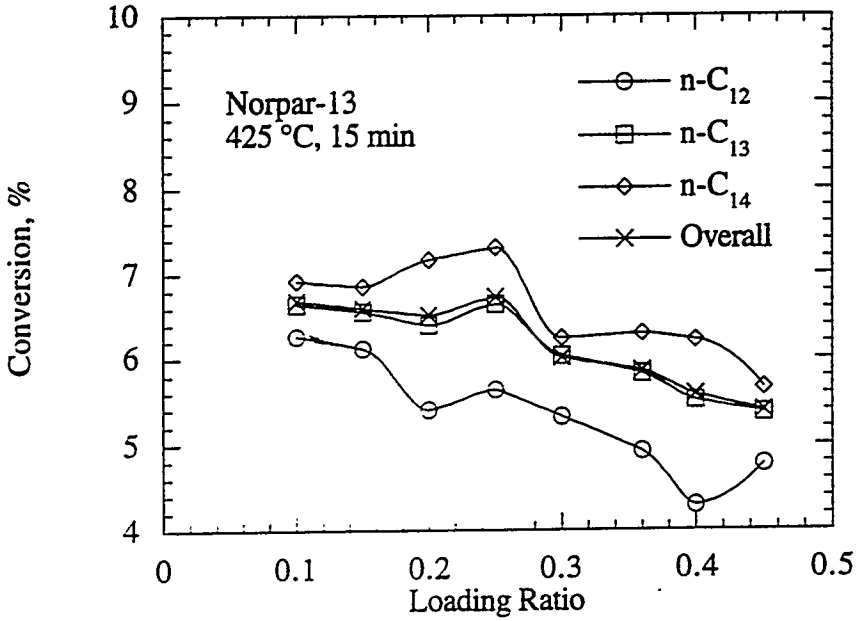

Figure 6. Changes in Conversion with Loading Ratio from Thermal Decomposition of Norpar-13 at 425 °C for 15 min.

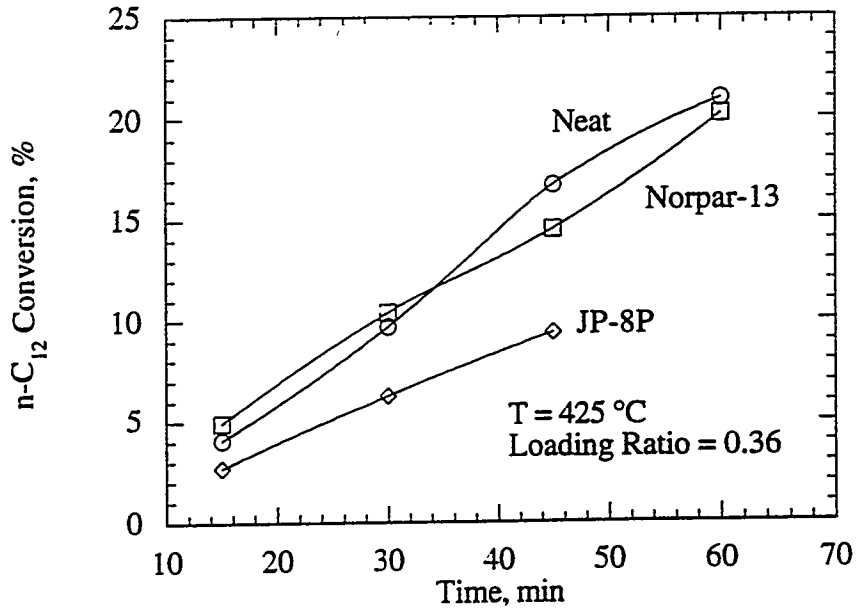

Figure 7. Changes in Conversion of *n*-C_{12} with Reaction Time from Thermal Decomposition of Pure Compound, Norpar-13, and JP-8P at 425 °C.

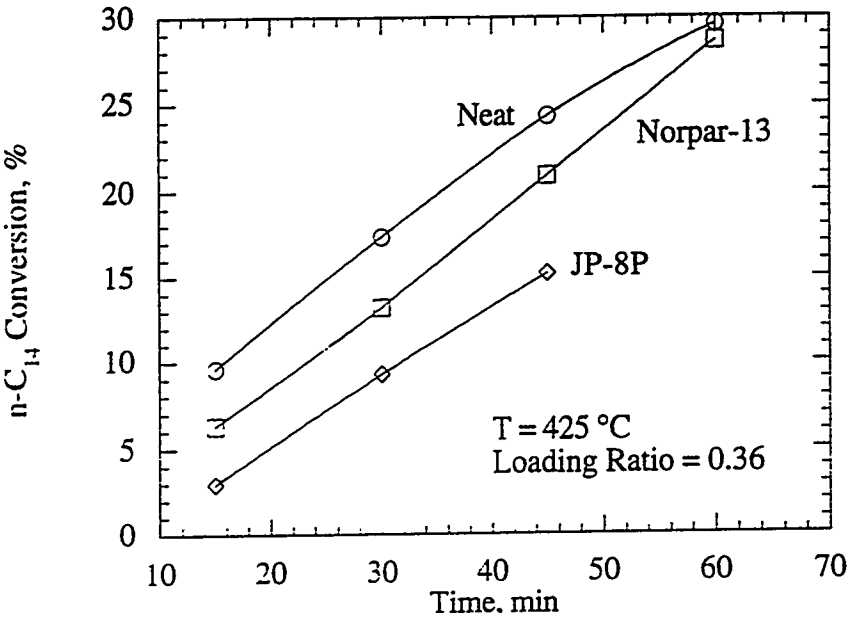

Figure 8. Changes in Conversion of *n*-C_{14} with Reaction Time from Thermal Decomposition of Pure Compound, Norpar-13, and JP-8P at 425 °C.

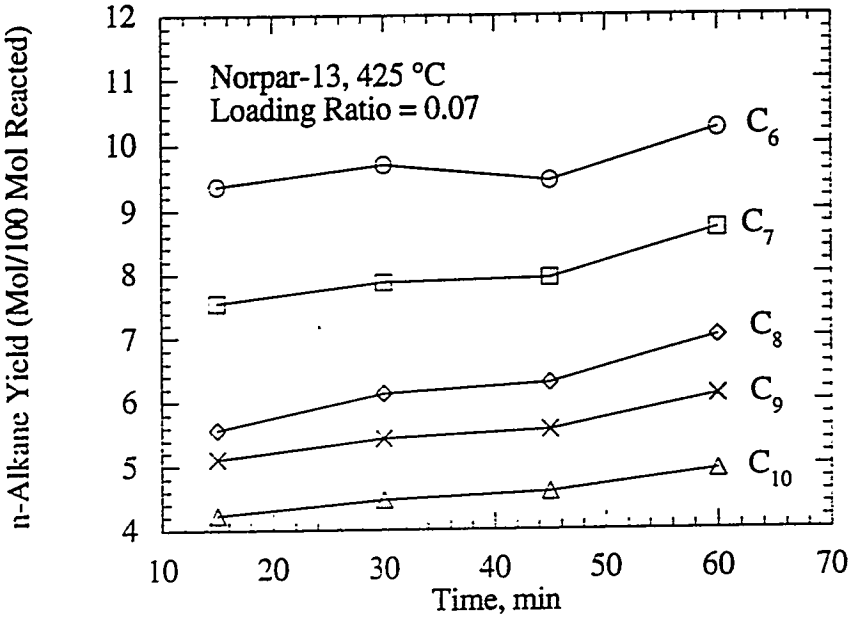

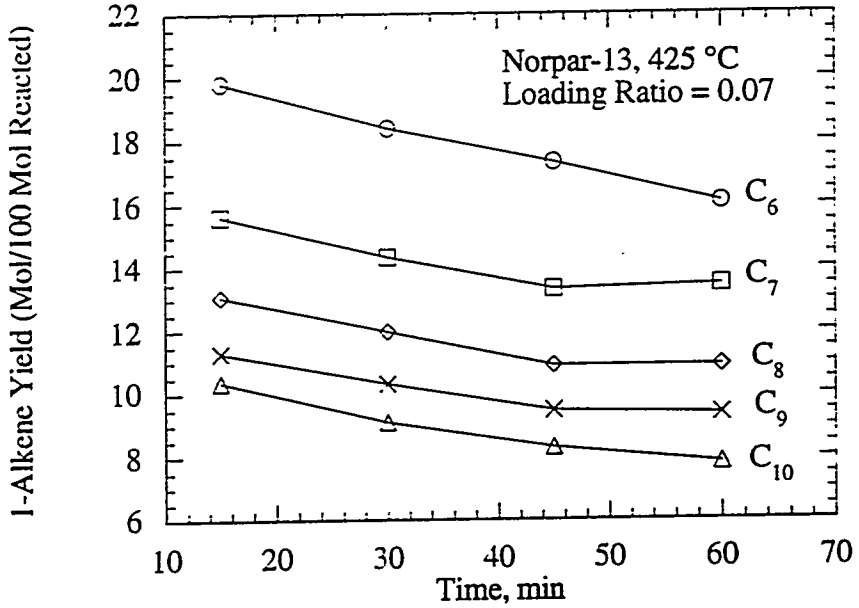

Figure 9. Changes in Molar Yields of C_6-C_{10} *n*-Alkanes and 1-Alkenes with Reaction Time from Thermal Decomposition of Norpar-13 at 425 °C and a Loading Ratio of 0.07.

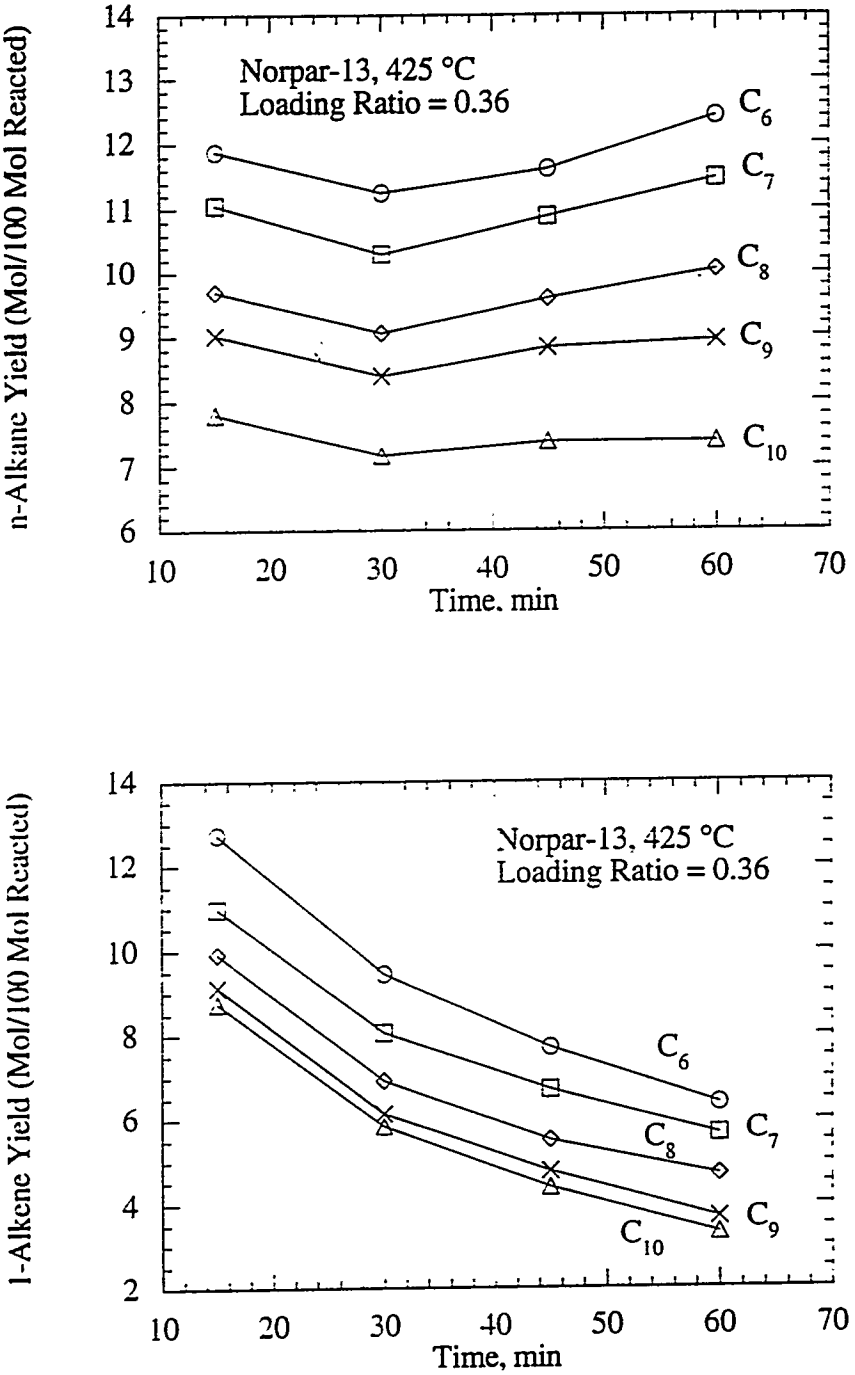

Figure 10. Changes in Molar Yields of C_6-C_{10} *n*-Alkanes and 1-Alkenes with Reaction Time from Thermal Decomposition of Norpar-13 at 425 °C and a Loading Ratio of 0.36.

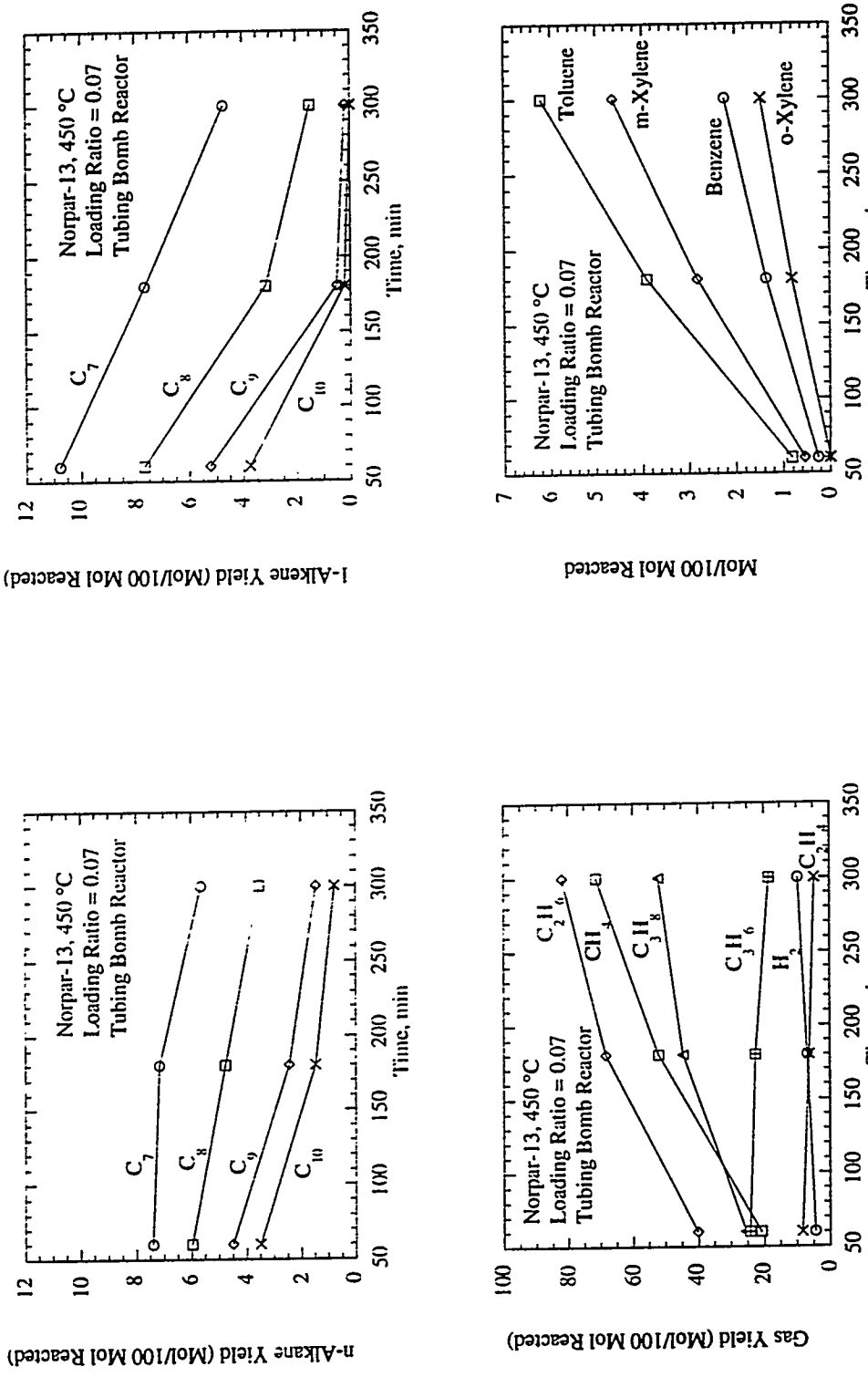

Figure11. Changes in Product Yields with Reaction Time from Thermal Decomposition of Norpar-13 at 450 °C in Tubing Bomb Reactor for a Loading Ratio of 0.07.

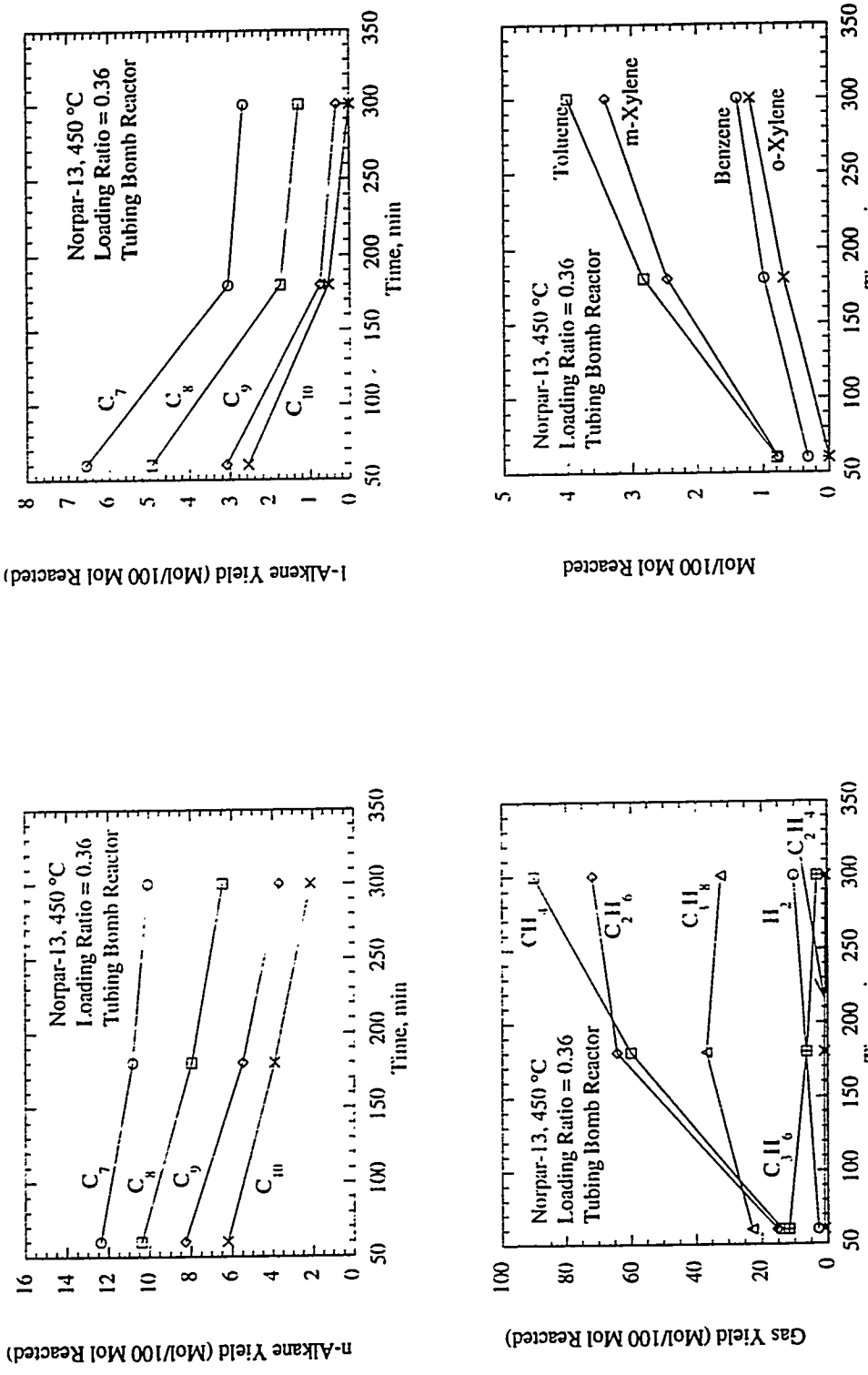

Figure 12. Changes in Product Yields with Reaction Time from Thermal Decomposition of Norpar-13 at 450 °C in Tubing Bomb Reactor for a Loading Ratio of 0.36.

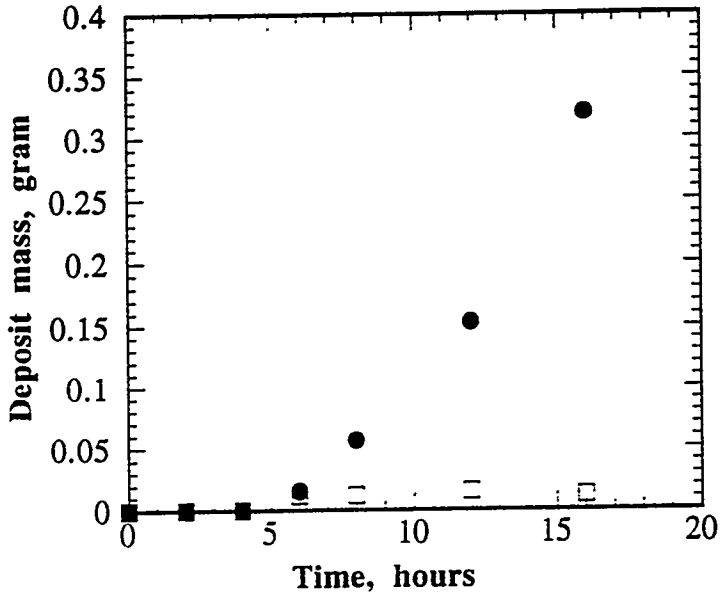

Figure 13. Mass of deposit formed on the wall (l) and formed in the bulk (o) versus time.

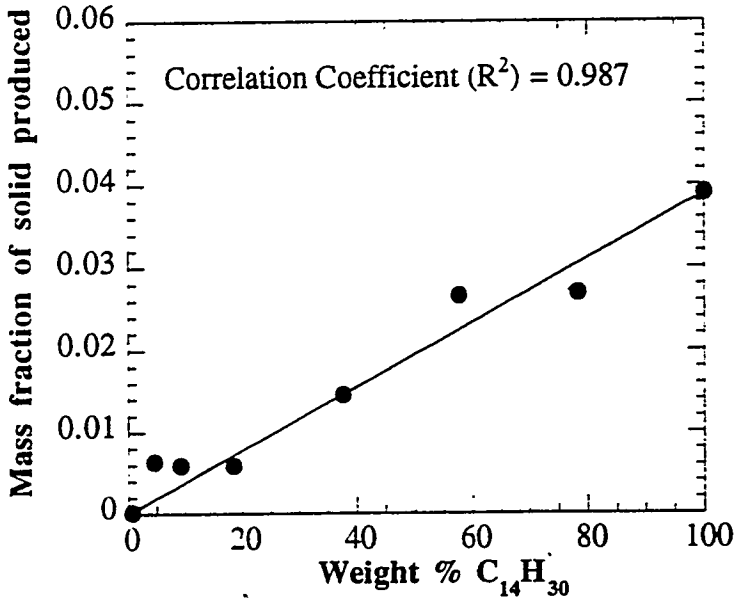

Figure 14. Mass fraction of solid produced versus initial weight% of tetradecane (l). Linear regression with $r^2 = 0.987$ (—).

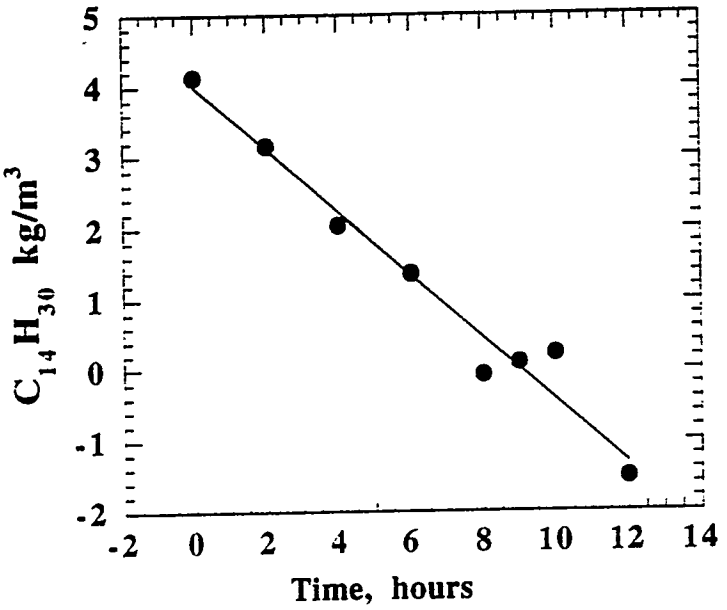

Figure 15. Concentration of tetradecane (l) plotted versus time. Linear regression with r^2 = 0.984 (—).

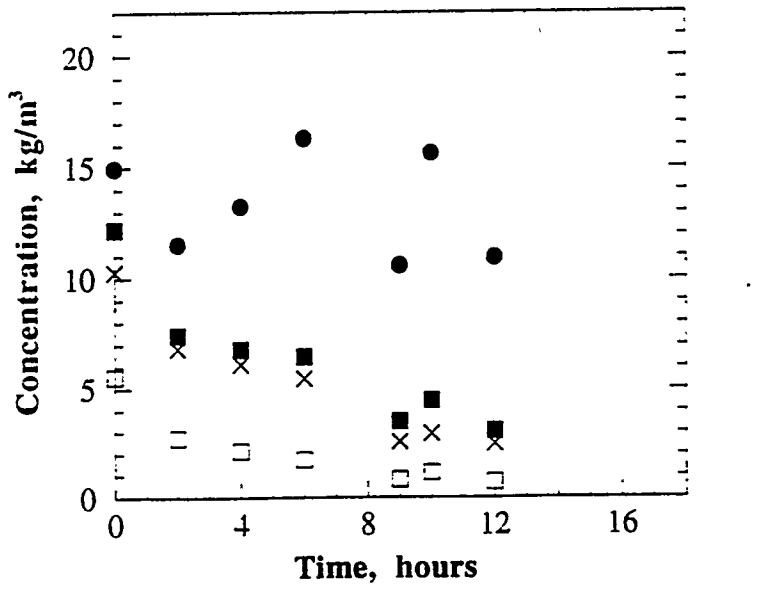

Figure 16. Concentration, Methyl cyclohexane (l), ethyl cyclohexane (n), propyl cyclohexane (o), ethyl-methyl cyclohexane (×) versus time.

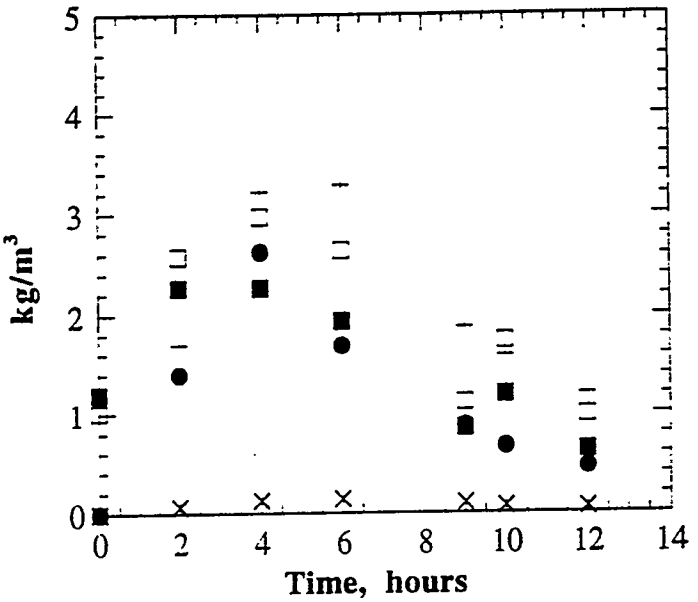

Figure 17. Concentration of octane (l), nonane (o), decane (n), hexane (×), heptane (+), versus time.

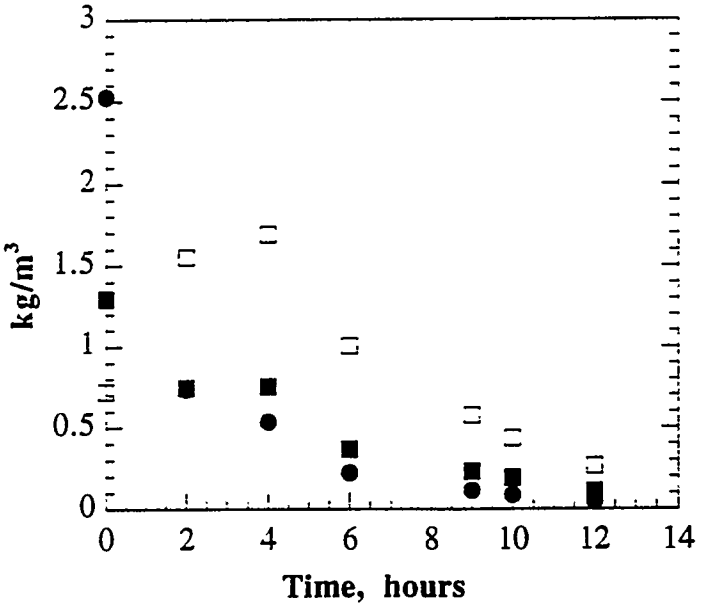

Figure18. Concentration of tridecane (l), dodecane (n), undecane (o), versus time.

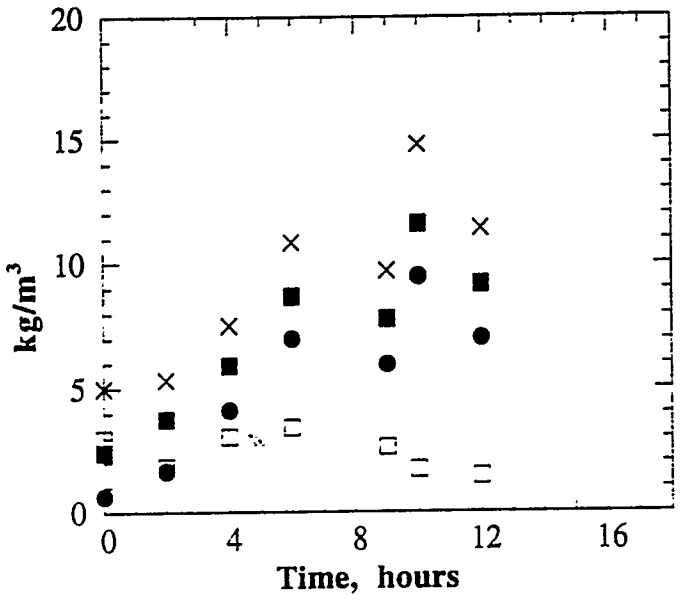

Figure 19. Concentration of methylcyclopentane (l), cyclohexane (o), toluene (n), xylenes + ethyl benzene (×) versus time.

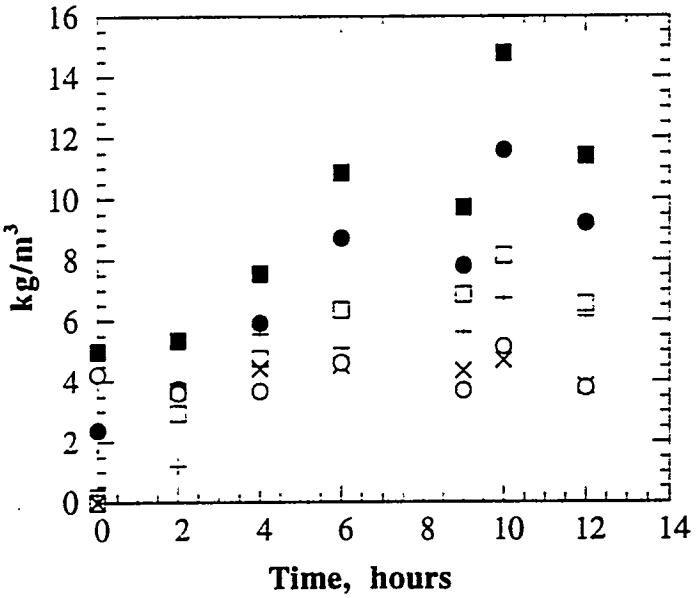

Figure 20. Concentration of toluene (l), xylenes + ethyl benzene (n), naphthalene c1 (o), naphthalene c2 (×), naphthalene(+), indan c1 (m) versus time.

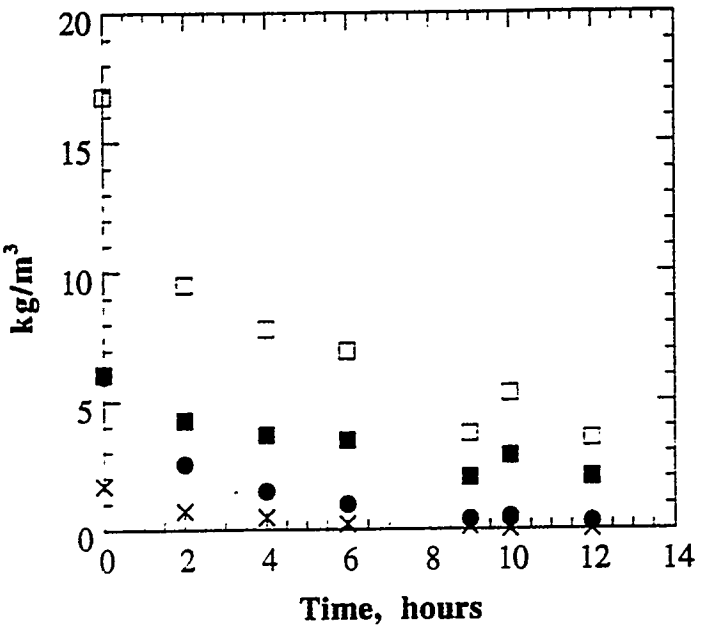

Figure 21. Concentration of tetralin (l), decalin c1 (n), decalin (o), tetralin c1 (×) versus time.

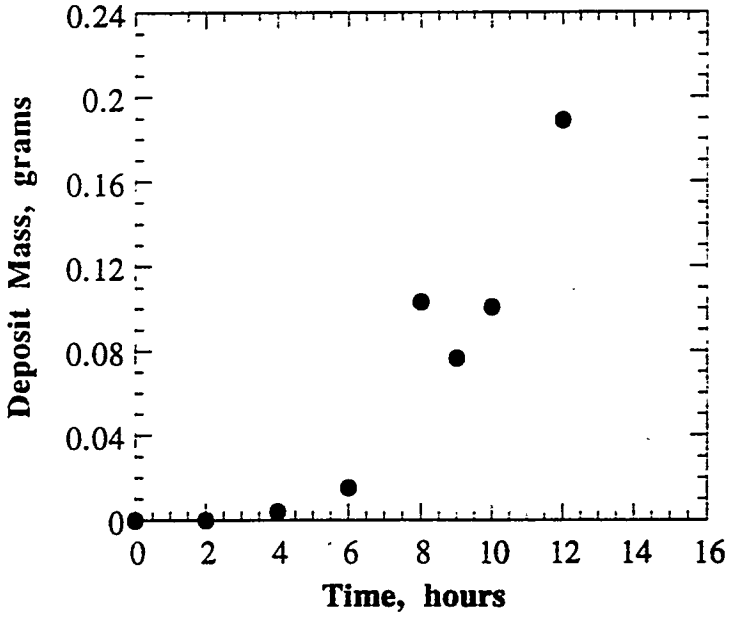

Figure 22. Deposit mass produced versus time.

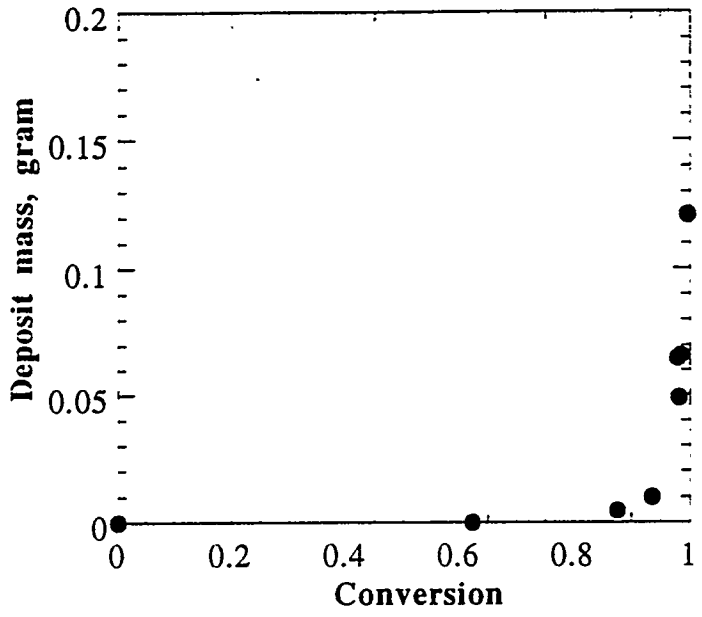

Figure 23. Deposit selectivity during tetradecane decomposition in a JP-8C mixture.

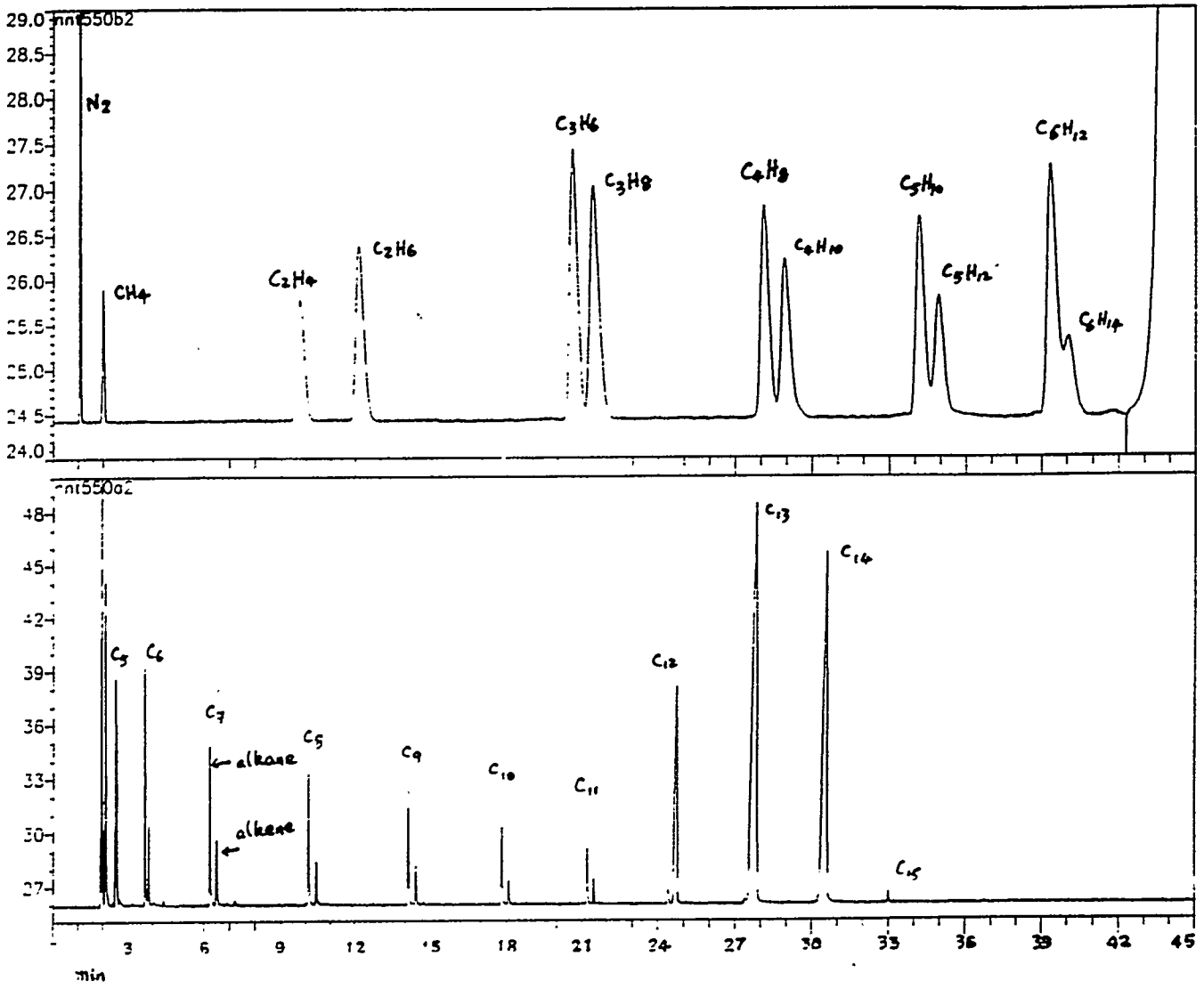

Figure 24. GC Chromatogram of Norpar 13 after Thermal Reaction in the Flow Reactor at 550 °C, 500 psig., 25 Second Space Time for 1 Hour.

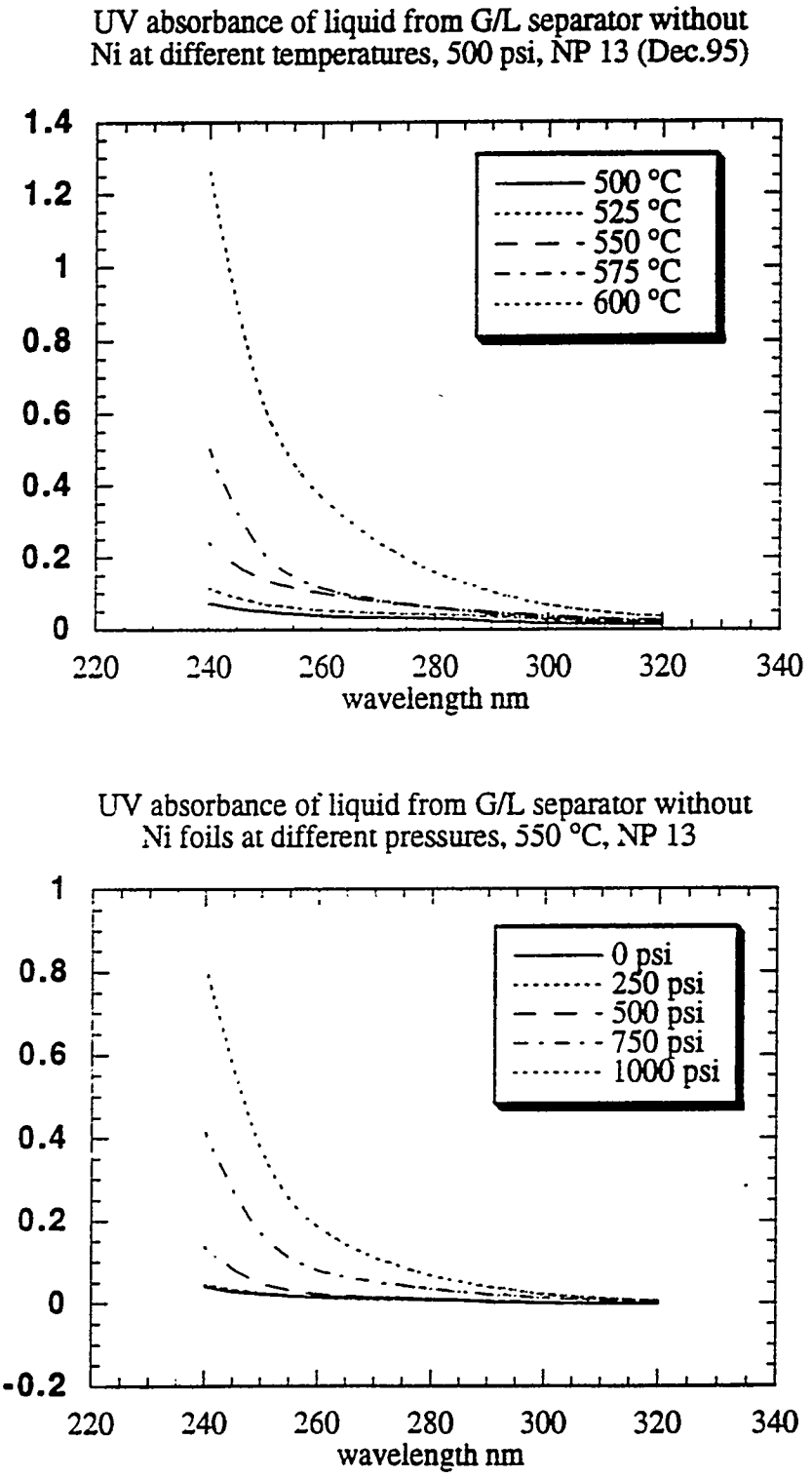

Figure 25. UV Absorbance Spectrum of Liquid from G/L Separator after Reaction of Norpar 13 without Ni at (a) Different Temperatures; (b) Different Pressures.

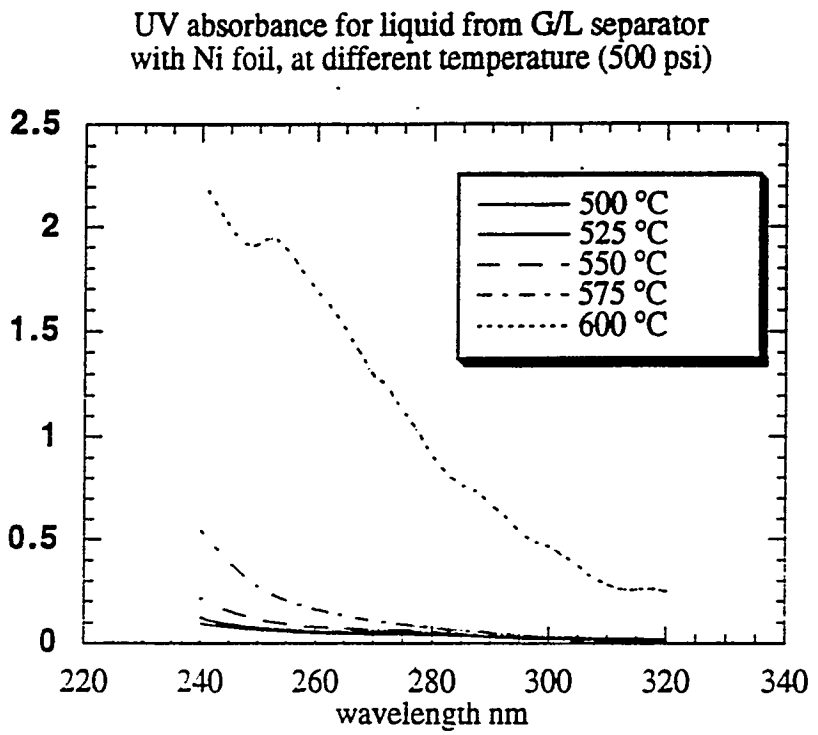

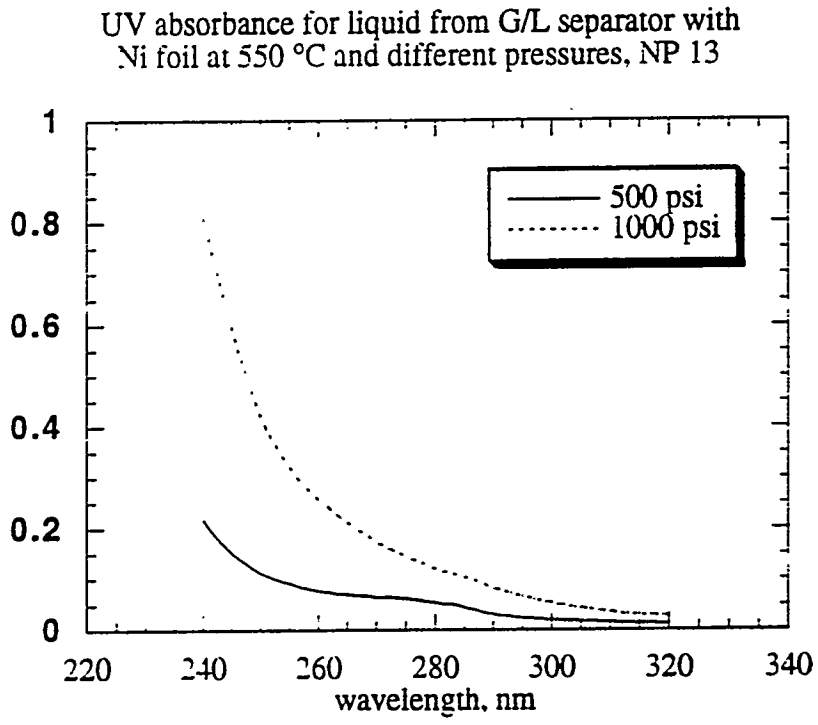

Figure 26. UV Absorbance Spectrum of Liquid from G/L Separator after Reaction of Norpar 13 with Ni at (a) Different Temperatures; (b) Different Pressures.

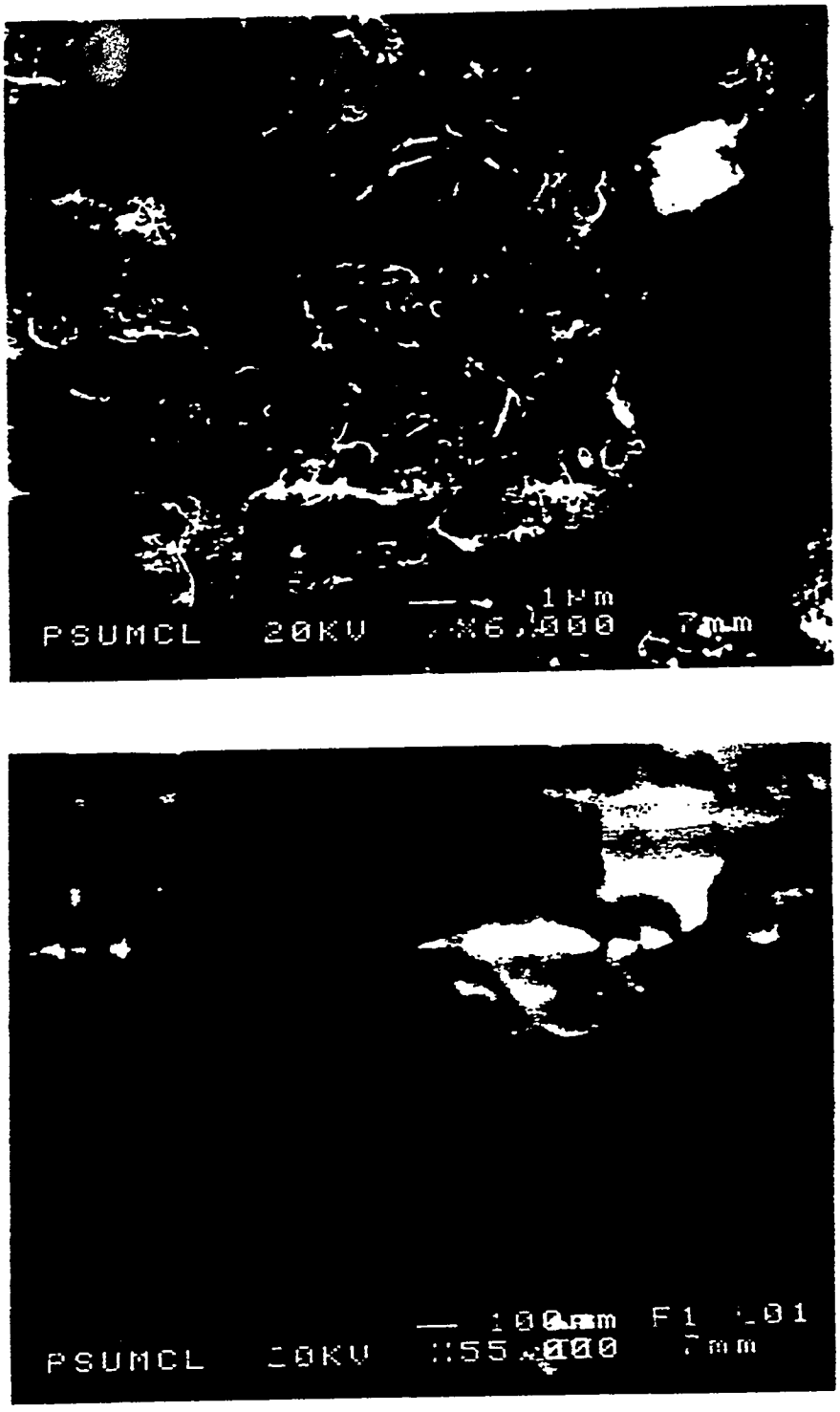

Figure 27. SEM Micrograph of Deposit from Reaction of Norpar 13 at 550 °C, 500 psig., for 5 Hour with Nickel Coupon (a) Filaments and Platelets (above), (b) Filaments (below).

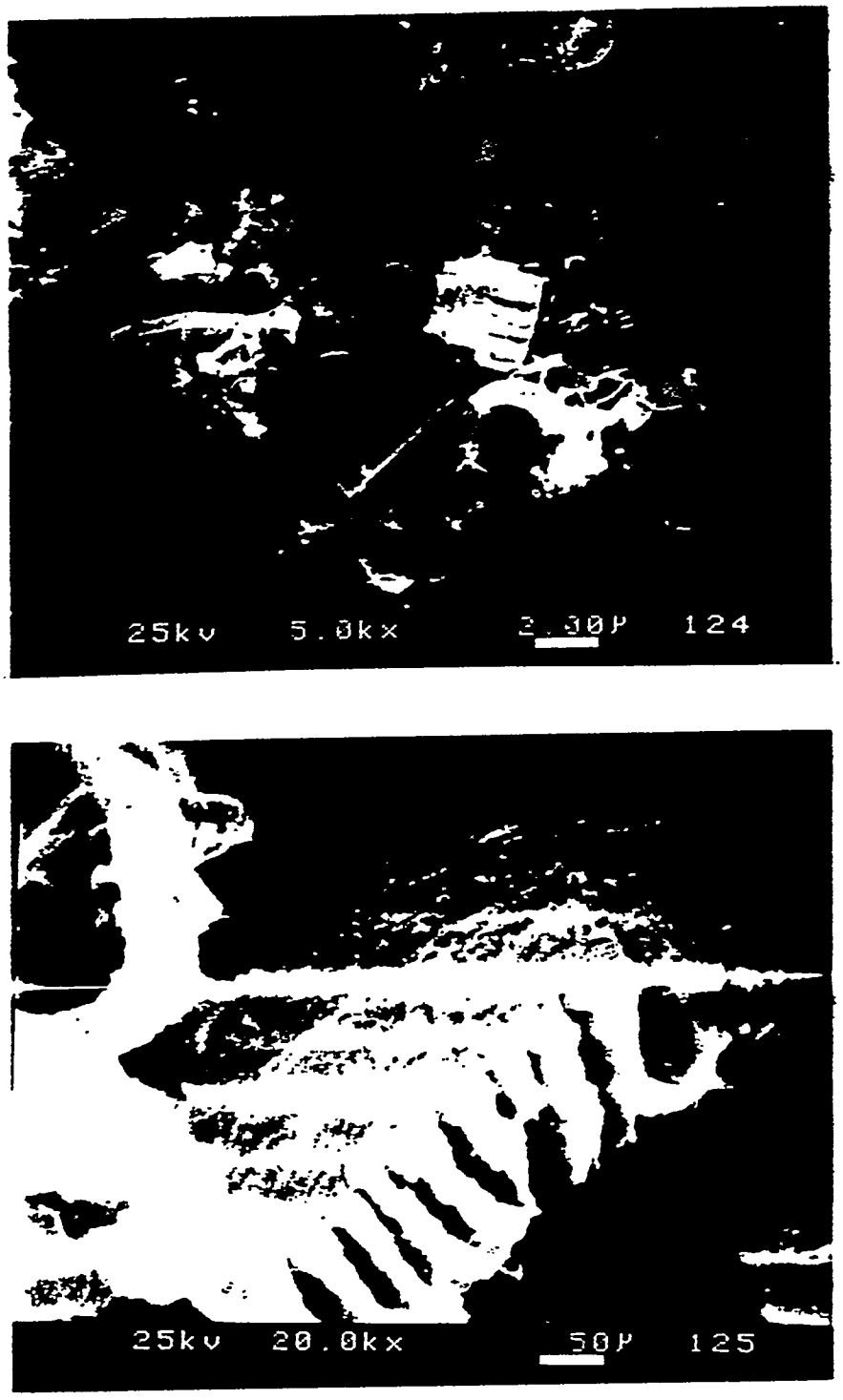

Figure 28. SEM Micrograph of Deposit from Reaction of Norpar 13 at 550 °C, 500 psig., for 5 Hour with Nickel Coupon (a) Filaments and Platelets (above), (b) Platelets (below).

Figure 29. TEM Micrograph of Deposit from Reaction of Norpar 13 at 550 °C, 500 psig. for 5 Hour with Nickel Coupon (a) Filaments (above), (b) Platelets (below).

Figure 30. TEM Micrograph of Deposit from Reaction of Norpar 13 at 550 °C, 500 psig. for 5 Hour with Nickel Coupon (a) Filaments-Entangled Platelets (above), (b) Platelets (below).

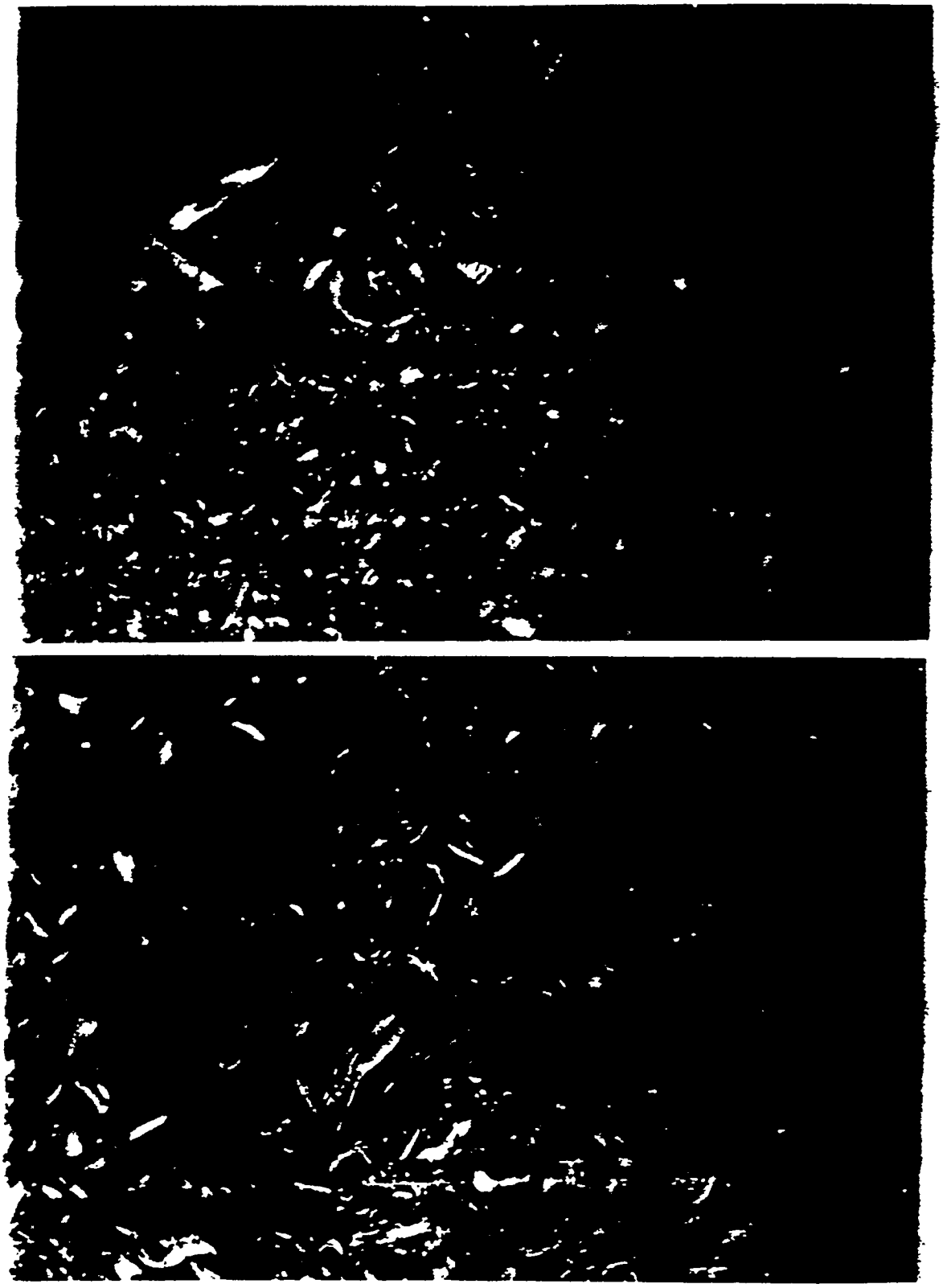

Figure 31. Polarized Optical Micrograph of Deposit from Reaction of Norpar 13 at 550 °C, 500 psig. for 5 Hour with Nickel Coupon Showing the Strong Anisotropic Texture of the Platelets (Yellow and Blue Blocks).

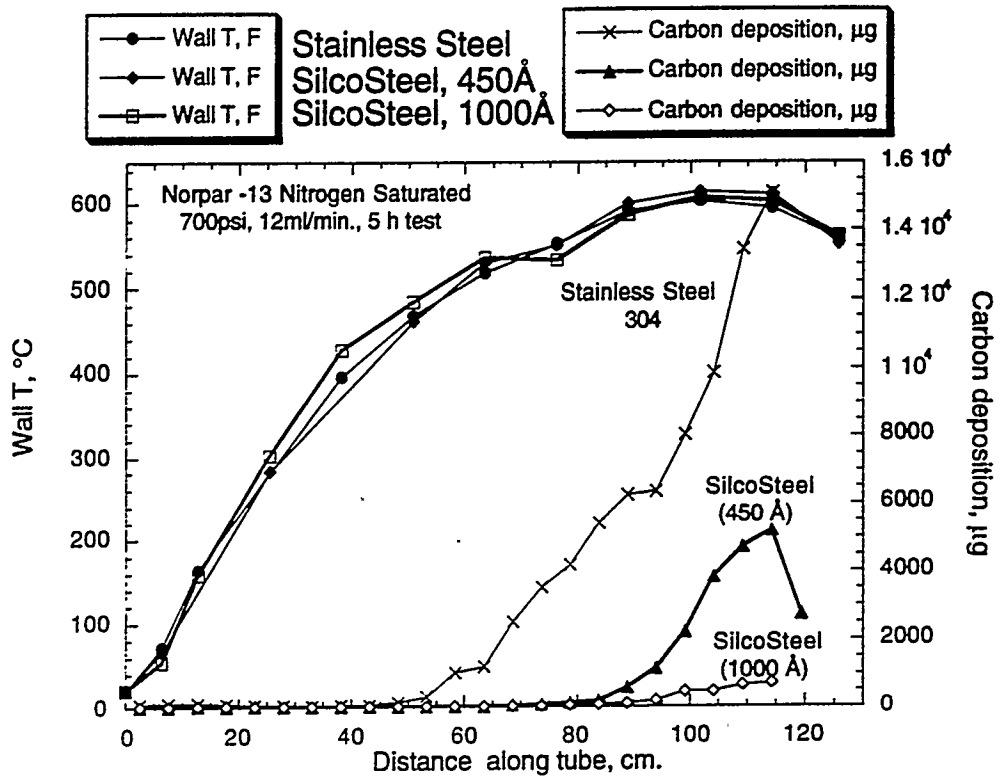

Figure 32. Deposition profile comparing stainless steel to SilcoSteel tubes.

Figure 33. FESEM micrograph of pyrolitic deposits on stainless steel, 330x.

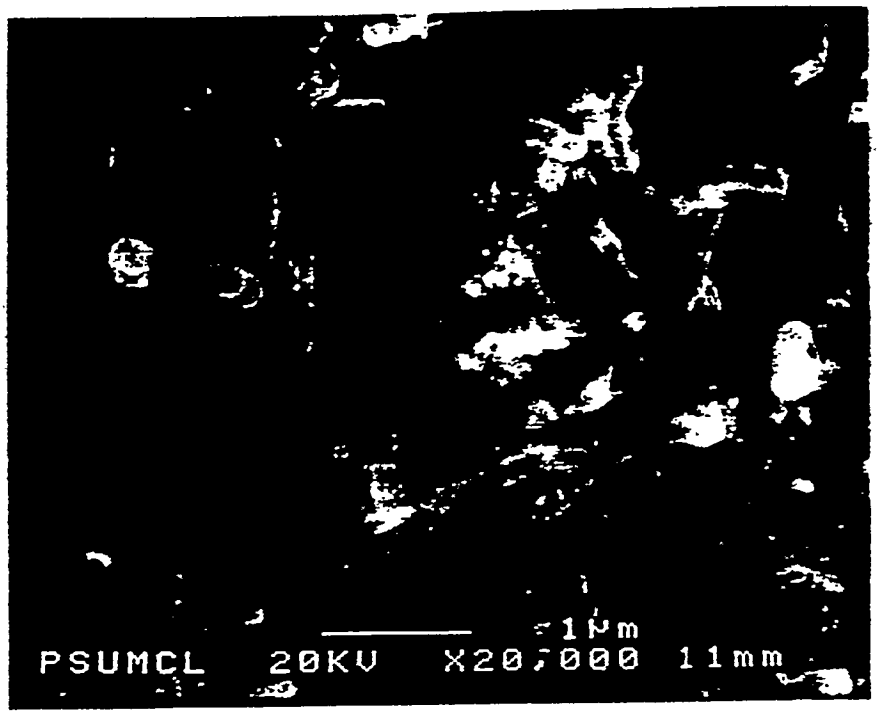

Figure 34. FESEM micrograph of pyrolitic deposits (filaments) on stainless steel, 20,000x.

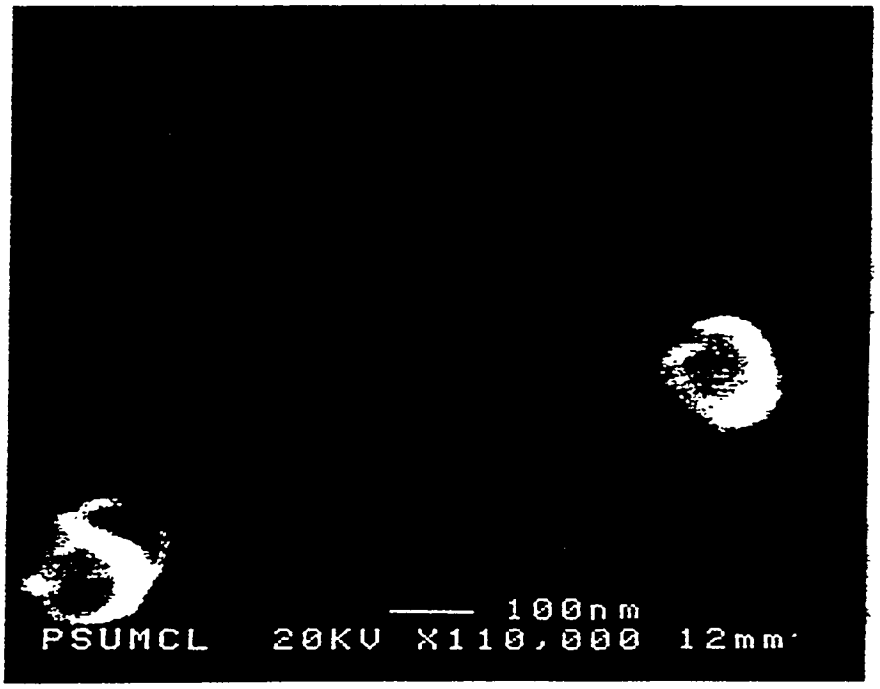

Figure 35. FESEM micrograph of a carbon filament deposit on stainless steel, 110,000x.

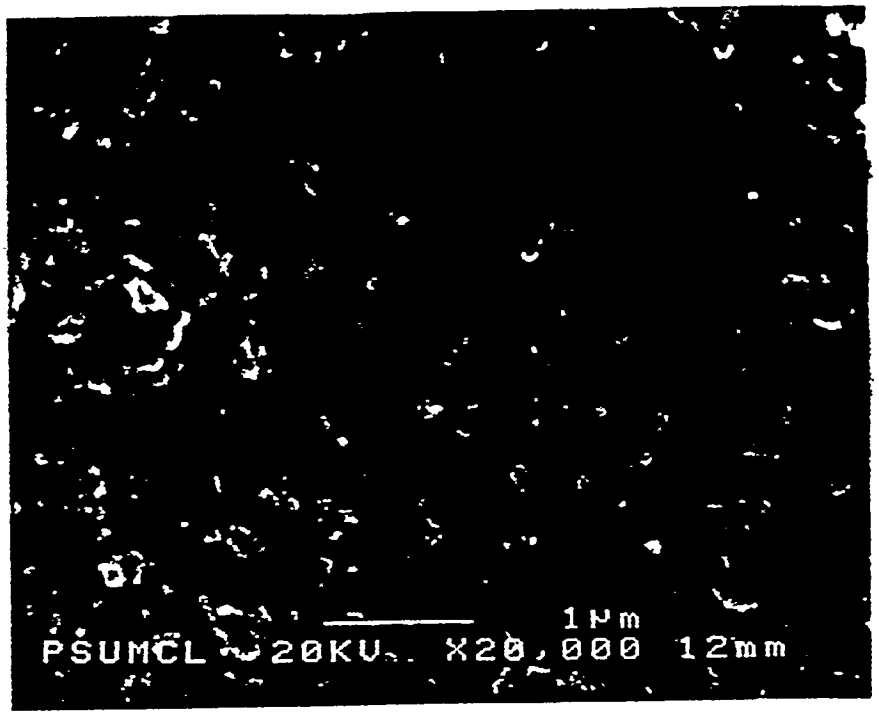

Figure 36. FESEM micrograph of pyrolitic deposits on 450Å thick SilcoSteel, 20,000x.

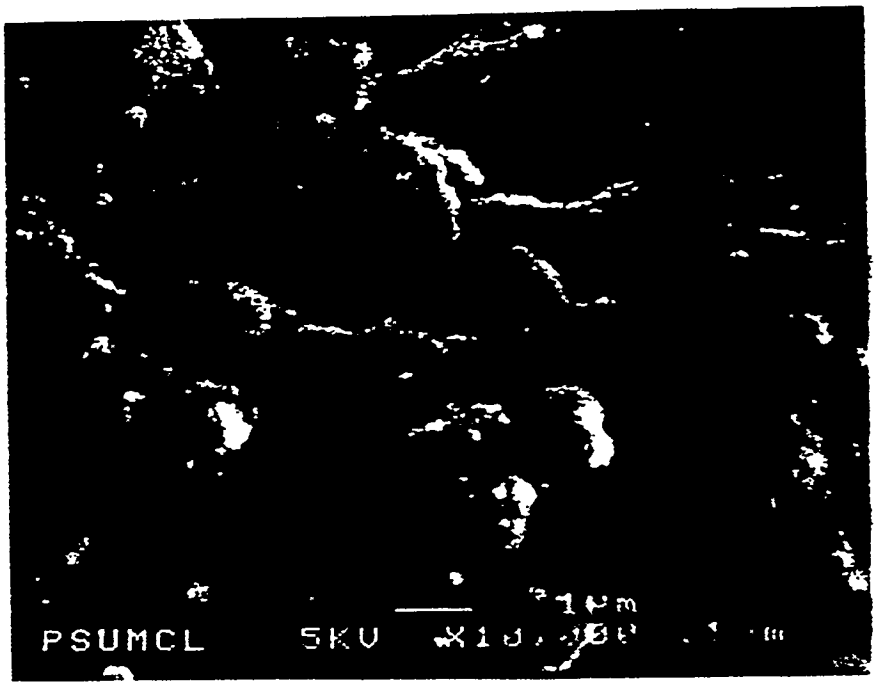

Figure 37. FESEM micrograph of oxidative deposits on stainless steel from a jet A fuel, 10,000x.

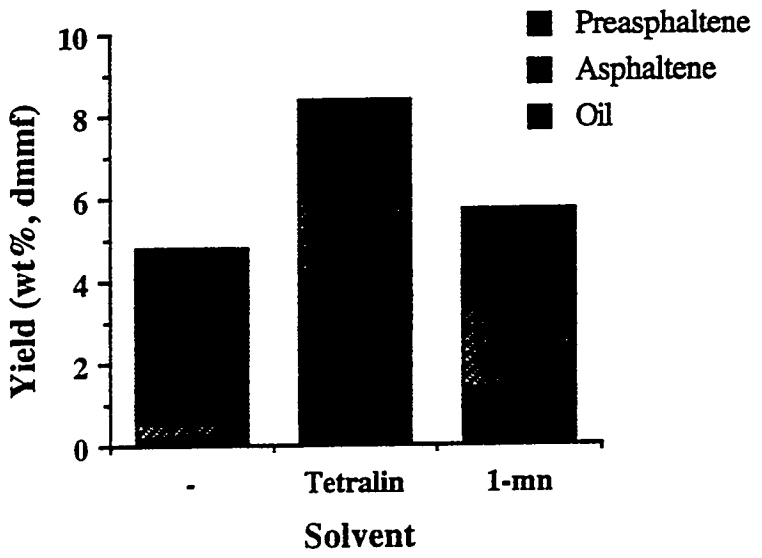

Figure 38. Yields of Soluble Products for Low Severity Non-Catalytic Liquefaction at 300 °C.

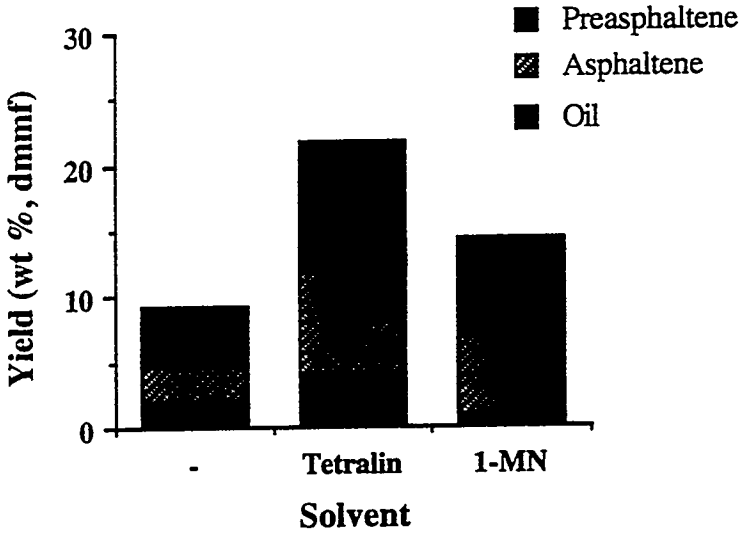

Figure 39. Yields of Soluble products for Low Severity Non-Catalytic Liquefaction at 350 °C.

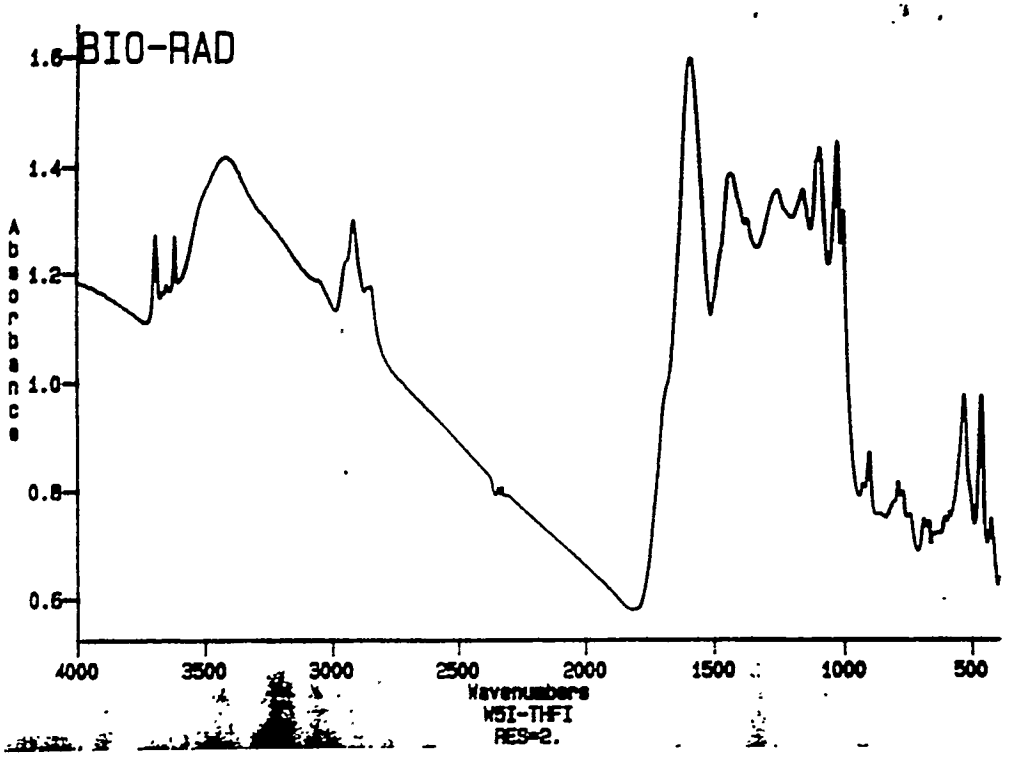

Figure 40. FTIR Spectra of THF-Insoluble Residue from Wyodak Coal Liquefied in Tetralin (300 °C, 6.9 MPa H_2, 30 min).

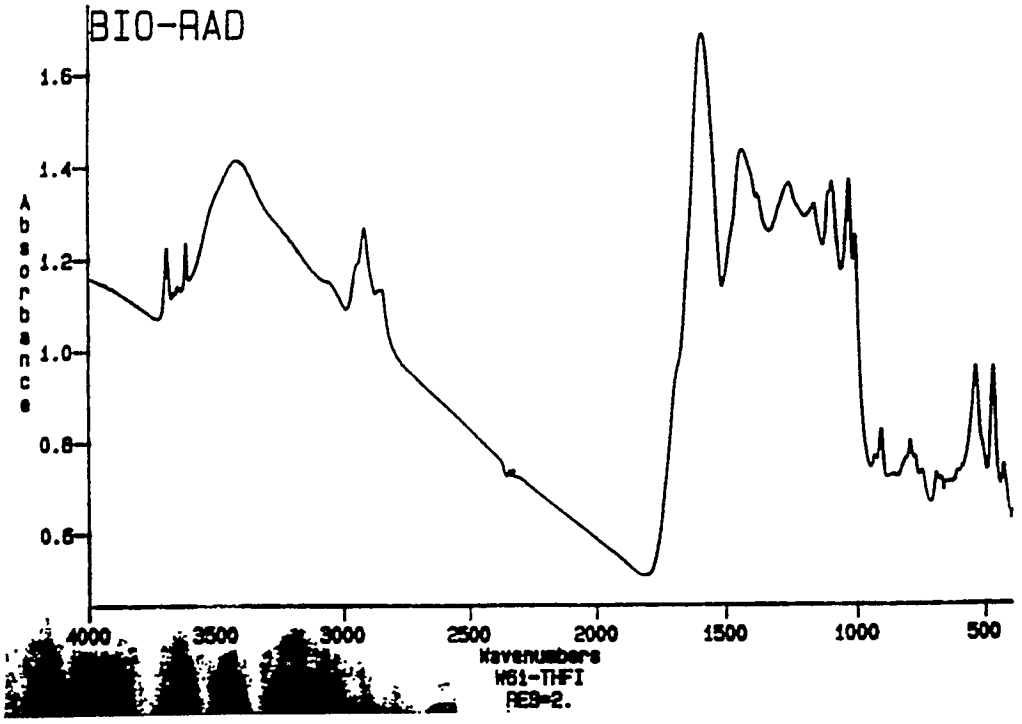

Figure 41. FTIR Spectra of THF-Insoluble Residue from Wyodak Coal Liquefied in 1-methylnaphthalene (300 °C, 6.9 MPa H_2, 30 min).

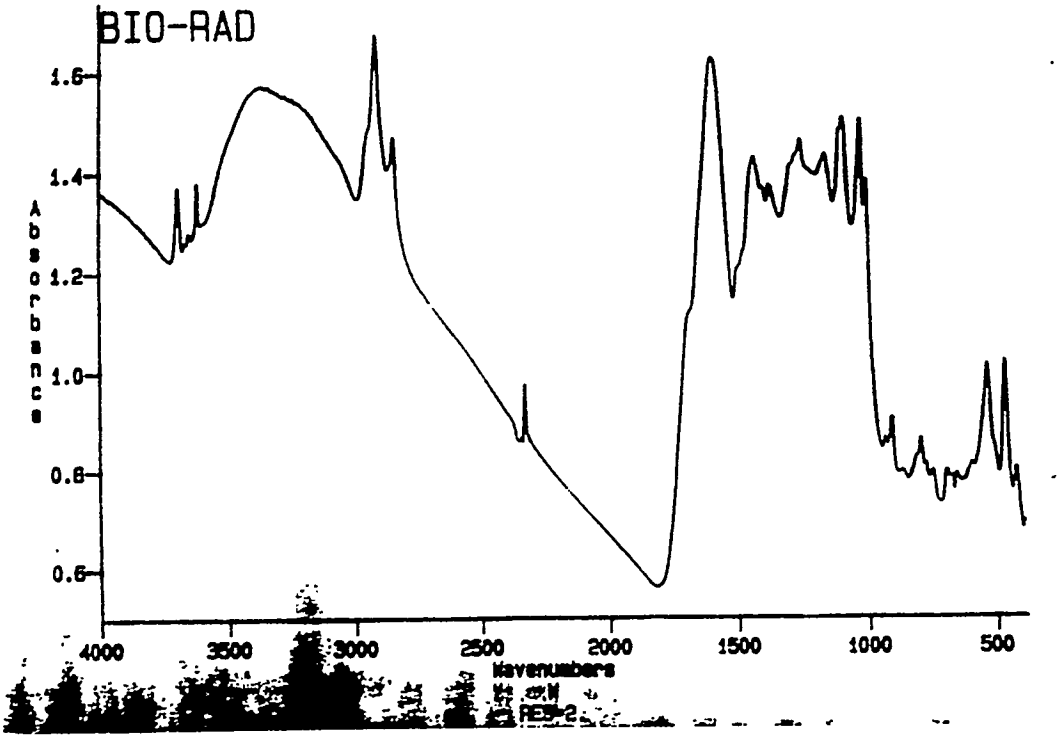

Figure 42. FTIR Spectra of THF-Extracted Wyodak Coal.

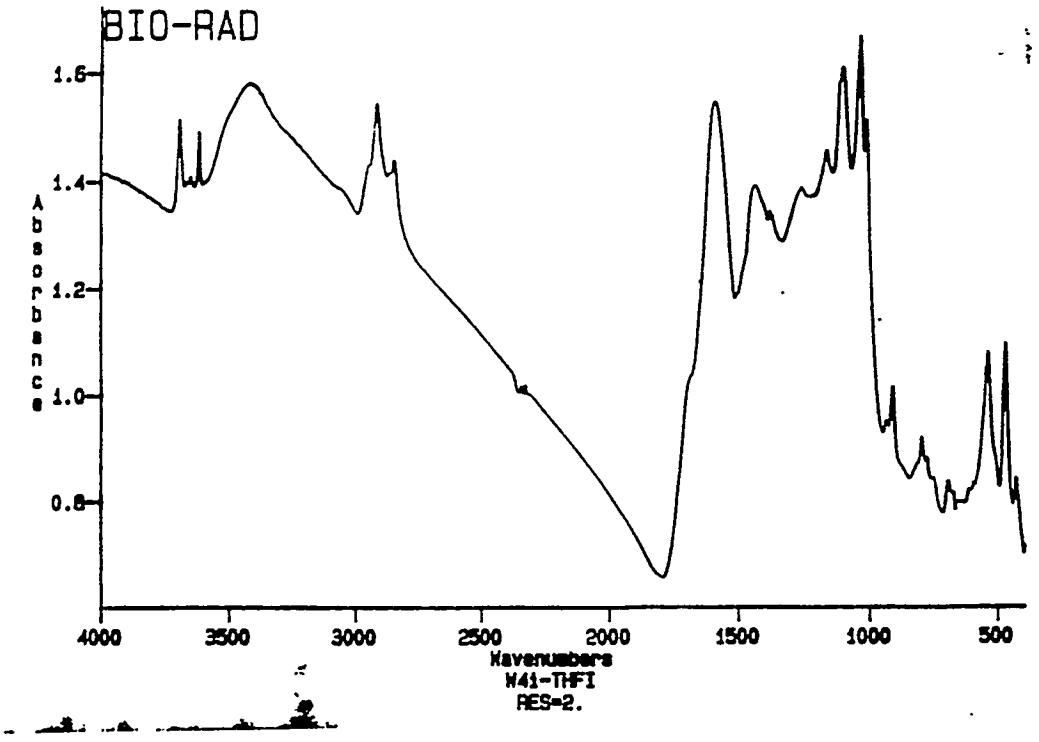

Figure 43. FTIR Spectra of THF-Insoluble Residue from Wyodak Coal Liquefied in Absence of Solvent (300 °C, 6.9 MPa H_2, 30 min).

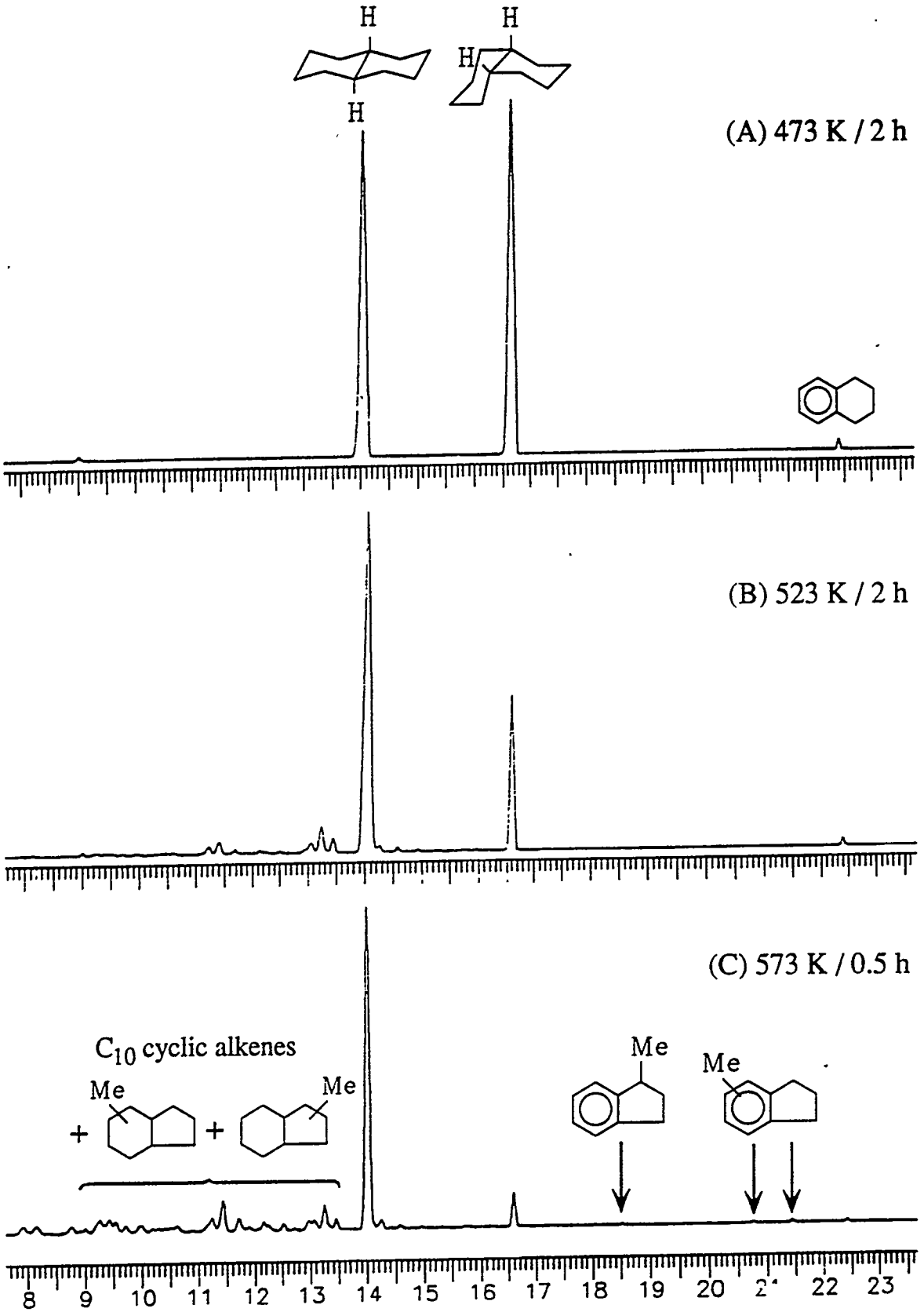

Figure 44.Expanded retention time window of GC profiles for three liquid products from decalin over LaHY: (A) 473 K / 2 h; (b) 523 K / 2 h; (C) 573 K / 0.5 h.

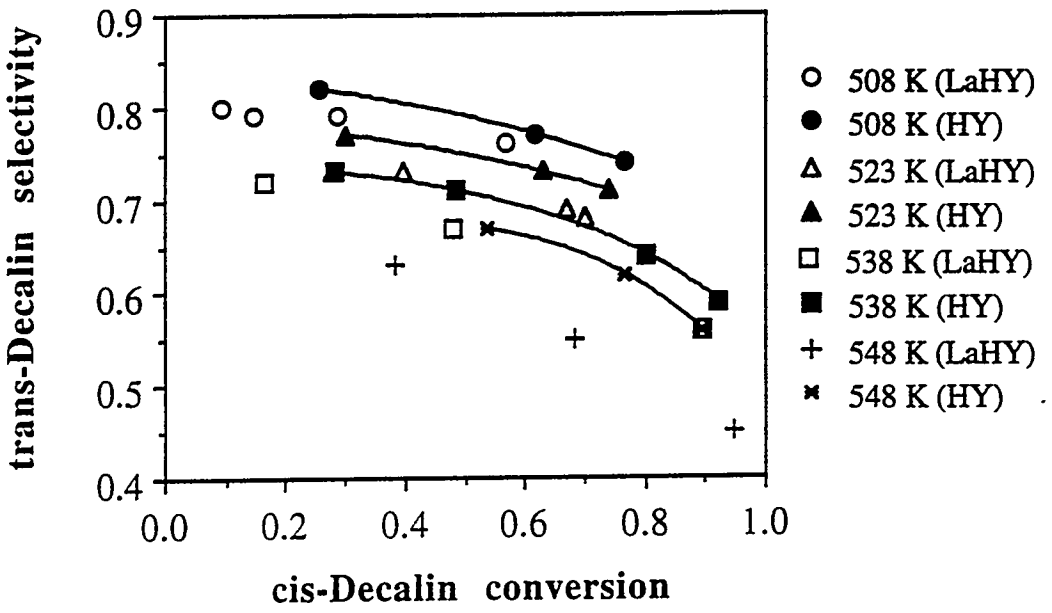

Figure 45. *trans*-Decalin selectivity vs *cis*-decalin conversion plots for LaHY and HY catalysts at four different temperatures.

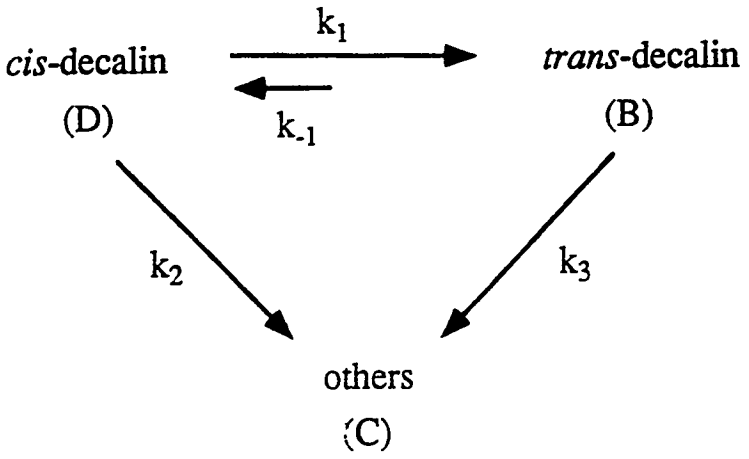

Figure 46. Overall reaction pathways for the catalytic reaction of *cis*-decalin. The dehydrogenation, ring-contraction, and cracking products are grouped as the "others".

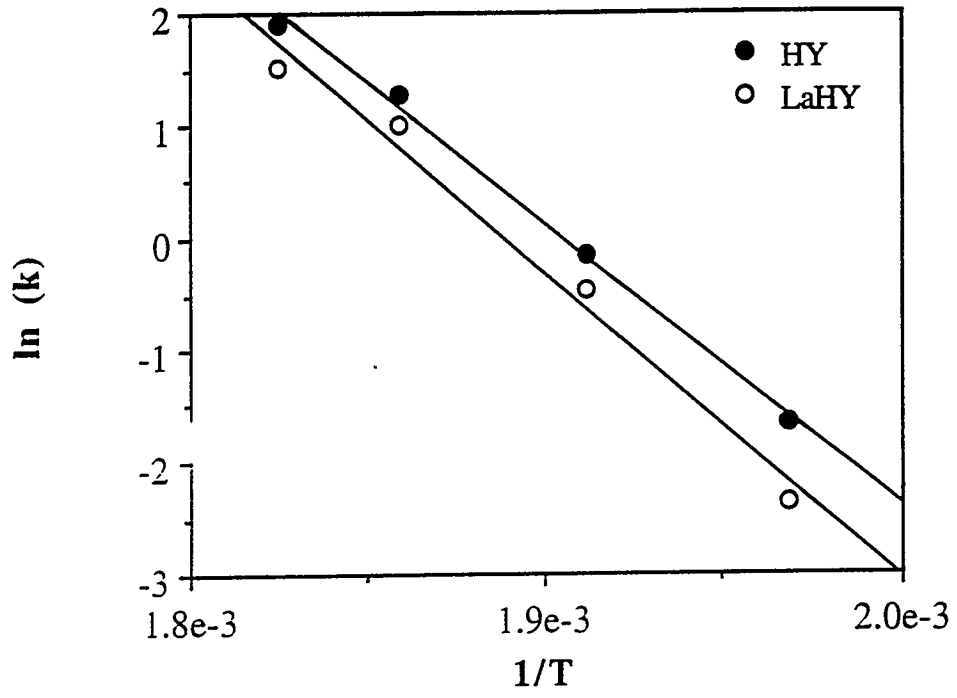

Figure 47. Arrhenius plots for LaHY and HY catalysts at temperatures 508 - 548 K.

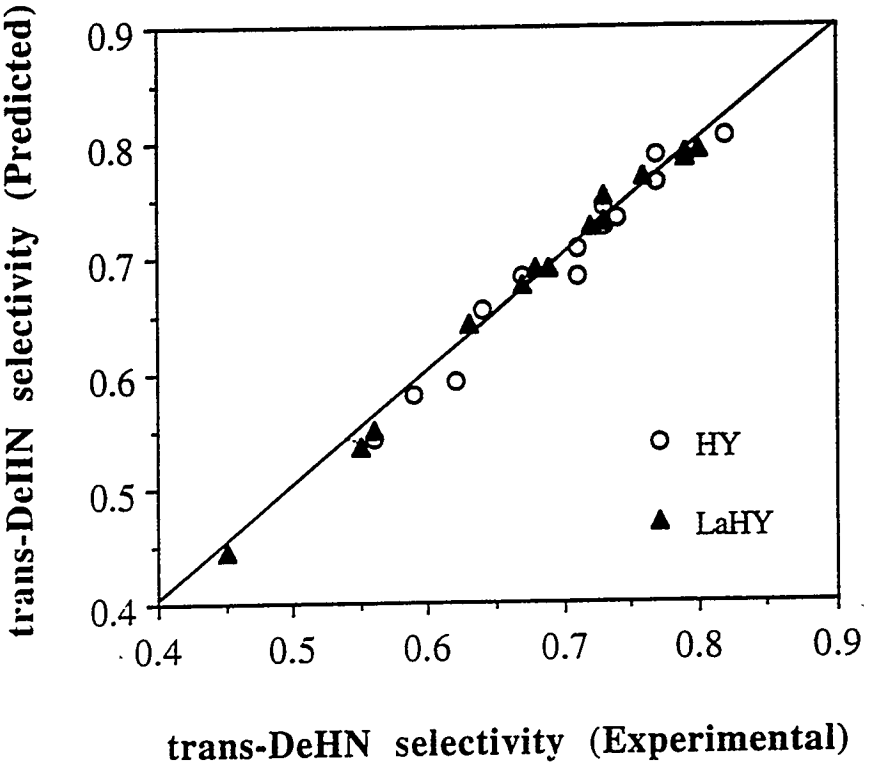

Figure 48. Predicted versus measured values of *trans*-decalin selectivity for the catalytic isomerization of *cis*-decalin using HY and LaHY at 508-548 K for 9-480 min.

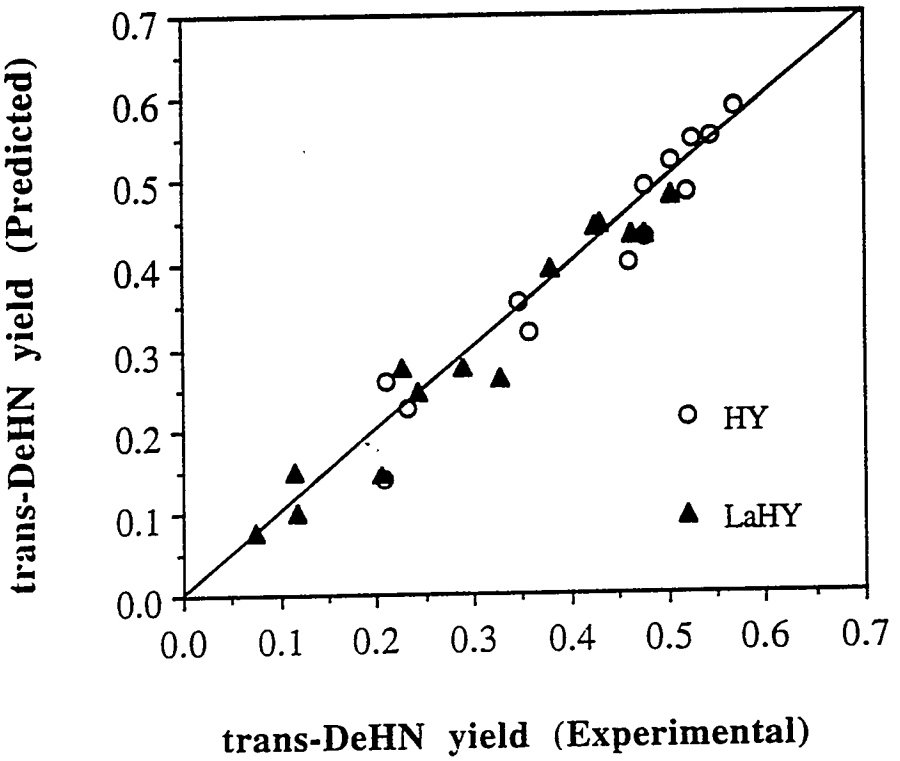

Figure 49. Predicted versus measured values of *trans*-decalin yield for the catalytic isomerization of *cis*-decalin using HY and LaHY at 508-548 K for 9-480 min.

APPENDIX III

SCHEMES

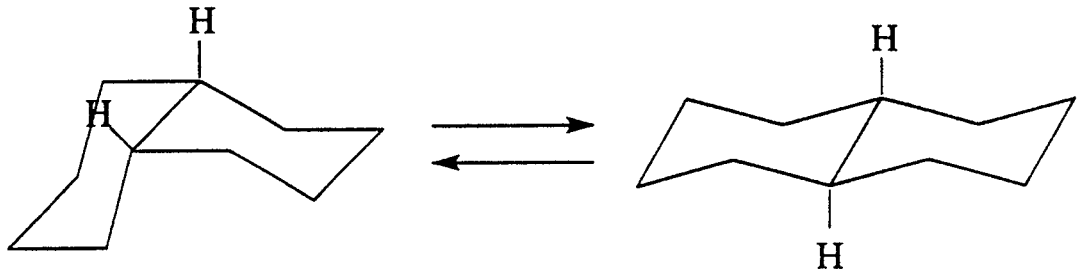

cis-DeHN *trans*-DeHN

Scheme 1. Conformational isomerization of *cis*-decalin to *trans*-decalin.

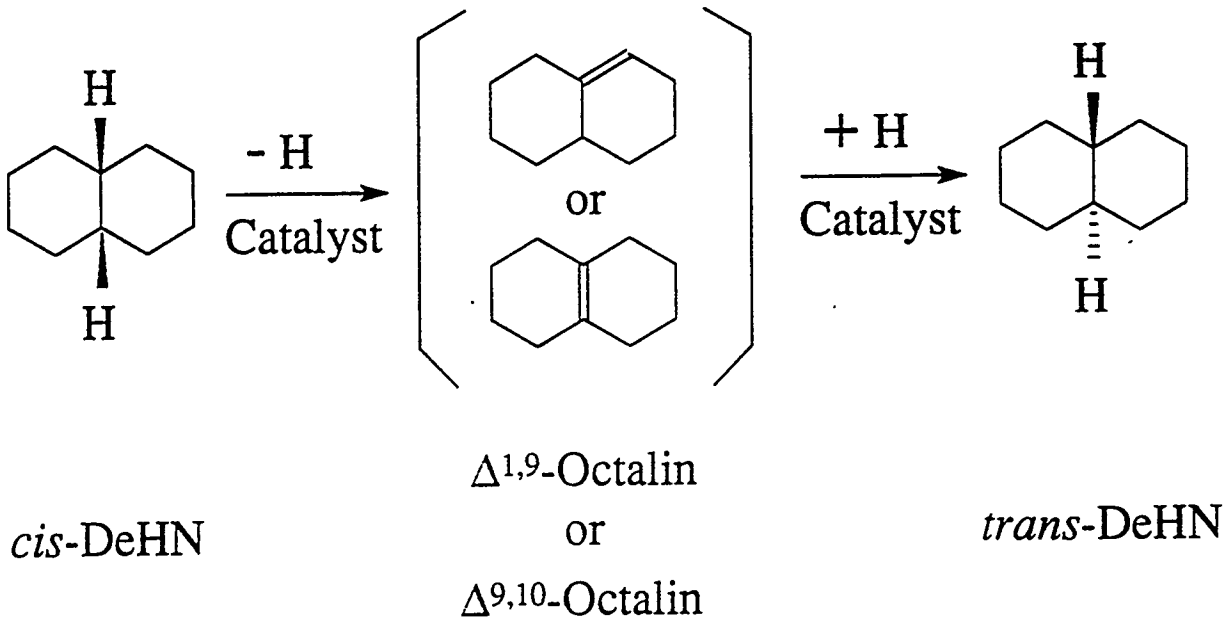

Scheme 2. Proposed reaction pathway for isomerization of *cis*-DeHN into *trans*-DeHN.